



UNIVERSITY OF BERGEN

Geophysical Institute

Master Thesis

**Study of Power Quality
Improvement for Grid-Connected
Floating PV Plant in Kilinochchi**

Author: Prindapan Santhakumaran

Supervisors:

Adjunct Professor Shujun Zhang

Professor Atputarajah Arulampalam

Professor Dhayalan Velauthapillai

June 2022

Abstract

In this study, four controllers have been provided for a grid-connected floating photovoltaic (FPV) system. Object of the study is to provide the utility grid high quality of power produced from the FPV plant. Solar technology is growing fast in Sri Lanka with the support from the government. A significant utilization of the solar resource has been envisaged by the Sri Lankan government and will play a major role in meeting the increasing energy demand in the country. In Kilinochchi at the premises of University of Jaffna 's campus, country 's first FPV plant is installed. Floating PV is gaining popularity around the as it can be a great alternative for the land based conventional solar plants. Control system proposed in this study is based on the FPV plant in Kilinochchi. Proposed controllers in this study are verified using the simulation test bed PSCAD/EMTDC. A Comparison between the controllers has been conducted as well as issues when intermittent sources are interfaced with the utility grid. The results show that some controllers where not applicable while other where proven to work quite efficiently.

Acknowledgement

I would like to express my gratitude to my supervisors, Adjunct Professor Shujun Zhang, Professor Atputarajah Arulampalam and Professor Dhayalan Velauthapillai. I am grateful to Adjunct Prof. Shujun Zhang for his guidance throughout this project and having patience with me.

I am thankful to Prof. Atputarajah who did not hesitate to help me from day one. Thank you for always finding time to answer all my queries and guided me in completing the task.

I am also thankful to Prof. Dhayalan Velauthapillai for suggesting me this thesis. It has been really interesting working on this project as it holds possibilities in enhancing future energy outlook in Sri Lanka.

I also thankful to University of Jaffna for providing me with required informations about the floating PV plant.

Last but not least, I really thankful for my family who have stood by me and encouraged me throughout this process. I made it this far thanks to my parents blessing and prayers.

Contents

1	Introduction	2
1.1	Energy outlook in Sri Lanka	2
1.2	Motivation	3
1.3	Object of the project	4
2	Overview on Grid-connected PV system	6
2.1	Solar cell physics	6
2.1.1	Fundamental of solar cell	6
2.1.2	Equivalent circuit	7
2.2	Requirement for grid-connected systems	8
2.3	Power Processing Unit	9
2.3.1	Voltage source converter	10
2.3.2	Structural arrangement in PV system	11
2.4	Transformer	13
2.5	Harmonics and Filter	14
2.5.1	L-filter	15
2.5.2	LC-filter	15
2.5.3	LCL-filter	15
2.5.4	LC-Filter design	16
2.6	Floating Solar Plant	16
2.6.1	Structure of floating PV plant	17
2.6.2	Floating Solar Plant in Kilinochi	21
3	Control of Grid-connected PV system	25
3.1	MPPT	26
3.2	DC-link voltage control	29
3.3	Proportional and integral controller	31
3.4	Power control	31
3.4.1	Clarke's & Park's Transformation	31
3.5	Principle of PWM technique	34
3.6	Grid Synchronization and Phase locked loop	36
3.7	Basis of Power flow	38
3.7.1	Instantaneous power theory	38
3.7.2	Voltage mode control and current mode control	40
3.8	Hysteresis control	41

4	Simulation of Grid-connected PV system	44
4.1	PV array design	45
4.2	MPPT control	47
4.3	PLL control	48
4.4	Control methods	49
4.4.1	Design of 1st controller	49
4.4.2	Design of 2nd controller	52
4.4.3	Design of 3rd controller	53
4.4.4	Design of 4th controller	56
4.5	Simulation Results	58
4.5.1	1st Controller	58
4.5.2	2nd Controller	63
4.5.3	3rd controller	64
4.5.4	4th controller	66
5	Conclusion & recommendation for future work	70
5.1	Conclusion and discussion	70
5.2	Future development for the system	72
A	PV topology	1
A.1	PV array design	1
A.2	DC-link capacitor calculation	2
A.3	LC-filter calculation	3
A.4	Clark and Park transformation on PSCAD	4
A.5	Pulse width modulation scheme	5
A.6	THD	6
B	Data about the FPV plant in Kilinochchi	8
B.1	SUNNY TRI POWER CORE1 Datasheet	8
B.2	PV module topology	9
B.3	Environmental condition	9

Chapter 1

Introduction

1.1 Energy outlook in Sri Lanka

A global response has been issued to progress from dependency from fossil fuels and pave a carbon neutral pathway in the future. With the purpose of fighting climate change, many countries have signed an international treaty known as the 'Paris agreement' in 2015. This aims to keep the rise of the global average temperature ideally to 1.5 degrees[49] in order to keep the temperature rise to the ideal value mentioned above. The emission needs to be reduced to 50% by 2030, and reach net-zero by 2050. Each country has devised their own pathways to strategically reduce their carbon emission annually. According to [49], by observing the global CO₂ emission from different countries in year 2018, Sri Lanka's share consisted of 20.6 million tons. In comparison to the world's total CO₂ emission, Sri Lanka's share consisted of only 0.06%. Even with low emission rate compared to rest of the world, the Sri Lankan government has the intention of reducing their emission by increasing their share of renewable energy sources to their energy mix. They intend to reduce the dependency of fossil fuel to meet the annually increasing energy demand. This is explained in the report from [49] which is Sri Lanka's long term generating expansion plan (LTGEP) devised for a period of 2022-2041. The report provided by the Ceylon Electricity Board (CEB) who have the key role in ensuring sufficient electricity supply for the country. Adhering to the government's policy on creating low carbon electricity supply system, LTGEP report presents a strategically devised plan for the gradual transition from conventional sources to renewable sources. This is done by studying the country's capabilities and limitation.

A milestone is set by the government which aims to ensure 50% of the generated electricity should come from RE sources by the year of 2030 [49]. Looking at the current energy mix in the country, petroleum and biomass are the major contributors in the primary energy supply. The share of petroleum is 40.2% and most of the source is imported as a finished product and as crude oil which will later be processed at the refinery in Sapugaskanda. 10.3% of the energy mix for electricity production is derived from coal. An immediate abandonment of the conventional technology is not recommended and thereby not included in the report. Gradual transition is essential for the current situation as the capacity of the RE would not be able to cover the energy requirement that the conventional sources generate. For this reason, in CEB's report further development of the sources of fossil fuels are planned. As an example initiative of oil and gas exploration has been conducted at

the Mannar basin located in the north-west coast. Still bearing in mind that the expansion plan has the interest of enhancing growth of other renewable energy (ORE) sources during the two decades.

The share of biomass in the energy supply is statistically known to be 36.2%. As biomass is an abundant resource in the country and the usage is difficult to document in domestic use, one can assume this percentage most probably be somewhat higher. Among the available indigenous resources, hydro power emerges as a primary resource among them. Its contribution in 2018's energy supply was accounted for 9.7%. Further development in the hydro power may be difficult since large amount of its 2000 MW capacity has already been utilized. Further large-scale development in hydro resource may lead to social and environmental consequences. According to CEB's report wind and solar energy can play a major role in providing energy to the country in the future. 3.7% of the energy supply is provided by wind and solar energy at present. The government intends to increase wind energy's contribution from 268 MW to 1,013 MW by the end of 2030. Solar energy's contribution to the country's energy mix will parallelly increase from 425 MW to 2,874 MW by the end of 2030. A further increase is expected according to the 20 years envisaged plan from CEB [49].

1.2 Motivation

Figure 1.1 presents the capacity growth of other renewable energy (ORE) resources. Among the resources a steep growth potential is envisaged for wind and solar during the period of 2 decades. The objective of this thesis is solely on solar energy and its current role in Sri Lanka's energy supply.

Sri Lanka being located around the equatorial belt which makes higher availability and potential of the resources. As it is illustrated in Fig.1.1, a significant increase of solar capacity is envisaged in CEB's plan and will be the leading form among ORE resources. Power generation from solar PV is gaining popularity around the world and the countries like Germany, Italy and India to mention [11][4]. With economical subsidy support from their governments, solar technology has grown in these countries and contributed in a large scale for their energy mix.

A similar trait can be seen in Sri Lanka where with economical support in the recent years local solar PV industry has gained momentum and has grown in both ground mounted solar PV and roof-top solar PV application. According to CEB's report a further development in this area is expected in both large and small-scale development. By 2025 an increase to 1,829 MW is planned and by 2030 an increase to 2,684 MW is expected with both large and small-scale projects. Sri Lanka's potentials in solar resource in the future which consist of three alternatives. Such as ground mounted solar, rooftop solar application and floating solar application. Among them large and medium-scale (10MW-100MW) developments are planned for ground mounted solar parks in the future [50]. With an increase in PV technology, motivation for this study will be based on the floating PV technology. Floating PV plant is an innovative way to harness the abundant source, and this technology is gaining popularity around the world[11]. Sri Lanka's first floating PV plant is located in the northern part of the country. The FPV plant is a pilot project conducted by the University of Jaffna and the research group ANCEHA. Number of FPV technology in Sri Lanka may increase in the near future as potential reservoir and sites have been discovered by Sri Lankan Sustainable Energy Authority [50].

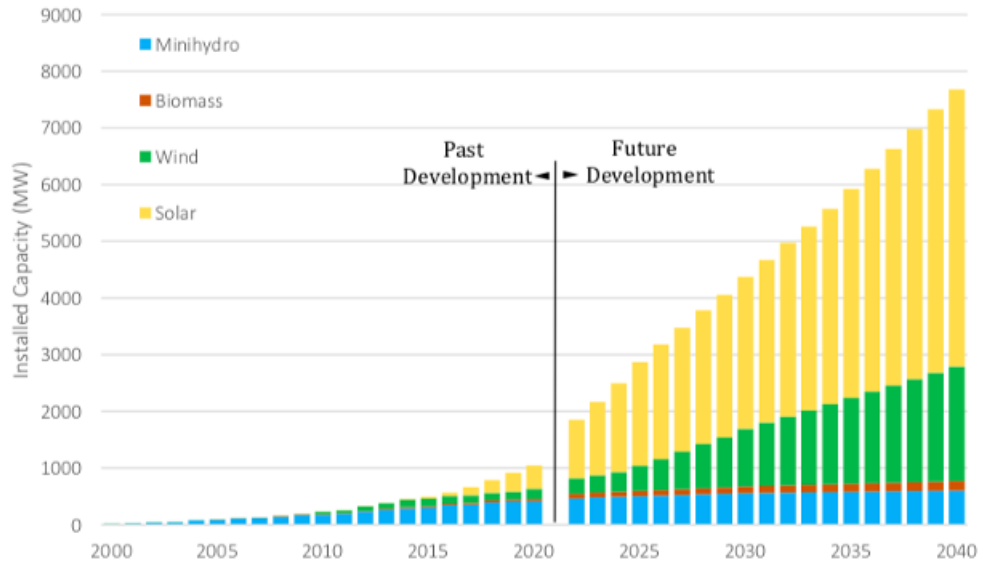


Figure 1.1: Past and the future ORE capacity in Sri Lanka [50]

1.3 Object of the project

Solar and wind are reliable resources to replace fossil fuel dependency to meet Sri Lanka's increasing energy requirement. As mentioned above, future development in solar resource is favored by the government. The government's intention is to have a transformation from phase 2 (less impact) to phase 3 (severe impact) as defined in Fig.1.2 which illustrates impacts of variable RE resources from non to severe [50]. Additionally, it indicates the challenges that must be considered to make the transition defined in Fig.1.2 possible.

Increased impact of solar resource to the utility introduces different dynamics because of its inherent characteristics. Proper control is essential and therefore the main object for this study is to design a controller for the grid-connected FPV plant which enables effective utilization of the solar resource and provides high power quality to the utility grid. Four different controllers have been designed in this study, and have been verified using the simulation test bed PSCAD/EMTDC.

This study is organized as following:

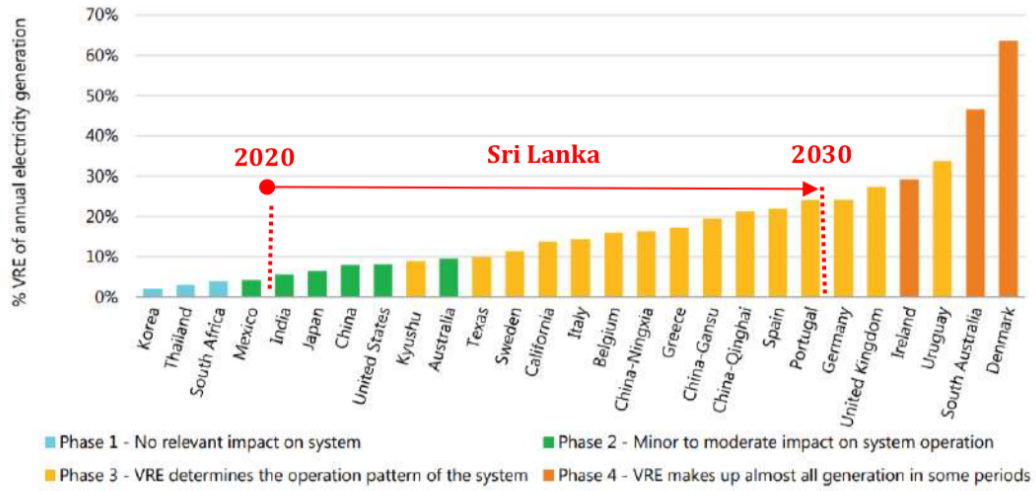
Chapter 2: Fundamentals components for a grid-connected PV system has been provided in this chapter to have a better understanding of the system. Additionally the FPV technology and the FPV plant in Kilinochchi has also been reviewed.

Chapter 3: Theory behind the control of power flow applied for the system is explained in this chapter.

Chapter 4: All four controllers designed for the system have been reviewed and the simulation

results has also been reviewed in this chapter.

Chapter 5: Conclusion of the report has been provided in this chapter. Additionally, a proposed further work has also been provided in this chapter.



Source: International Energy Agency

Figure 1.2: Impact from VRE sources in different stage [50]

Chapter 2

Overview on Grid-connected PV system

Essential components needed for a conventional grid-connected PV system is illustrated in Fig. 2.1. Similar topology applies for the FPV plant as well. Details about necessary components needed for a grid-connected operation are provided in this chapter to understand the function of the system. By the end of the chapter, a detailed explanation about FPV technology and the FPV plant in Kilinochchi will be presented.

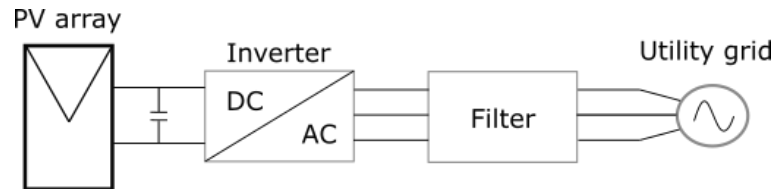


Figure 2.1: Grid connected, transformer-less PV system

2.1 Solar cell physics

2.1.1 Fundamental of solar cell

A brief explanation of the solar cell technology is provided here, with the purpose of understanding how the efficiency of a PV module in the system can be influenced. Physics of solar cell technology is similar to a diode with pn-junction. When the surface of a solar cell is being illuminated with solar irradiance, with sufficient photon energy the electrons can be lifted from valence band to conduction band. A potential gradient is now created in the junction region with increase of mobile electrons in the conduction band. The mobile electron will get accelerated due to applied electric field. The hole left by the excited electron will flow in the opposite way of electron. This motion of charges results in a current flow, I_{ph} through the external circuit [38].

The power generated from a single solar cell is around 1W. For application of large power production several solar cell must be combined in series and parallel for larger output. In Fig.2.2 the differences between a cell, module and an array are shown. Several cells connected in series forms a module with an output of 100-330Wp. For large-scale power applications (10-100kW), a single module won't be sufficient to produce the desired output value. Modules needs to be connected in a combination of series and parallel connection to meet the desired value. This arrangement of several modules is called an array [27].

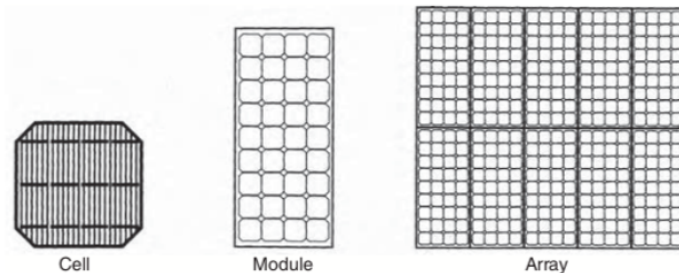


Figure 2.2: Differences between PV cell, module and array [27]

2.1.2 Equivalent circuit

An equivalent circuit for a single diode PV cell is depicted in Fig.2.3. The photon current I_{ph} generated from the current source is from solar illumination. In an ideal case the shunt resistance R_{sh} is equal to infinity and the series resistance R_s is equal to zero, meaning the resistance can be ignored in an ideal case. According to [4] in real case scenario, these resistance can't be ignored since they have an impact on the efficiency of the PV cell. According to [27] the values of R_s and R_{sh} in silicon varies between $0.05 - 0.10\Omega$ for R_s , while R_{sh} varies between $200 - 300\Omega$. I_D is the current through the diode, and I_{sh} is the current through the R_{sh} . I_{pv} is the output current of the PV cell. By applying Kirchhoff's current law, gives the following equations:

$$\begin{aligned}
 I_{pv} &= I_{ph} - I_D - I_{sh} \\
 I_{pv} &= I_{ph} - I_o \left[\exp\left(\frac{q(V_{pv} + I_{pv}R_s)}{AN_sKT}\right) - 1 \right] - \frac{V_{pv} + I_{pv}R_s}{R_{sh}}
 \end{aligned} \tag{2.1}$$

Where the I_o is the reverse saturation current of the diode, q is the electron charge ($1.602 \cdot 10^{-19}$ C), K is the Boltzmann constant ($1.38 \cdot 10^{-23}$ J/K), T is the cell temperature, A is the ideality factor which is a constant depended on PV cell technology, and N_s is the number of cells connected in series.

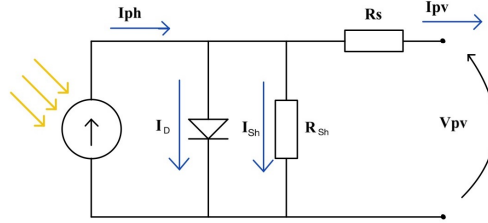


Figure 2.3: Equivalent circuit of single-diode solar cell

In [18] by Ramdani Youcef and Moulay Fatima gives a proper understanding on how the PV cell technology is dependent on the atmospheric conditions using equation (2.1). The output power of the modules is proven to increase or decrease based on variation of the irradiation and temperature. By studying the relationship between the current and voltage curve in Fig.2.4, it can be observed that the maximum point for the voltage and current changes when the irradiation and the cell temperature varies. The design of the PV array must consider the fundamental aspect of the PV technology and should be designed having the atmospheric condition as a factor to increase the system efficiency. In section 3.1 a more detailed explanation of the environmental influences for the system will be provided in designing a maximum power point tracking (MPPT) controller for the system.

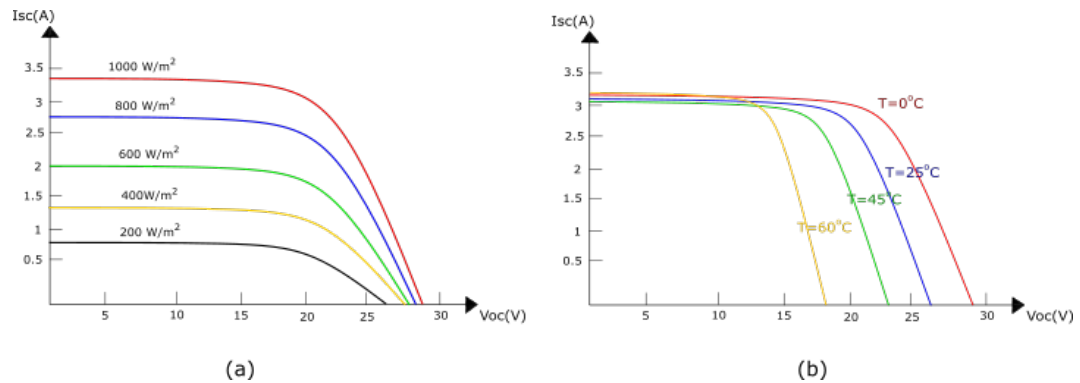


Figure 2.4: Caption

2.2 Requirement for grid-connected systems

Solar is an intermittent source and when interfaced to the utility grid it influences the operation of distributions systems dramatically. When designing the control for the grid connected PV system, international and national standards are needed to be considered to ensure safe and reliable operation. These guidelines typically accommodate the principle of power quality requirements, general technical requirements, power control, voltage regulation and measurements of action taken

for abnormal conditions. Design of the system must comply with these standards given by the utility company so that safety and protection of the grid connected PV system is guaranteed. There are several standards in place for governing the safety of distributed resources connected to the grid. Among them IEEE 1547 and IEC 61727 are the widely recognized standards in this field, where the IEEE 1547 standard addresses for the interconnected generation up to 10 MVA while the IEC 61727 addresses standards specifically for PV system connected to the grid with generation at 10 kVA or lower [36][55]. IEEE 929 is another standard developed for PV system providing guidelines concerning safety, power quality and operation of the utility system [55]. Additional to the international standards that were mentioned, national standards have also been considered in the design aspect for the grid connected PV system in Sri Lanka. SLS 1543 and SLS 1547 are the national standards for utility interface of PV system in Sri Lanka. SLS 1543 incorporates the (or is similar to) standard IEC 62109 which addressed the requirements for the converter used in PV systems, while the SLS 1547 incorporates standard IEC 61727:2004. [33][34]

	IEC 61727	IEEE 1547	IEEE 929
Harmonic currents (order-h)limits	(3-9)4% (11-15)2% (17-21)1.5% (23-33)0.6%	(< 11)4% (11-17)2% (17-23)1.5% (23-35)0.6% (>35)0.3%	(3-9)4% (11-15)2% (17-21)1.5% (23-33)0.6% (> 35)0.3%
DC current injection	Less than 1% of rated output current	Less than 0.5% of full rated output current	The PV system should not inject DC current > 0.5% of the rated inverter output current into the AC interface under either normal or abnormal operating conditions
Voltage range for normal operation	85-110% (196-253 V)		88-110% of nominal voltage. Inverter should abnormal and respond
Frequency range for normal operation	50 ± 1Hz		59.3-60.5 Hz

2.3 Power Processing Unit

A power processing unit (PPU) is an essential part for the grid connected PV system. The DC power generated from the PV array is processed and transformed to AC power using a PPU. Grid connected PV systems can be defined based on number of power stages in its system. In Fig.2.5, two conventional topologies are illustrated, where Fig.2.5a) is a single stage inverter, where the control

tasks for the system is being handled by an inverter. A two-stage inverter is proposed in Fig.2.5b) where there is a dc-dc converter connected between the PV array and the inverter. The dc-dc converter works as voltage regulator as either boost converter, buck converter or cuk converter [4]. Control complexity is reduced in two-stage topology as the control task can be divided between the dc-dc converter and the inverter. However, two-stage topology results in increased cost and decrease in efficiency compared to the single-stage system. Single-stage converter can be summarized as having good efficiency, minimized cost and simple implementation, but at the expense of increased complexity in its control scheme [2].

Tasks considering the PPU are the following:

MPPT control: In a PV system operation, the power produced from the solar arrays will vary with environmental changes. It is required from the system control to utilize the maximum possible power provided from the arrays at any given moment [39]. This is achieved using an MPPT control.

Control of injected voltage and current: Among the basic control expected from PV system. Either voltage or current generated from the inverter must be controlled to follow the same frequency as the grid parameter for proper synchronization. The control must also ensure enhanced power quality by ensuring harmonic contents in the current are within a certain limit.

Voltage regulation: DC-link voltage regulation control ensures the voltage from PV injected to the converter is at a constant value as this may vary because of the nature of the system.

Islanding detection and protection: In case of abnormal situation, the control of the system needs to detect the problem and disconnect from the grid as soon as possible to avoid further damages.

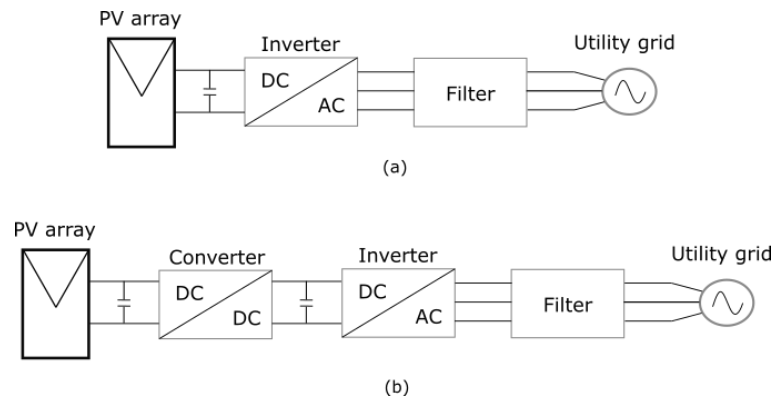


Figure 2.5: Structural topology of PV system a) single-stage inverter and b) two-stage inverter

2.3.1 Voltage source converter

The output of a grid-interfaced inverter can either be a single-phase or three-phase system. Depending of the power level application for the system, the output of the inverter is either single-phase or three-phase. Single-phase rectifiers are mostly employed for lower power circuits, while three-phase

are employed for medium- and high-power circuits [7]. Structure of a rectifier and an inverter are similar. The difference is depended on the operation and application of the system. As mentioned, the inverter transforms the dc power supplied from a dc source (PV array or a battery) and converts it into sinusoidal ac waveform. A rectifier's operation is the opposite of the inverter's. An ac load or utility grid is the source and supplies the rectifier. Purpose of the rectifier operation is to transform the ac waveform to dc waveform and supply a dc load[7]. Operation of four-quadrant operation is a basic concept which is required from the inverter [30]. When the instantaneous voltage and current are both positive, the power flow is also positive with a power flow direction from dc to ac. This is under the operational interval 1. In interval 3 is also an inverter operation as the two negative instantaneous current and voltage results in positive power flow. Interval 2 and 4 are when the current and voltage are opposite, at this moment the VSC is in rectifying mode. Generating reactive power either to ac or dc based on the phase angle of the current [30].

Inverters and rectifier have common structure where both consist of controllable semiconductor switches for its operation. MOSFET, IGBT or BJT switches can be used with a PWM scheme applied to regulate the duty ratio of the switches to attain the desired waveform. The switches can be replaced with diodes or thyristors, in that case a PWM scheme can not be applied to control the switches. Rather the voltage of the supply line will determine the turn-off sequence. These converters are classified as line-commutated converters while self-commutated converters can use PWM techniques. According to [andrzej m trzynadlowski notitle 2016] the voltage and current waveform generated from line-commutated waveforms are distorted and the total harmonic distortion (THD) from the rectifiers are high. While waveforms from self-commutated rectifier results in lower THD level. A PWM scheme improves the waveform but due to the switching it also increases the switching losses of the system. In section 3.5 a detailed explanation on how PWM scheme works and different techniques is presented.

2.3.2 Structural arrangement in PV system

For both single stage systems and two-stage systems, inverter and the PV modules can be arranged in different ways where different topologies will influence the efficiency of the system. Some of the available topologies have been reviewed below.

Centralized inverter: Topology of a centralized inverter is shown in Fig.2.6. Several modules are connected in series are called strings, doesn't require voltage amplification as the modules in string generates high voltage. These series connected modules are then connected in parallel with other strings to get maximum power output before connecting to a single inverter. This topology is a well-established one applied in the past. This topology is applicable for large PV system with high power output. Single inverter is only used makes the topology economical viable compared to the other. However, has disadvantage in power reliability having only one MPPT tracking the maximum power and power losses in the string diodes [2] [42].

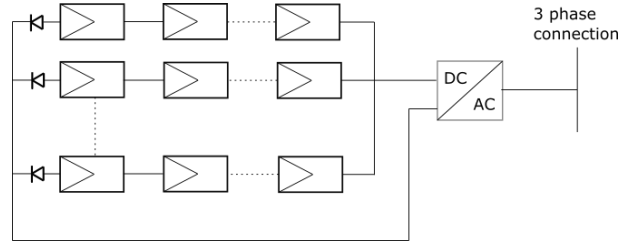


Figure 2.6: Centralized inverter topology

String inverter: Structural arrangement for the string inverter is illustrated in Fig.2.7, with similarity of the centralized inverter the modules are connected in series to amplify the input voltage to the inverter. According to [15] taking the European requirement defined, 16 modules are required to amplify the voltage to applicable or acceptable level. It is possible to apply this technology with less modules, in that case a transformer or a boost converter is needed for voltage amplification. The disadvantage seen from the centralized inverters with losses in string diodes is avoided here and each modules have its own MPPT tracker installed. The mismatch between the panels is also reduced but not eliminated. Overall efficiency compared to the centralized inverters are better in the string inverter topology. The flexibility of the design is increased as new strings can be added to increase system's power output. Economical aspect may be a disadvantage with this kind topology with increased inverter [41][2].

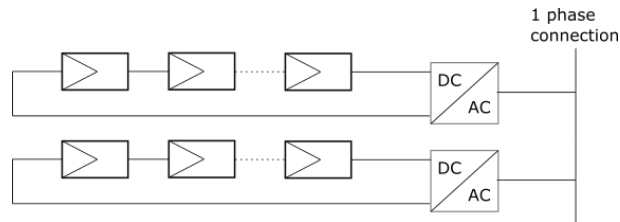


Figure 2.7: String inverter topology

Multistring inverter: Fig.2.8 shows the arrangement of the multistring inverter and presents more flexibility and higher efficiency compared to both centralized and string inverter. Between modules connected in strings and the inverter, dc-dc converters are connected here to track the MPP and for voltage amplification. This architecture benefits from the advantages of both previous topologies, using single inverter to lower the cost and separate MPP tracking enhances the efficiency. But compared to the string inverter, the reliability decreases and losses from the dc-dc converter will be added to the system as well [2][41][40].

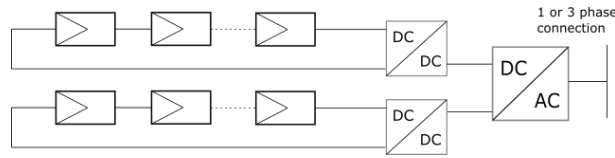


Figure 2.8: Caption

AC modules: Topology for the AC module is illustrated in Fig.2.9, it is a simple topology with one module connected to an inverter. Since there is only one module, losses due to partial shading is reduced and overall better efficiency is achieved with this topology. However, the AC modules is only applicable for low power applications, using several inverters will increase the cost of the system [2].

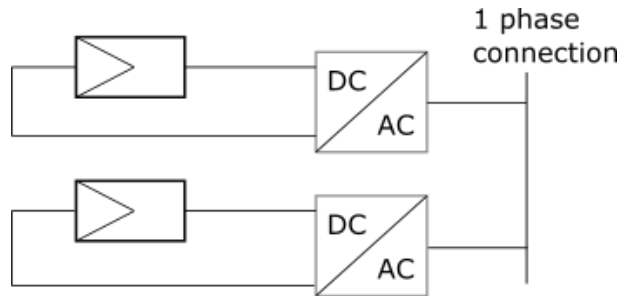


Figure 2.9: Caption

2.4 Transformer

In conventional structure of a PV system, transformer is usually embedded with object of increasing the voltage ratio and to ensure proper grounding or galvanic isolation between the PV module and the grid. The transformer can be embedded as low frequency transformer on the grid side suppressing the dc component. However, this arrangement decreases systems overall efficiency and increases the size and cost of the system. An alternative is inserting high-frequency transformer in front stage of the PV, but this topology gives a complex power processing unit without any improvement in its efficiency [48] [26][19].

Without a proper grounding, leakage current may follow through, increasing system losses, current harmonics, and lead to safety hazards. Therefore, in some standards there are required proper grounding of the system and required to monitor the faults. Permissible inject dc current to grid is also given in standards which varies between 0.5% and 1% of the rated current (section x.x standards). While other standards require groundings of the equipment's in absence of galvanic isolation [48].

Having a transformer in the PV system affects system's overall efficiency and cost, while 20 kW transformer-less PV inverter reported in [48] was able to attain 99% efficiency. Compared to

a conventional system with transformer embedded, the transformer was accounted for 49% of the system losses. A transformer-less PV system will be a better option for a PV system, with increased efficiency and lower cost. But proper techniques need to be studied and applied for transformer-less system to minimize the leakage current and to improve the power quality. In [48], improved PWM scheme, different inverter topologies and common mode filters are proposed as methods to reduce the leakage current. Similar methods are mentioned in [26] as well.

2.5 Harmonics and Filter

Object of the inverter is to generate a waveform as close to pure sinusoidal as possible. By using non-linear loads, such as power converters, power sources and uninterruptible power supply (UPS), the output waveform will be superimposed of waveform with fundamental frequency with other waveform consisting of harmonic frequencies. The amplitude of the superimposed waveform will also be modified. With increase in use of the non-linear loads, harmonics are a part of the system that needs to be addressed during the design process. Harmonics distortion on the output waveform needs to be attenuated since it causes detrimental effects on the electronic components influencing the power quality. As defined in equation (2.2), harmonics in voltage and current waveform is of a frequency equal to an integer, given as h , multiplied with the fundamental frequency f_1 .

$$f_h = h \cdot f_1 \quad (2.2)$$

Frequencies can be given as f_1 (the fundamental), f_2 , f_3 , f_4 , f_5 , and so forth. The harmonics that needs to be attenuated or filtered are the odd harmonics while the even harmonics gets cancelled due to its symmetry. Fig.2.10 shows the sinusoidal waveform of a distorted current containing 3rd, 5th and 7th harmonic. observing the waveform it can be seen that the amplitude is also affected and have been adjusted in its total value. Each waveform portrayed in the figure can be defined with following equations:

$$I_1 = Im_1 \sin(\omega t) \quad (2.3)$$

$$I_3 = Im_3 \sin(\omega t - \delta_3) \quad (2.4)$$

$$I_5 = Im_5 \sin(\omega t - \delta_5) \quad (2.5)$$

$$I_7 = Im_7 \sin(\omega t - \delta_7) \quad (2.6)$$

Where the peak amplitude is defined as Im_h for the given harmonic current h . The distorted current waveform is the sum of equation from (2.2) to (2.5).

$$I_{total} = I_1 + I_3 + I_5 + I_7 \quad (2.7)$$

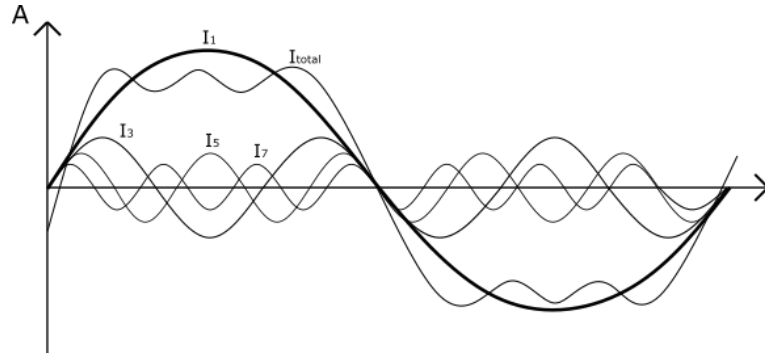


Figure 2.10: Distorted sinusoidal waveform with 3rd, 5th and 7th harmonics

To suppress the harmonic generated from inverter and avoiding injecting it to the grid, a filter is connected in between to achieve low current distortion. As illustrated in Fig.2.11 three possible filter topologies are presented where the simplest one consist of an inductor.

2.5.1 L-filter

The topology of a L-filter is shown Fig.2.11a) and it consist of an inductor connected in between the VSC and the load or grid to eliminate the harmonics. L-filter is a first order filter with attenuation of 20 dB/decade and is suitable for converter operation with high switching frequency. For a better attenuation of the harmonics, a larger filter will be required that may be bulky and more expensive. Due to this disadvantage and the voltage drop on the inductance causing poor system dynamics, L-filter wont be the right choice for the grid-connected system [22].

2.5.2 LC-filter

Another filter that presents better damping option than the L-filter is the second order filter, LC-filter (Fig.2.11b)). With inductor in series and capacitor connected in parallel, the value of the inductor can be decreased meaning the cost and size of the filter can also be decreased. This filter presents a 12 db/decade attenuation after the cut-off frequency f_0 , and has resonance frequency as well at f_0 . A resistor can be added to the circuit in either parallel or series to damp the frequency near the cut-off frequency. Disadvantage of the LC-filter is the dependency of the resonant frequency with the grid impedance [17].

2.5.3 LCL-filter

Compared to the two former filter topologies, the LCL filter emerges as a favour among them since it reduces the disadvantages caused from the the L- and LC-filter. A cheaper and filter with better attenuation is achieved with LCL-filter.

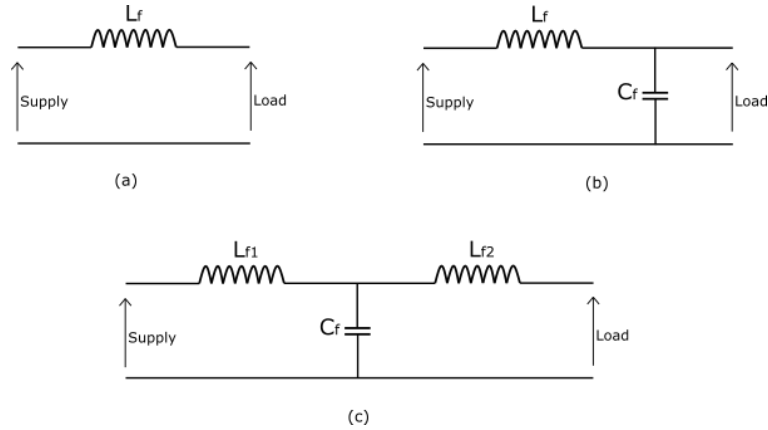


Figure 2.11: Filter topologies: a) L-filter, b) LC-filter and c) LCL-filter

2.5.4 LC-Filter design

The grid connected PV system that has been simulated in this study, uses an LC-filter to attenuate the harmonics. Ripple current $\Delta i_{L,max}$ is usually chosen between a value of 10-25% of the rated current. High value of the ripple current may increase switching losses and conduction losses, thereby low ripple current value is desired. However, large inductor result in larger coil and core losses. Thereby a trade between the size and the switching losses must be considered. Equation (2.8) is used find the maximum current ripple and can also be used to find the filter inductor L_f [3]:

$$\Delta i_{L,max} = \frac{1}{8} \cdot \frac{V_{DC}}{L_f \cdot f_{sw}} = 10\% i_{rated} \quad (2.8)$$

Following equation (2.9) is used to find the appropriate filter capacitance which is a trade-off between reactive power from the capacitor at fundamental frequency and the coil inductance.

$$C_f = 10\% \frac{P_{rated}}{3 \cdot 2\pi f \cdot V_{rated}^2} \quad (2.9)$$

Value of the capacitance must be chosen to an appropriate value. Since large capacitance means more reactive power will flow through the capacitor and will increase the current demand. This result in decreased efficiency. The capacitance can not be too low value either as a larger inductance would be required to attenuate the harmonics. For the LC filter designed in this system, the reactive power is considered to be 10% of the rated power [3].

2.6 Floating Solar Plant

Principle behind the power production for a floating PV system is similar to a conventional PV system. The only difference is the placement of the installation. Conventional solar design is usually known as panels installed on solid ground as its foundation. PV modules can also be installed on the surface of any water body, like pond, reservoir, or dam to harness the solar energy. These types of designs are known as floating PV (FPV) plant. It is an innovative way to harness the abundant

source and is gaining popularity around the world for its potential and the advantages apart from power production [21]. The grid-connected design simulated and presented for this thesis uses the FPV plant in Sri Lanka as its base model.

From the contingency plan established by CEB seen in first chapter [50], government are looking to utilize the abundant resource of solar for large scale production. Harnessing solar energy for power production will aid in meeting their energy demand with cleaner resources. Disadvantage with the conventional land-based solar plant is the land requirement and can act as a barrier for further development of a PV plant. Expansion project developing from small-scale to large-scale will require more land area to install the PV modules. Pakistan and India have had similar issue and solved it by implementing FPV plant in their available dam or pond [20][8]. Including solving the issues with land limitation, FPV benefits also in reducing the water evaporation of the water body it is installed on. Additionally, having panels mounted on water decreases the algae production in water due to shading of the water surface which results in less contaminated water enhancing the aquatic life. According to [8] it is proven that the efficiency from FPV plant is 10% better than the conventional land-based PV system due to the cooling effect provided by the surface water. Higher cell temperature will impact the efficiency of solar cell, as seen from I-V characteristics in section 2.1. The surface water enables a cooling effect that enhances plant's efficiency. Shading of a PV module will also affect the efficiency which is reduced when the module is installed on water surfaces area where there is less tree to block or cause shade on the panels. Fewer incidents of dust occurring on the panels will also be reduced for a FPV. Besides the improvements in the generation efficiency, compared to the conventional land-based PV system, FPV also benefit in economical aspect. Cost of land area for PV installation is reduced significantly and as mentioned in [8] electricity generated from land-based cost USD 0.05/kWh while electricity generated from FPV will cost USD 0.026/kWh which is 48% less.

China, Singapore, United states, and Japan are some countries to be mentioned that have added FPV installation with China leading the list with an installed capacity of 376,50 MW [21]. Hybrid approach has been suggested in [20][6][21], where the FPV plant is installed on a reservoir combining with hydropower technology. Study in [20] exercises the hybrid solution on Ghazi Barotha dam, which benefits for both FPV technology and hydropower technology. FPV installed on reservoir benefits in grid connectivity with all the necessary components (transformers, transmission lines, etc.) are in accessible distance. Additionally, hydropower may also act as a battery solving the intermittence characteristic of solar. Water evaporation is decreased with FPV plant installed on the reservoir, which benefits the hydropower technology.

Currently, Sri Lanka has only one FPV plant and this number may increase in near future. According to CEB's report, potential areas and sites have been located for large-scale grid interfaced FPV projects [50]. A detailed explanation of the FPV plant and its necessary components are given in section 2.6.1, then leading up to section 2.6.2 which will explain in detail about the FPV plant in Sri Lanka.

2.6.1 Structure of floating PV plant

Fig.2.12 illustrates the necessary components needed for a FPV plant technology, which consist of:

1. Floating system: The floating system represents the part or the body where the PV modules

rest on. Important that these structures have a buoyancy while having the capacity to withstand the weight of the panels.

2. Mooring system: Mooring system works as an anchor for the FSPV, keeping the structure steady as possible under incidents of wave propagation.
3. PV system: Devices needed for power generation are installed on top of the floating system, PV modules, junction box, MPPT etc.
4. Cables and connectors: The generated power from the solar array is transported to the substation by use of cables. The cables are specially designed for the use in FSPV, to endure high temperature and are designed to be robust.

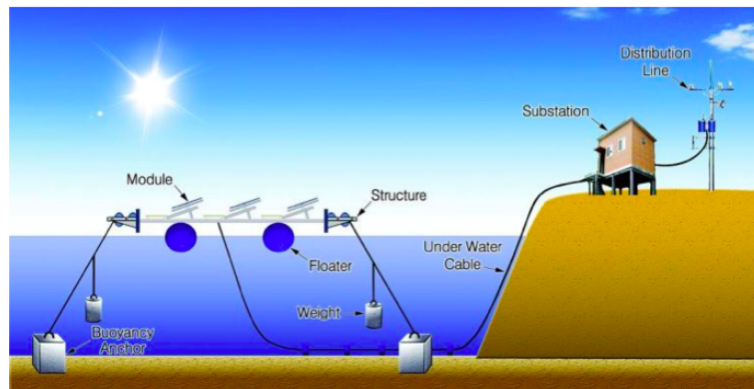


Figure 2.12: Structure of floating solar plant

It is essential that the PV modules are installed on a desired tilt angle to harness the optimal power as possible from the solar irradiance. This applies for all type of solar technologies and applies for the FPV as well. The design of FPV structure must be designed based on the angle. Study in [13] shows research on FPV plants in India, and according to this research the structural design for the FPV technology can be characterized as either PV module tracking based, or based on the floating system used. Fig.2.13 illustrates the differences, and the PV module tracking based system can be classified further in two parts; as fixed-type -and tracking-type floating PV.

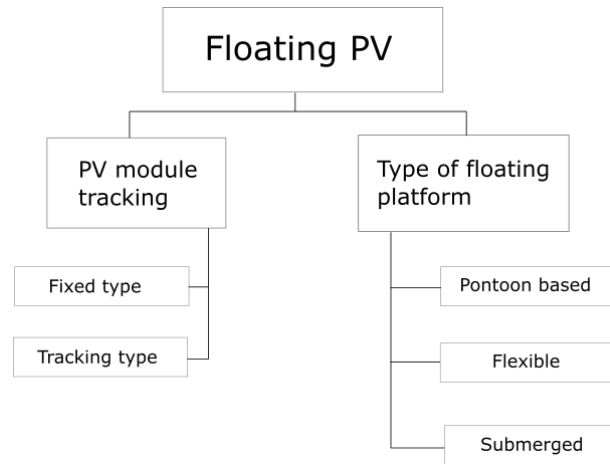


Figure 2.13: Floating solar plant classification[54]

A **fixed-type** is presented in Fig.2.14 and as the name suggest the panels in fixed-type are tilted in a certain angle and mooring system is adjusted to keep fixed in place with less movement. For this type the weight of modules can be reduced, which makes it a convenient structure to design.



Figure 2.14: Fixed-type system[13]

The construction for the **tracking-type** is more complex compared to fixed-type since by using an algorithm, the solar panels are rotated towards the optimal sun radiation at a given time of day. One may argue for increased cost for a complex structure but pays off in efficiency. In [13] it is stated that a Floating Tracking Cooling Concentrator has 60-70% higher efficiency over a fixed-type. Fig.2.15 presents a tracking-type FPV system.



Figure 2.15: Tracking type[13]

The second classification is based on the floating system, here the **pontoon Based floating system** are made from medium density polyethylene (MDPE) and is designed to have a buoyancy while withstanding the weight of PV modules. It is a simple structure that can only hold a certain number of panels and is not made to endure severe environmental conditions. An example of the pontoon based FPV is shown in Fig.2.16

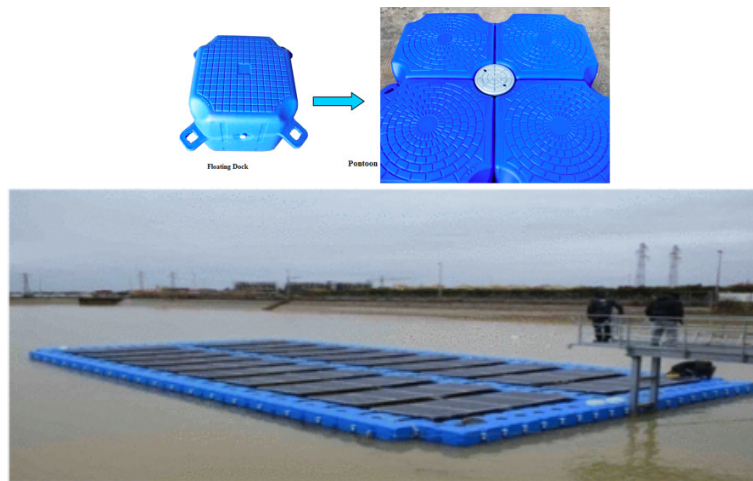


Figure 2.16: Pontoon based FPV[13]

Figure2.17 shows a picture of a thin film **flexible floating PV system**. Purpose behind this design is to be able to interact with the surface of the water without having any remarkable impact on the electrical performance. As a results, due to the cooling effect from the water a 5% efficiency gain is seen compared to land-based PV [13].



Figure 2.17: Flexible type[13]

Submerged floating system is shown in Figure 2.7 for PV installment in shallow water. By submerging the PV in water in depth, according to the [13][47] a modification of solar radiation spectrum and decrease of temperature is reported which has an impact on module's energy performance.

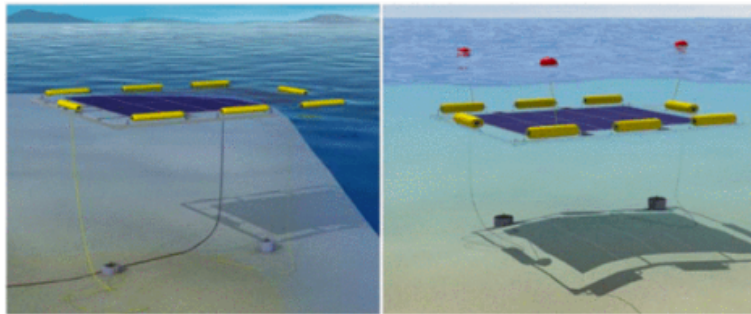


Figure 2.18: Submerged Floating PV[13]

2.6.2 Floating Solar Plant in Kilinochi

In Kilinochchi Ariviyal Nagar at the campus of University of Jaffna, a FPV plant is installed here with a capacity of 42.5 kW in year 2020. The FPV plant presented here is a pilot project established by the research group ANCEHA, Current Solar and the University of Jaffna. With the help from the Norwegian government, Sri Lanka's first ever FPV plant was realized and marks as a revolutionary step for the country.

The floating solar plant is placed on a pond inside the premises of the campus. An ariel view of the pond is provided in Fig.2.19 and picture of the plant is provided in Fig.2.20. As it can be seen from Fig.2.20, the PV modules are fixed on a certain angle, positioned in the middle of the pond. PV modules are fixed properly on a white beam structure. According to Current Solar (provider of the PV modules and the floating structure), the material is made from glass fiber and resin which are of same materials used for boat production. Several pipes of high-density polyethylene (HDPE) are applied under the beams to make the structure float on the water. Ropes are used to tie the end of the structure on trees nearby to secure the plant is anchored properly. Among the different

available characterization for a FPV plant, the FPV plant in Kilinochchi can be categorized as system based on tracking with fixed angle.



Figure 2.19: Aerial view of the pond and the FPV plant



Figure 2.20: Floating PV plant in Kilinochchi

Fig.2.21 shows the installation set up of the PV array at the FPV plant in Kilinochchi. In total there are 144 panels installed with half of them consisting of 295 Wp Twin Peak while the

other half consists of 320 Wp N-peak. As mentioned above, the panels are fixed in a certain angle, connected in a triangle shape where half of the PV modules facing east while the other half facing west. 18 Twin peak modules facing west connected in string, are connected in parallel with 18 other Twin peak modules facing the same direction. The 36 modules make up to be an array. Should be noted that the Twin peak modules are only connected to Twin peak modules to avoid power mismatch. This is then connected to one of six available MPPT ports in the SUNNY TRI POWER CORE1 inverter from the SMA company. In a similar manner, an array is formed from N-peak modules facing west and is connected to an available MPPT port in the inverter. Connection for the remaining modules facing east is done in same way. Data sheet for the inverter is provided in Appendix, in Table 2.1 a summarized table of the parameters are given.

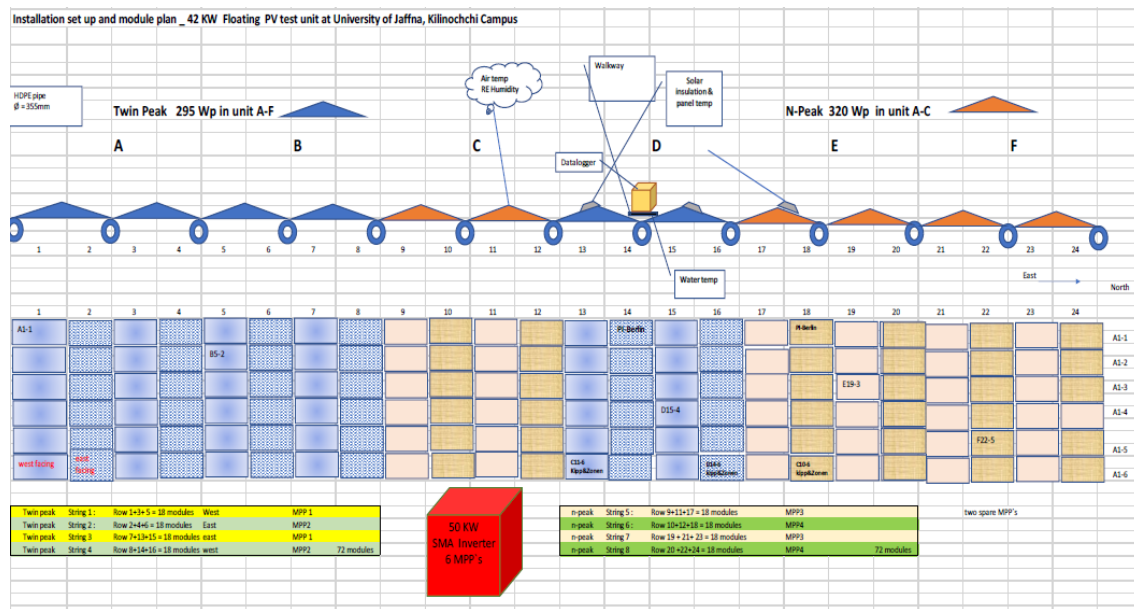


Figure 2.21: Overview of the PV module installation

The structural arrangement of array's connection to the inverter can remind of a combination between the structure of a centralized inverter and a multistring inverter. A single inverter is used, with 36 modules formed as an array connected to one of the MPP tracker port on the inverter. Four out of the six available ports are currently in use for the FPV plant while the fifth one is connected to ground based 2.5 kW reference PV plant. Approximately, 45 kW is produced and supplied to the utility grid ($230V_{rms}$, 50 Hz). Location of the SMA inverter is in close proximity of the FPV plant. A small storage room encircled in red in Fig.2.19 shows its location. Cables from the FPV are water resistance and are connected to the inverter through underground connection. Figure y.1 shows the grounding for the FPV plant and the junction box for connection to the MPPT ports.

With the information provided by the University of Jaffna, a curve of environmental data from the site is shown in Fig.2.22. This curve shows the irradiation and temperature values for 24 hours

Parameters	Values
$V_{dc.rated}$	670V
P_{rated}	50 kW
Apparent power S	50 kVA
AC nominal voltage, V_{RMS}/V_{ll}	230V/400V
AC grid frequency, f_g	50 Hz
Rated output current, I_{rated}	72.5A
PF	1
THD	< 3%
Max efficiency, η_{max}	98%

Table 2.1: SUNNY TRI POWER CORE1 inverter parameters

in May which is the warmest month. Peak power production from the FPV plant will be when the irradiation is at its highest point. In Fig.2.22 this is approximately at noon, 12 pm. Lowest production of the power is shown to be when the sun sets which is after 5 am. Average ambient temperature on the site can be seen to be around 30°C.

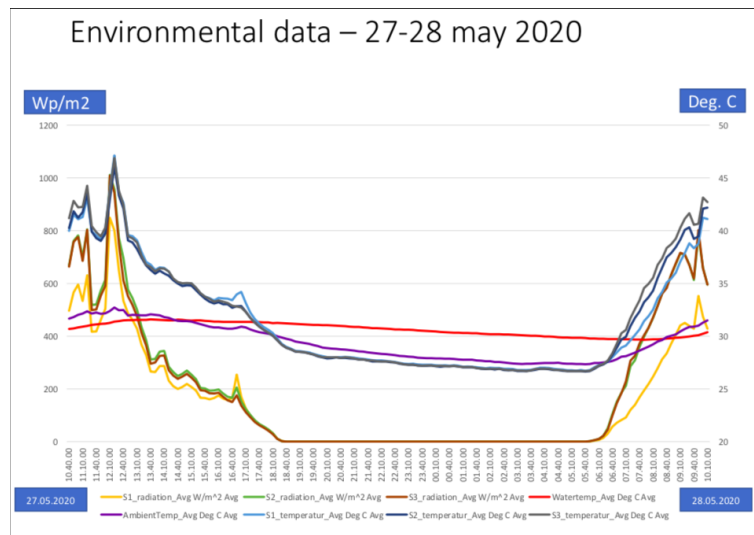


Figure 2.22: Environmental data of the site from 27th to 28th of May 2020

Chapter 3

Control of Grid-connected PV system

A brief overview of the necessary component blocks for a PV system was introduced in the previous chapter. In this chapter the control aspect for a grid-connected PV system will be reviewed. A PV system can be categorized as either a grid connected system or as a stand-alone system based on their application and configuration.

The FPV plant in Kilinochchi is a grid-connected system, where the power generated from the PV is supplied to the utility grid. Arrangement of implementing an alternate energy storage device to the grid-connected application is increasing. Benefit from this configuration is that the power from the PV can charge the energy storage devices at time when the demand for power is low. Other advantages are energy storage device can get access to power from the grid at times when the PV or battery is not available, or sell the excess energy produced during peak hours. A general issue with PV technology is solar's nature of intermittency, with an energy storage to the configuration, a flexibility to the power management is achieved where the peak load demand can be met by the power charged in the energy storage device.

Configuration of the stand-alone PV system is similar to the grid-connected systems, but instead of a utility grid, the PV system supplies an AC or DC load. The stand-alone application is suitable for operations in meeting the low power demand in rural areas and can be applied in a hybrid application.

In both cases, an inverter or referred as dc/ac converter is a key element in its operation to supply the power to the grid or load. Further in this paper, control of a single-stage grid-connected inverter will be focused on in detail as a similar inverter is used for the FPV system in Kilinochchi. The object is to design a controller that enhances the efficiency and the power quality of the grid-connected system by optimal control of the active (P) and reactive (Q) power flow. This is the main task for the controller. The main object of the controller can be subdivided in following tasks:

- Maximum power point tracker (MPPT) control
- DC-link voltage control

- Grid synchronization
- Reference current and voltage generation
- Voltage and current control

3.1 MPPT

In section 2.1 the impact from variation in environmental conditions on the output power from the PV array was shown. A maximum power point tracker (MPPT) technique is applied to realize the maximum efficiency of a PV array. The I-V characterization has a non-linear relationship that changes with the atmospheric condition (irradiance and temperature). From sunrise to sunset, numerous curves can be depicted. An MPPT algorithm is applied to track the maximum power point for voltage and current, V_{MPP} and I_{MPP} . This way, the optimal production of the array can be realized despite the environmental changes. A P-V, or I-V curve is shown in fig. 3.x which shows the relationship between the parameters for an array at given temperature and irradiance. Peak of the curve is marked as P_{MPP} , V_{MPP} and I_{MPP} as this point is the MPPT control must track. As suggested in [4][51] there are several methods available track the MPPT. Key factor for all of them are to track the MPP to realize optimal production for the system. Different techniques vary in terms of complexity, number variables used for control, convergence speed, cost of hardware and technique's popularity. Suitable method is also decided based on these terms.

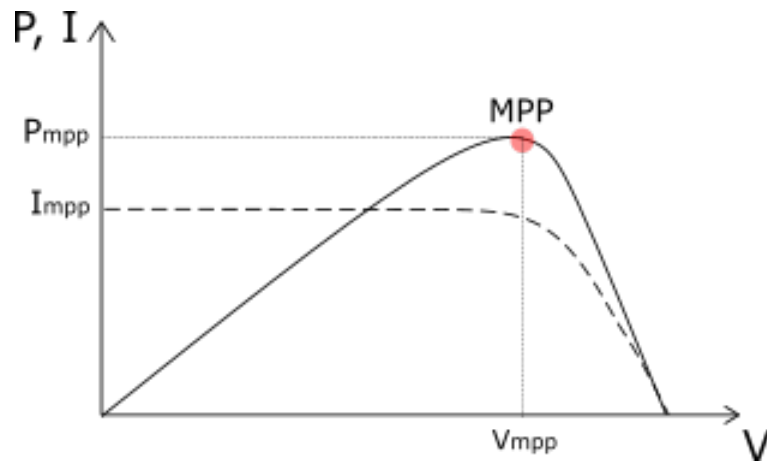


Figure 3.1: P-V and I-V curve of for an array

MPPT methods can be divided as either mechanical tracking or electrical tracking [4]. In mechanical tracking the arrays are adjusted to the sun's movement over time to catch the peak irradiation of the sun. In electrical tracking otherwise, an algorithm is applied. In [43] the different methods in MPPT are separated as either direct or indirect methods. Indirect methods are based on estimating a MPPT value with given data, as a result an approximated value is given for MPP. However, the direct method gives a better reliability. Voltage and current of the PV is used here. By

perturbing the operation point, it will be moved closer to appropriate point eventually. Advantages of the electrical tracking and the direct method is that it would not be dependent on changes of irradiance and temperature [4][43].

Among the available methods, perturb and observe (P&O), incremental conductance (INC) and the constant voltage has been reviewed in this paper.

Constant voltage:

The constant voltage method is an indirect method where the ratio between the voltage at MPP and open circuit voltage is used to decide to track the MPP. According to [43][39], the operating voltage must be a value of a ratio between 0.73- 0.8 which changes to the environmental conditions.

P&O method:

This method is an example of the indirect method and is one of the favored methods among MPPT techniques because of its simple implementation. The operation point tracks the MPP based on increase or decrease in power. If $\frac{dP}{dV} > 0$ then the algorithm perturbs the operating point to move towards the positive direction, which means it moving towards the MPP. The opposite is true if $\frac{dP}{dV} < 0$, then the operating point is moving away from, and the algorithm needs to reverse the operating point [51][39][43]. Disadvantage of the P&O is the oscillation that being created around the MPP point. A flowchart of the method is provided in Fig.3.2

INC method:

The INC method is another example on direct method and uses the slope of the PV array power curve to move the operating point closer to MPP. Value of the slope informs if the operating point is at left side of MPP, on the right side of MPP or at the desired MPP. This can be summarized from (3.1) [39][40]. A flowchart of the method is presented in Fig.3.3. Advantage of the method is a fast tracking can be achieved with this method with large increment. Has a similar disadvantage to the P&O method, where precise MPP might not be detected and an oscillation around the MPP can be experienced due to this [51]. From equation (3.2) the tracking of the MPP can be defined as shown in (3.3) instead. By comparing the measured value I/V with the incremental conductance dI/dV .

$$\begin{cases} dP/dV = 0, & \text{at MPP} \\ dP/dV > 0, & \text{left side of MPP} \\ dP/dV < 0, & \text{right side of MPP} \end{cases} \quad (3.1)$$

Since $P=IV$, this equation can be rewritten as:

$$\frac{dP}{dV} = \frac{d(IV)}{dV} = I + V \frac{dI}{dV} \quad (3.2)$$

From equation (3.2) the tracking of the MPP can be defined as shown in (3.3) instead. By comparing the measured value I/V with the incremental conductance dI/dV . A flowchart of the method is presented in Fig.3.3. Advantage of the method is a fast tracking can be achieved with this method with large increment. Has a similar disadvantage to the *P&O* method, where precise MPP might

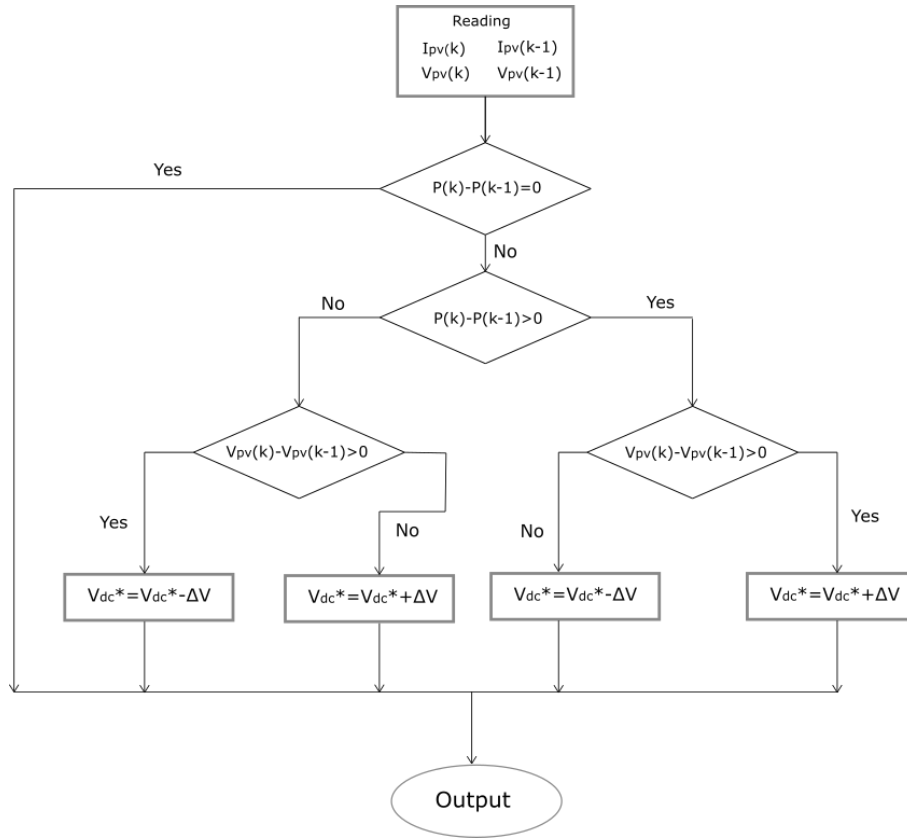


Figure 3.2: Flowchart for the P&O method

not be detected and an oscillation around the MPP can be experienced due to this [51].

$$\begin{cases} dI/dV = -I/V, \text{ at MPP} \\ dI/dV > -I/V, \text{ left side of MPP} \\ dI/dV < -I/V, \text{ right side of MPP} \end{cases} \quad (3.3)$$

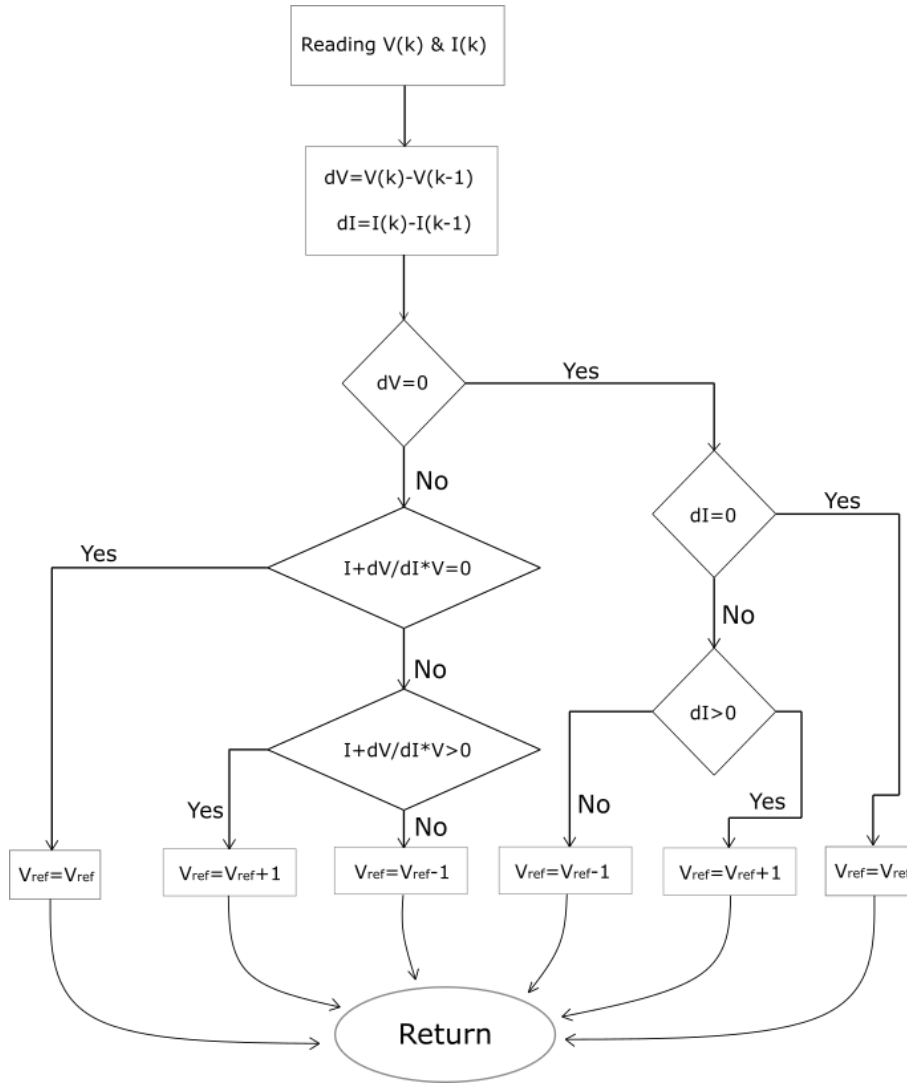


Figure 3.3: Flowchart for the INC method

3.2 DC-link voltage control

Voltage from the PV module is injected to the inverter with oscillation and ripple. This endangers system's power quality by not operating at the maximum power point (MPP) and decreases inverters lifetime as well. The oscillation needs to be reduced to achieve a stable operation, ensuring the dc-link voltage is constant. This can be done by applying a large dc-link capacitor to attenuate the ripples but this is not favored. The reason is increased cost and size of the capacitor makes the inverter less compact and less reliable. Therefore, the design of the dc-link capacitor and control of the dc-link voltage is a vital control part for the grid-connected operation of the single stage inverter.

In Fig.3.4 is illustrated how the dc-link capacitor is connected for a single-stage topology, where the inverter implements the MPPT control, therefore the dc-link capacitor is connected between the PV array and the inverter. As for the two-stage topology which has a dc-dc converter to handle the MPPT, the dc-link capacitor is connected between the dc-dc converter and inverter, while a boost capacitor is connected between the PV array and dc-dc converter [28]. Fig.3.4 illustrates how the power produced from array flows through the capacitor, P_{pv} is the power from PV, P_c is the power flow to the dc-link capacitor and P_{inv} is the power injected to inverter. Different studies are available explaining how the control of the dc-link voltage is implemented [56][16][25][52], where for example in [52] the dc-link voltage is controlled by regulating the amplitude of the injected ac current. In this study equation (3.4) was provided, revealing the relationship between P_{out} which is the injected power to the inverter and the dc-link capacitor C_{dc} . High power injected to the inverter, will result in decrease of the dc-link capacitor and increase of the Vdc ripple.

$$\Delta V_{dc.rip} = \frac{P_{out}}{\omega C_{dc} V_{dc}} \quad (3.4)$$

For the dc-link voltage control presented in [25], the controller for the single phase grid connected converter focuses on three points for its design which is 1) measured voltage must track the reference voltage with zero steady state error, 2) active power injected to VSC wont be stable, when this occurs, the ripple must be minimized, and 3) ac current must not present any harmonic content. Other studies [56] [16][52] and [24] have the same object with different methods to control the dc-link voltage. The control of the dc-link voltage for this study is controlled by applying the frequently used method by applying a PI controller with constant PI gains.

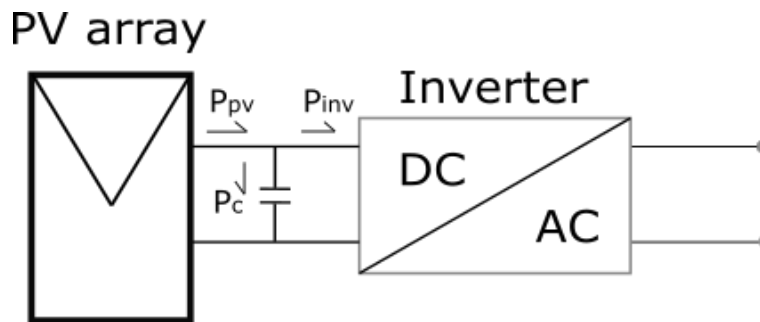


Figure 3.4: DC-link capacitor

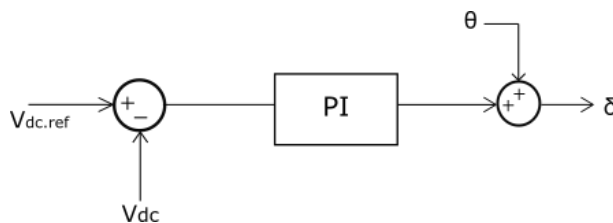


Figure 3.5: Control block for DC-link voltage control

3.3 Proportional and integral controller

Proportional and integral controller are commonly used in control algorithm. PI controllers are essential when parameters are transformed from natural frame (abc) or from stationary ($\alpha\beta$) to synchronous frame (dq). PI compensators are applied to reduce the error between signals to zero. PI controller can be defined as

$$H_{pi}(s) = K_p \frac{1 + T_i s}{T_i s} \quad (3.5)$$

With a transfer function for a system the process can be controlled. PI controller used for the proposed controllers in this study is based on "Trial and error" method.

In most of the controllers applied are transformer from natural frame to synchronous frame to enable easier control option with two phase instead of three phase.

3.4 Power control

To be able to inject power to the utility grid, the voltage supplied from inverter must be larger than the grid voltage V_s . If not the power flow will be in the opposite way. For the simplicity, a steady state condition has been considered for the system meaning the power loss has been neglected while in reality this must be considered. As for this case, the input power is equal to output power (supplied to grid).

3.4.1 Clarke's & Park's Transformation

Clark and Park transformation are two approaches applied in the three-phase power system analysis applied to control the three phase variables in two phases instead, decreasing the complexity of the control. A brief explanation of the Clark and Park transformation are introduced.

In Fig.3.6a) and Fig.3.6b), v_a , v_b and v_c are instantaneous balanced three phase voltages given as:

$$v_a + v_b + v_c = 0 \quad (3.6)$$

In terms of the three phase voltages v_{abc} , a voltage space vector is defined \vec{v} in fig.3.6a). The voltage space vector \vec{v} , can be defined in real and imaginary axes, which is called the $\alpha\beta$ -frame shown in Fig.3.6c) and in Fig.3.6d). This transformation is called the Clark's transformation, and the corresponding matrix for this transformation is gives as [46]:

$$\begin{bmatrix} v_\alpha \\ v_\beta \end{bmatrix} = T_c \times \begin{bmatrix} v_a \\ v_b \\ v_c \end{bmatrix} \quad (3.7)$$

Where T_c is the matrix used to realize the transformation, defined as:

$$T_c = k \times \begin{bmatrix} 1 & -\frac{1}{2} & -\frac{1}{2} \\ 0 & \frac{\sqrt{3}}{2} & -\frac{\sqrt{3}}{2} \end{bmatrix} \quad (3.8)$$

The value of k is a transformation constant and can either be chosen to of 2/3 (amplitude invariant) or $\sqrt{2/3}$ (power invariant) [12]. It is based on the application, by applying the k-value for amplitude invariant, then the amplitude will stay as a constant while the power changes. However, the opposite is true when k-value is chosen to be power invariant. In the Clark 's transformation (3.8) $k = \frac{2}{3}$ as recommended in [46].

$$\begin{bmatrix} V_\alpha \\ V_\beta \\ 0 \end{bmatrix} = \frac{2}{3} \times \begin{bmatrix} 1 & -\frac{1}{2} & -\frac{1}{2} \\ 0 & \frac{\sqrt{3}}{2} & -\frac{\sqrt{3}}{2} \\ \frac{1}{2} & \frac{1}{2} & \frac{1}{2} \end{bmatrix} \times \begin{bmatrix} V_a \\ V_b \\ V_c \end{bmatrix} \quad (3.9)$$

The before mentioned equations are vectors defined in two phase that varies with time. The Park's transformation which is also known as dq0 transformation enables the vector to become independent of the time in synchronous frame and the following equation for transformation from $\alpha\beta$ -frame to dq-frame is shown:

$$\begin{bmatrix} V_d \\ V_q \\ 0 \end{bmatrix} = T_p V_{\alpha\beta 0} \times \begin{bmatrix} \text{Cos}\theta & \text{Sin}\theta & 0 \\ \text{Sin}\theta & \text{Cos}\theta & 0 \\ 0 & 0 & 1 \end{bmatrix} \quad (3.10)$$

Here is T_p the transformation matrix required to realize the Park transformation. With this equation the AC waveform can be controlled as DC quantity enabling the control to become much simpler than it was to begin with. Transformation from abc-frame to dq-frame can also be done in a direct manner by using the matrix T. The equation for this is defined below:

$$\begin{bmatrix} V_d \\ V_q \\ 0 \end{bmatrix} = T \times \begin{bmatrix} V_a \\ V_b \\ V_c \end{bmatrix} \quad (3.11)$$

$$T = \frac{2}{3} \begin{bmatrix} \text{Cos}\theta & \text{Cos}(\theta - \frac{2\pi}{3}) & \text{Cos}(\theta + \frac{2\pi}{3}) \\ \text{Sin}\theta & \text{Sin}(\theta - \frac{2\pi}{3}) & \text{Sin}(\theta + \frac{2\pi}{3}) \\ \frac{1}{2} & \frac{1}{2} & \frac{1}{2} \end{bmatrix} \quad (3.12)$$

Matrix T is product of the matrices T_c and T_p . A transformation from the synchronous reference frame (dq) back to natural frame is also necessary, this is called an inverse Park transformation:

$$T^{-1} = \frac{2}{3} \begin{bmatrix} \text{Cos}\theta & \text{Sin}\theta & \frac{1}{2} \\ \text{Cos}(\theta - \frac{2\pi}{3}) & \text{Sin}(\theta - \frac{2\pi}{3}) & \frac{1}{2} \\ \text{Cos}(\theta + \frac{2\pi}{3}) & \text{Sin}(\theta + \frac{2\pi}{3}) & \frac{1}{2} \end{bmatrix} \quad (3.13)$$

$$\begin{bmatrix} V_a \\ V_b \\ V_c \end{bmatrix} = T^{-1} \begin{bmatrix} V_d \\ V_q \\ 0 \end{bmatrix} \quad (3.14)$$

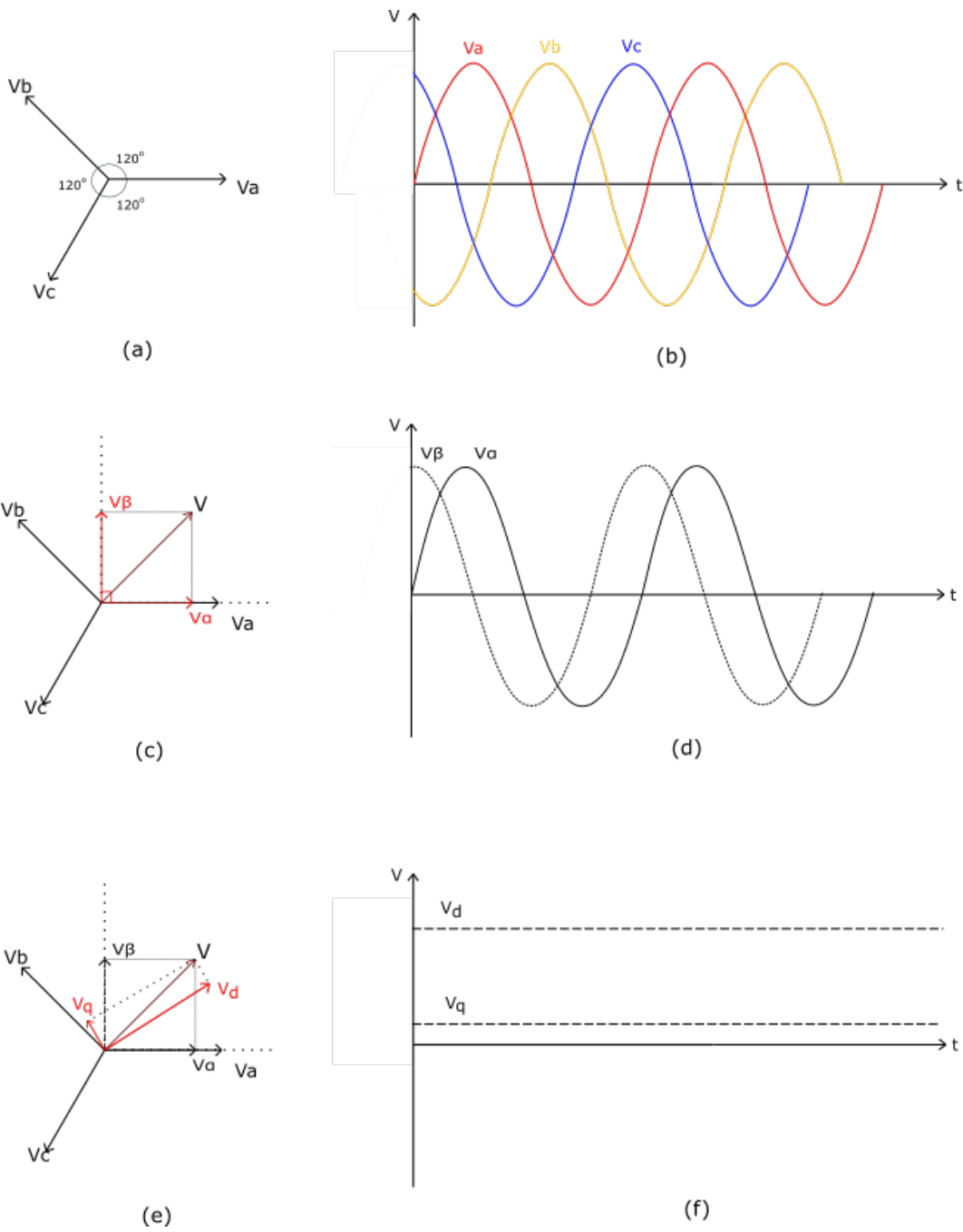


Figure 3.6: Clark and Park transformation

3.5 Principle of PWM technique

The dc-ac converter or referred as inverter, converts a rectified waveform into sinusoidal waveform. This is realized through applying a modulation technique to regulate the injected dc power from PV array into a sinusoidal AC waveform as an output. Pulse signals are sent to the controllable switches (IGBT or MOSFET) in the inverter to regulate its duty ratio. This modulation scheme is called pulse width modulation and its object is to control the magnitude and the frequency of the output voltage waveform. There are several techniques proposed for the PWM scheme like the space vector PWM [9] or the unipolar inverted sine PWM for the multilevel inverter. As half-bridge, two-stage inverter is ought to be used for the three-phase system for this study, the focus will be of the conventional sine PWM scheme applied for this inverter [30].

Sine PWM: Sine PWM (SPWM) method or carrier based PWM (CBPWM) is the most common PWM scheme among varies other techniques carried out for the regulation of pulse signals sent to controllable switches [30][5]. In SPWM, a control voltage, $v_{control}$, with sinusoidal waveform is compared with a carrier waveform to generate the pulse signals. The control voltage consists of desired amplitude and frequency f_1 (50Hz). The carrier waveform, V_{tri} , is a repetitive triangular wave propagating through time between 1 and -1 with high frequency. This frequency illustrates the switching frequency f_{sw} for the controllable switches (IGBT) and ranges between 6-20 kHz [30].

For the simplicity, Fig.3.7 shows an illustration of the comparison between $v_{control}$ and V_{tri} for a single-phase inverter with two switches in one leg. Signals generated from the switches are of pulsed waveforms as shown in Fig.3.7. Switches S1 and S2 are upper and bottom switches and are commanded to turn On/Off based on the intersection of the waveforms. Can be summarized as following:

$$S1 = \begin{cases} 1, \text{Switch is on} \Rightarrow & v_{control} > V_{tri} \\ 0, \text{Switch is off} \Rightarrow & v_{control} < V_{tri} \end{cases} \quad (3.15)$$

$$S2 = \begin{cases} 1, \text{Switch is on} \Rightarrow & v_{control} < V_{tri} \\ 0, \text{Switch is off} \Rightarrow & v_{control} > V_{tri} \end{cases} \quad (3.16)$$

The duty ratio of the switches are being regulated when a reference sinusoidal waveform is compared with a repeating triangular waveform with high frequency. Amplitude modulation ratio, m_a , and frequency modulation ratio, m_f , are two essential terms here for characterising the two waveforms. As the name suggest, the m_f gives the harmonic content of the fundamental frequency f_1 . Since the output of the inverter will always consist some harmonics, the m_f will show the harmonic content of f_1 . The harmonic can be mitigated through a filter between the inverter and the grid it is supplying to. Another way is to increase the switching frequency f_{sw} which is the frequency of V_{tri} . Having high value of f_{sw} , the switches will act faster on its switching sequence reducing the amount of harmonic content produced at the output. The normal value chosen for f_{sw} is in between 6 kHz and 20 kHz. The equation for the frequency modulation ratio is given as:

$$m_f = \frac{f_{sw}}{f_1} \quad (3.17)$$

Similarly the equation for the amplitude modulation ratio can be given as:

$$m_a = \frac{\hat{V}_{control}}{\hat{V}_{tri}} \quad (3.18)$$

The desired value of the amplitude modulation ratio is defined as the linear region:

$$m_a \leq 1$$

From Fig.3.7, a value greater than 1, is when the $v_{control}$ exceeds the amplitude or the peak value of the V_{tri} . This is called the overmodulation region [30]. At this condition, some of the switching sequences are missed with the $v_{control}$ being larger than V_{tri} . As a consequence, larger content of harmonics can be seen for the output waveform. Operation in overmodulation region is undesired, and needs to be avoided because of higher harmonic content. The overmodulation region can be defined as:

$$m_a \geq 1$$

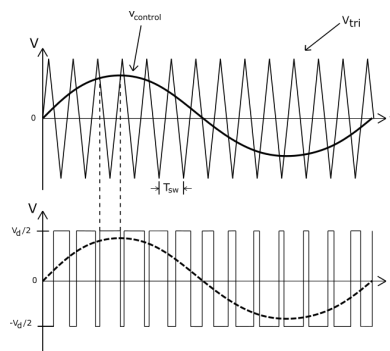


Figure 3.7: Pulse width modulation for single phase

The SPWM scheme applied for the single-phase inverter can be realized for a three-phase inverter as well. For the single-phase inverter, consisted of one leg with two switches. Three-phase inverter has three legs each phase, and each consist of two controllable switches. Instead of one $v_{control}$, now three control voltages each displaced by 120° are compared with V_{tri} .

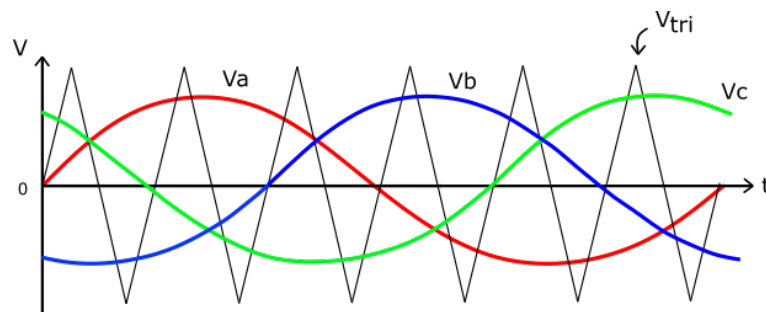


Figure 3.8: PWM for three-phase inverter

3.6 Grid Synchronization and Phase locked loop

For the grid-connected PV system, proper synchronization with the grid is essential to ensure the power converter and the grid works in unison. Proper synchronization between the inverter variables and the grid variables is essential to ensure stable operation of the system. Information on utility voltage's phase angle, amplitude and frequency are essential for the grid synchronization. Grid synchronization and grid monitoring are two concepts that are relevant to each other. By monitoring phase-angle, amplitude and frequency at the point of common coupling (PCC), information can be achieved to see if the synchronization process was a success. At the same time, the task of monitoring these variables is essential during fault conditions or abnormal operation conditions. Since the inverter supports the grid with frequency and voltage, during casualties like faults, disturbances or resonance on the system, the grid stability and its safety is threatened at the same time. Standards are in place by the utility companies. If the grid variables observed at the PCC exceeds the limit defined in the standards, the connection between the inverter and the grid will get disconnected immediately to avoid further damages of the system. Voltage variables will still be monitored during the disconnected time, when the fault or the disturbance ceases, the inverter reconnects with the grid again.

The control for the grid synchronization is a vital part in the control aspect for the grid-connected PV system. Since the information generated from this algorithm is later used in different level of control. For the PWM technique seen in previous section, required information to regulate the duty ratio of the switches are the voltage amplitude, frequency and the phase angle information that are sensed from the synchronization control. Additionally, the synchronization technique can also be used to detect harmonic components. Thereby, the technique for grid synchronization can be divided in two domains, frequency- and time domain [37]. Grid synchronization based on time-domain has been studied for this thesis. As the frequency domain will be beyond the scope of this study, more information about this technique is provided in [37].

A phase locked loop (PLL) technique is a time-domain based synchronization technique. PLL is applied to enable proper synchronization and certifies it happens fast and accurate. PLL is a feedback control system which adjust the phase-angle of a generated signal to match a reference signal. The general structure of the PLL is illustrated in Fig.3.9 consisting of fundamental blocks as phase detector (PD), loop filter (LF), and voltage controlled oscillator.

- **PD:** error signal e is generated which is a comparison between the desired phase angle with the measured phase angle sent as feedback.
- **LF:** Loop filter block usually consist of a PI controller. Input to the LF block is the phase error signal from the PD. PI controller will minimize this error signal to zero and provide a driving signal to VCO.
- **VCO:** Consist of an integrator block. The driving signal, which is frequency ω is generated as a phase angle as the output oscillation. It acts as a resettable block where the value drops down to zero each time the output angle reaches 2π .

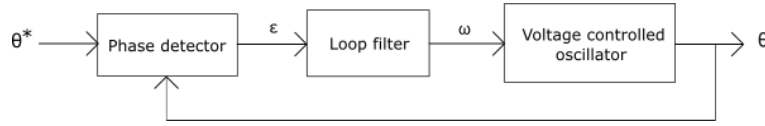


Figure 3.9: Fundamental blocks of PLL

In the article of [1] different techniques are mentioned for the PLL control. PLL based on Inverse Park transformation, Hilbert transformation and synchronous reference frame PLL (SRF-PLL) have been reviewed with special attention to its tracking precision and its dynamic response of the different PLL techniques. When designing the PLL control, it must be a trade-off between the tracking precision and the dynamic response, since a fast dynamic response can result in lack of tracking precision [1]. Key object for these techniques are same, but differentiate in the structure of the PD block.

Synchronous reference frame PLL

Structure of the SRF-PLL presents a simpler form compared to PLL techniques with the inverse park transformation and Hilbert transformation. The complexity of SRF-PLL is also simpler compared to the other, thereby the SRF-PLL is the favored technique among them. Detailed illustration of SRF-PLL topology is presented in Fig.3.10.

Voltages observed at PCC are denoted as V_s and are generated from the inverter. To improve the tracking precision, the VCO is augmented with a feedforward term of the angular frequency (50Hz). Voltage variables are transformed from natural reference frame (abc) to synchronous frame (dq) using Park's transformation block in Fig.3.10. In Fig.3.11a) the d-q component of the respective voltages is given as $V_s d$ and $V_s q$ rotating at an arbitrary frequency. Angular position of the d-component is controlled by the feedback loop to line up with the utility voltage. As a consequence, the q-component is controlled to zero. Fig.3.11b) shows how the voltage vector are with proper synchronization. Voltage generated from the inverter will have the same amplitude, phase angle and frequency as the utility grid voltage.

Study in [1] shows that compared to the other techniques, the SRF-PLL does not contribute to attenuate the output harmonics. Enhanced PLL (EPLL) and the quadrature PLL (QPLL) present better attenuation than the SRF-PLL. Thereby, an external filter is necessary for system implementing the SRF-PLL for grid synchronization.

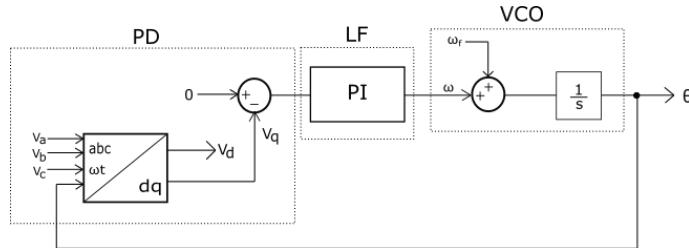


Figure 3.10: SRF-PLL

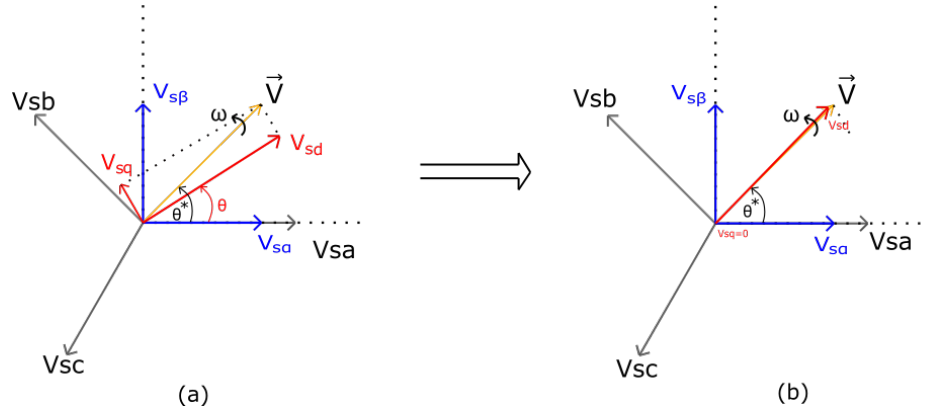


Figure 3.11: Synchronization with SRF-PLL: a) before synchronization and b) synchronized with utility voltage.

3.7 Basis of Power flow

In this section the fundamentals of the power flow in a three phase grid-connected PV system will be reviewed. Inverter's importance has been introduced in section 2 reviewing its main goal in a grid-connected system. Additional to MPPT control, DC-link voltage control and ensuring power quality injected to the grid, the inverter must also control the power flow of active and reactive power injected to the grid. Controllers designed for the FPV plant is based on the fundamentals and basis of the power flow theory. Thereby, control of the instantaneous active power and reactive power components exchanged between VSC and the AC system at PCC will be explained by reviewing the instantaneous power theory.

3.7.1 Instantaneous power theory

The instantaneous active and reactive power is controlled by regulating the amplitude and the phase angle of the voltages [10][6]. Given an ac circuit as shown in 3.12 with voltage generated from the the inverter is denoted as V_{inv} and the receiving end voltage at the ac side is the grid voltage denoted as V_{grid} . For the simplicity of the understanding, the figure illustrates for a single phase but the theory is applicable for three phase system as well. In [10] a phasor diagram is depicted for the ac circuit in Fig. 3.12 and is shown in Fig.3.13. Phasor diagram from [10] takes as a model of a transmission line. Compared to the inductance on the line, the resistance has a lower value, and is therefor considered negligible in the phasor diagram. Using this phasor diagram, equations 3.19 and 3.20 [44] where depicted illustrating that the active power P sent to the AC side can be controlled by adjusting the inverter voltage amplitude and the angle between the sending end voltage (V_{inv}) and the receiving end voltage (V_{grid}) which is angle δ . Similarly the reactive power Q is proportional to the magnitude of the voltage generated from the inverter. Angle θ on the phasor diagram is the power factor angle, which is the angle between the current component and the receiving end voltage V_{grid} .

$$P(t) = \frac{V_{inv} - V_{grid}}{\omega L} \delta \quad (3.19)$$

$$Q(t) = \frac{V_{inv} - V_{grid}}{\omega L} V_{grid} \quad (3.20)$$

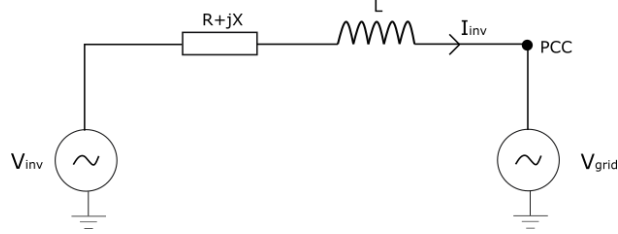


Figure 3.12: Equivalent 1-phase ac circuit

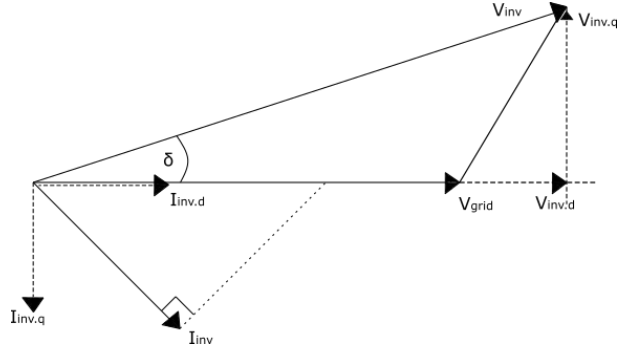


Figure 3.13: Phasor diagram

From equation 3.19 and 3.20 it is known that the control of the power flow is by controlling the phase angle δ and voltage magnitude. Usually a grid connected controller requires operation in unity power factor (PF). Meaning the controller designed must be able to limit the reactive power production to zero. By applying Kirchoff's voltage law at the point of common coupling (PCC) of Fig.3.12 following equations are achieved transformed from abc three phase quantities to rotational reference frame dq-axis:

$$V_{inv,abc} = V_{grid,abc} + (R + L \frac{d}{dt}) I_{abc} \quad (3.21)$$

$$V_{inv,abc} - V_{grid,abc} = R I_{abc} + L \frac{dI_{abc}}{dt} \quad (3.22)$$

By applying Clark's and Park's transformation seen in section 3.4.1, the three phase quantities can be seen and controlled as two phase quantities instead. Equation (3.23) and (3.24) shows the equation in stationary frame:

$$V_{inv.\alpha\beta} - V_{grid.\alpha\beta} = RI_{\alpha\beta} + L \frac{dI_{\alpha\beta}}{dt} \quad (3.23)$$

$$V_{inv.dq} - V_{grid.dq} = RI_{dq} + j\omega LI_{dq} + L \frac{dI_{dq}}{dt} \quad (3.24)$$

With the phase angle information, above equation can be transformed to synchronous frame shown in (3.25) and (3.26). Losses of the system can be considered to be bare minimum for the simplicity of the system and the resistance R can be neglected.

$$V_{inv.d} - V_{grid.d} = L \frac{dI_d}{dt} - \omega LI_q \quad (3.25)$$

$$V_{inv.q} - V_{grid.q} = L \frac{dI_q}{dt} + \omega LI_d \quad (3.26)$$

As mentioned earlier, by controlling the dq-component of the current and the dq-component of the voltage, the active and reactive power generated and absorbed can be controlled. An additional phasor diagram showing for P and Q is illustrated in Fig.3.14 where it can be confirmed that Q is controlled by regulating $V_{inv.q}$ or by I_d , similarly flow of P is regulated by $V_{inv.d}$ or I_q . Four different controllers were designed in this thesis for the FPV plant, where most of the controllers are based on the mentioned control theory for the exchange of the power flow between the VSC and the PCC at the AC system. The different controller will be defined in the following sections.

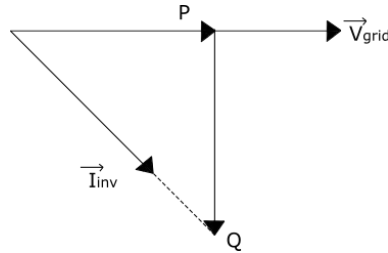


Figure 3.14: Phasor diagram for power flow

3.7.2 Voltage mode control and current mode control

According to [53], two controllers were introduced here for the control of the active power P and reactive power Q from the inverter. The first method is called the voltage-mode control. Active and reactive power is controlled based on the phase angle and the amplitude, similar to control theory explained in the previous section above. The voltage-mode control is a simple control that can be implemented with few numbers of loops. Absence of current control makes the voltage mode controller unreliable under fault conditions as it is not protected under overcurrents. Current mode control is the second method mentioned in [53] and is the mostly used method for active and reactive power control. Since the current at AC side is sensed and controlled, second controller is more preferred as it has superior dynamics and higher control precision.

3.8 Hysteresis control

The hysteresis current control (HCC) method is one of the simplest control method available that can be applied for the grid-connected inverter control. HCC is characterized in terms of stability, fast response time and good accuracy [31][45]. Studies in [32][23][29][35] has implemented the HCC method for different applications, both for three phases and single-phase systems. Desired switching signals are generated in a different way with HCC. In sine PWM scheme or carrier based PWM scheme desired pulse signals were sent to IGBT switches by comparing a reference sinusoidal waveform with a carrier waveform. In HCC, pulse signals are sent to the switches by comparing instantaneous current waveform with a reference current waveform in a predefined band called the hysteresis band. This has also been illustrated in Fig.3.15. Object of the controller is to track the reference current and realize a waveform as close to reference current waveform as possible. How the instantaneous current i follows the reference current i_{ref} is projected in Fig.3.15, and in Fig.3.16 a control block of the HCC is presented. The control block shows that HCC is a closed loop control where the upper and lower boundary limit of the hysteresis band is defined as e_{max} and e_{min} respectively, defining the limitation of inductor currents pathway with purpose of following i_{ref} as close as possible. Switching signals are sent and regulates the phase leg switches to $V_{dc}/2$ when the value of i is less than δ_{HCC} . Vice versa, the phase leg switches to $-V_{dc}/2$ when the i is larger than δ_{HCC} . The error value e is the compared value between the measured current i and i_{ref} as it can be seen in Fig.3.16. The switching signals can be summarized in following terms considering a single-phase inverter or a rectifier, with upper and bottom switches of the converter of one leg is S1 and S2, respectively [45]:

$$\begin{cases} i < \delta_{HCC} \rightarrow \frac{V_{dc}}{2}, S1 = 1 \text{ and } S2 = 0 \\ i > \delta_{HCC} \rightarrow -\frac{V_{dc}}{2}, S1 = 0 \text{ and } S2 = 1 \end{cases} \quad (3.27)$$

In three phase systems with three legs, the same switching logic can be applied to the other two phases. Choosing a proper bandwidth δ_{HCC} is vital for the controller since it can control the average frequency for the inverter application and decide which bandwidth had the optimal performance for the grid connected application.

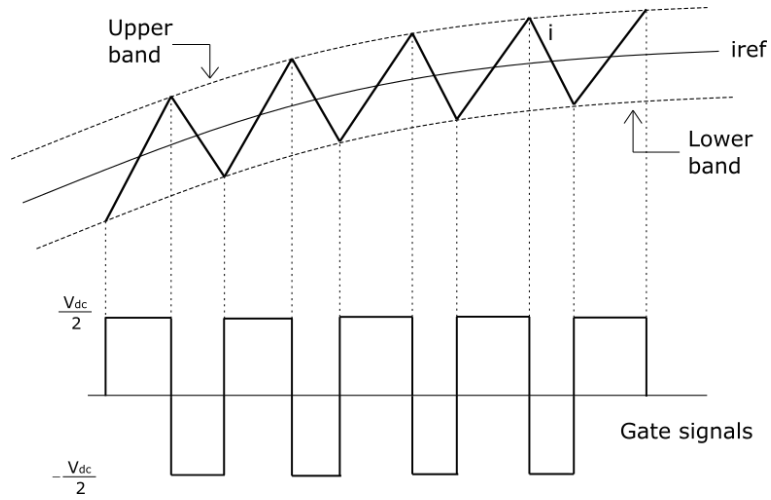


Figure 3.15: Hysteresis current control

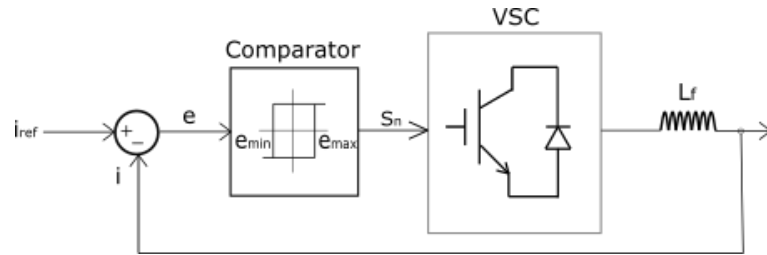


Figure 3.16: Hysteresis current control block

Different studies are available presenting an enhanced method of the conventional HCC, presenting strategies that can overcome the limitation of the control. In [35] there were three different HCC strategies are introduced and simulated for the grid connected PV system; conventional HCC, adaptive bandwidth HCC and the vector-based HCC. Disadvantage of the conventional method lies in variation of the modulation frequency in the hysteresis band resulting in undesired outcome of the ripple current. In the adaptive bandwidth HCC method, a relationship between the f_{sw} and the tolerance of the bandwidth δ_{HCC} is derived with the object of making up for conventional method. The tolerance bandwidth of δ_{HCC} is regulated by using the equation (3.27), with variation of the instantaneous reference current and the dc link voltage V_{dc} , the distortion of the current waveform could be reduced [45].

$$\delta_{HCC} = \frac{0.125V_{dc}}{f_{sw}L_f} \left[1 - \frac{4L_f^2}{V_{dc}^2} \left(\frac{V}{L_f} + \frac{di_{a.ref}}{dt} \right) \right] \quad (3.28)$$

Simulation results conducted in [35] reveals that the vector-based HCC is a better control applied for the grid connected PV system significantly reducing the ripple output of the inverter, reducing the switching frequency and at the same time keeping the simplicity of the controller which is

overlooked in the adaptive method. As the name suggests, the vector-based method selects the zero and non-zero voltage to follow the reference current vector. Additional to hysteresis band width δ_{HCC} defining the tolerance band, the vector-based have another level of tolerance band $\delta_{HCC} + \Delta\delta_{HCC}$ constructing the current error vector to be kept within a hexagonal region. An in-depth description of the vector-based control is beyond the scope for this study. The HCC control applied for the grid connected VSC seen in this study is the adaptive method. The control strategy is enhanced with PLL control additionally implemented to the system. A detailed description of the vector-based method is provided in [35].

Chapter 4

Simulation of Grid-connected PV system

Duration time of the simulation conducted for each controller where for 10s with a $25\mu s$. Results from the MPPT and PLL controller where the same for all four designs, therefore the results for these controllers are defined in its respective sections. As the DC-link voltage control is directly related to the control of the active power flow, its control implementation varies for each controller. Topology for the grid-connected system simulated in PSCAD environment is presented in Fig.4.1. Topology consist of six IGBT switches with a diode connected in parallel. Since it is a three phase system, there are three legs with two switches in each. Two dc-link capacitors are provided to supply constant ripple free voltage as input to the inverter. An LC-filter is connected between the grid and inverter to reduce the current ripple generated from the inverter before it supplies the grid. Usually, a resistance, R , is connected in series with L_f , since the system is considered under steady state, R has been ignored. For the ease of the project, a stiff grid has been considered so the focus will be on understanding how the designed controller can provide high quality power to the grid. In Table.4.1 all the values for the parameters are given. As it can be seen the proposed simulation will not be based on the 42 kW FPV plant at Kilinochchi. Instead, the simulation will be based on lower power output of 6.4kW. Four proposed controllers will be simulated under STC and site condition. Change in environmental conditions will have an impact on the power production as it is shown in Table.4.1 and this will be observed in the simulation results as well. Under STC, the array can produce 6.4kW as input to the inverter, while the power is increased at site condition to 7.2kW.

System Parameters	Values under STC	Values under Site condition
Input Power P_{pv}	6.4kW	7.2kW
Input Voltage $V_{dc}/2$	677V	670V
Input Current I_{dc}	9.3A	10.7A
DC link capacitor C_{DC}	$260\mu F$	$260\mu F$
Filter Inductor	9mH	9mH
Filter Capacitor	$1.5\mu F$	$1.5\mu F$
System frequency	50 Hz	50Hz
Grid voltage V_{ph-ph}/V_{rms}	400V/230V	400/230V
Grid side filter R	0.1Ω	0.1Ω

Table 4.1: Overview of system parameters for the proposed grid-connected topology

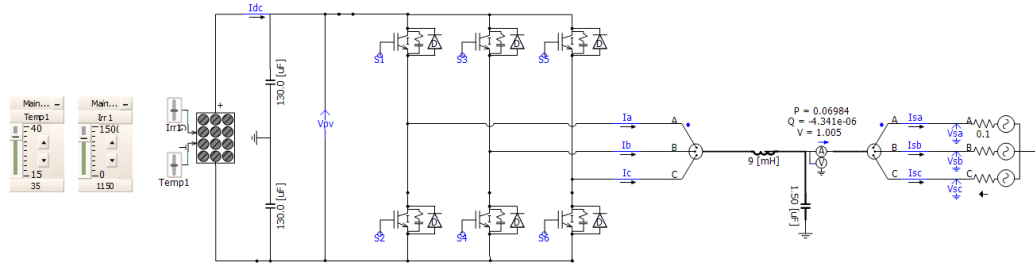


Figure 4.1: Half-bridge inverter applied for the system with IGBT switches

4.1 PV array design

An appropriate design of the PV array was established based on the parameters of the SUNNY Tri Power Core1 inverter used at the FPV plant in Kilinochchi. Datasheet of the inverter is provided in the Appendix chapter. The PV array was designed to match the required input MPP voltage range which is between 500V and 800V. A PV array with an MPP voltage in the vicinity of 677V was designed. Parameters of the array is given in Table4.2. Fig.4.2 provides the characteristics of the array under STC ($1000W/m^2$ and $25^\circ C$), while Fig.4.3 shows the characteristic under site condition. According to measured data from Institute for Energy Technology (IFE), peak irradiance and temperature where measured to $1150.5W/m^2$ and $35.7^\circ C$ in may 2021. The impact on the environmental changes can be observed in Fig.4.3. Compared to the STC condition, maximum power provided by the PV array has increased to 7.2 kW.

Parameters	Value
I_{mpp}	9.3A
V_{mpp}	677V
P_{mpp}	6.4kW
I_{sc}	10A
V_{oc}	834V

Table 4.2: PV array parameters

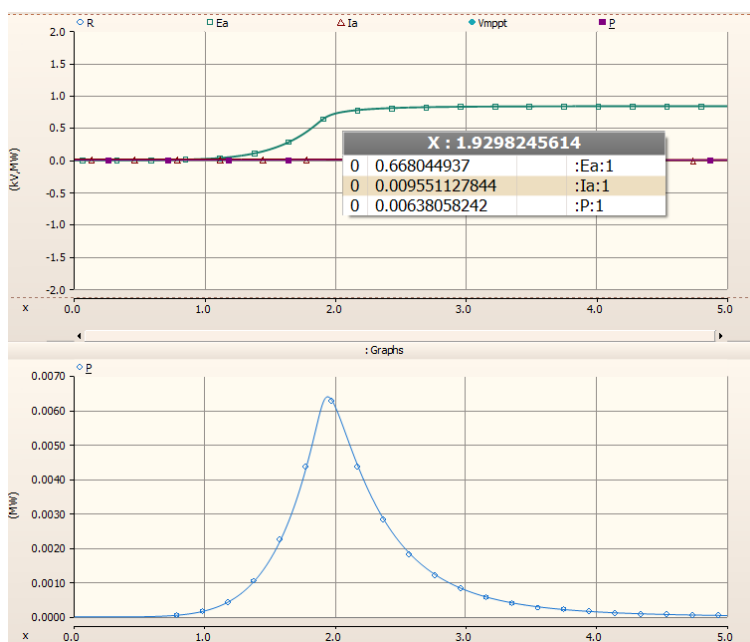


Figure 4.2: PV array characterisation under STC

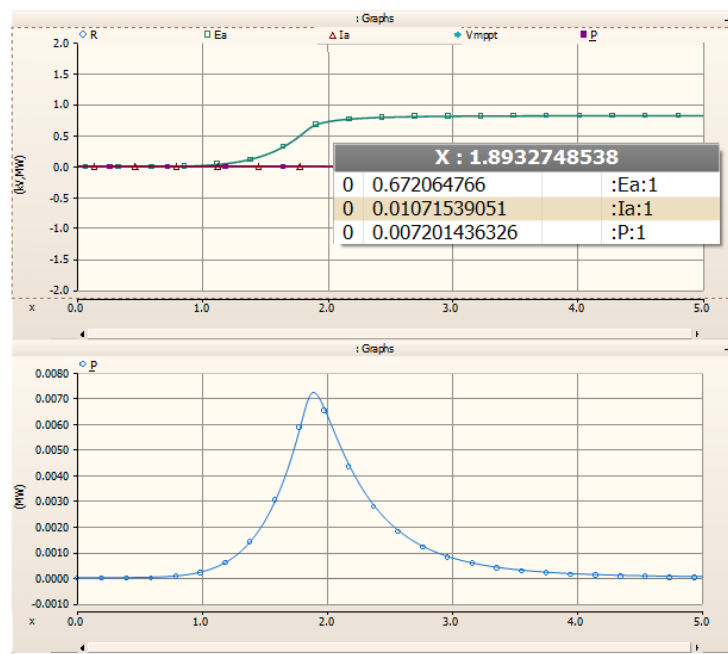


Figure 4.3: PV array characterisation under site condition

4.2 MPPT control

The incremental conductance method was applied for the MPPT control of the system. The MPPT block is provided from PSCAD environment and is presented in Fig.4.4. As seen in Fig.4.4, I_{sc} , V_{oc} and the initial MPP voltage from PV array characterisation under STC is defined for the INC method. The instantaneous voltage provided by the array V_{pv} and the instantaneous current i_{dc} are the required input values for the MPPT block. A detailed representation of the INC method is provided in section 3.x.

In Fig.4.5 results of the INC method is presented, where the dc link voltage V_{pv} tracks the MPP voltage with high precision under varying environmental condition. This shows that the object of the MPPT control is realized for the system. The provided MPPT control is achieved from the simulation results from 2nd controller. A similar tracking precision is seen for the other controllers with some deviations.

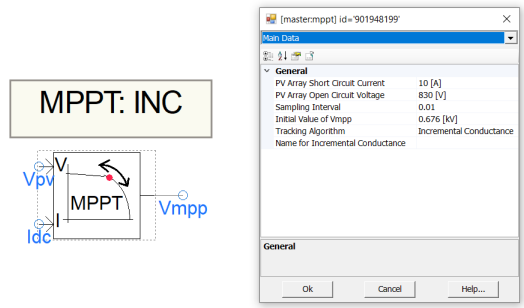


Figure 4.4: MPPT block: Incremental conductance

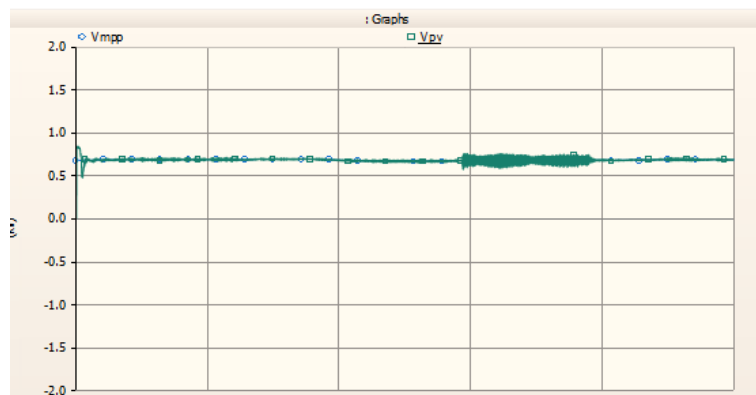


Figure 4.5: Tracking precision from the MPPT control

4.3 PLL control

Control block for the grid synchronization is shown in Fig.4.6 and the results of the synchronization is shown in Fig.4.7. The generated angle θ is a repetitive waveform, propagating from 0 to 2π at 50 Hz.

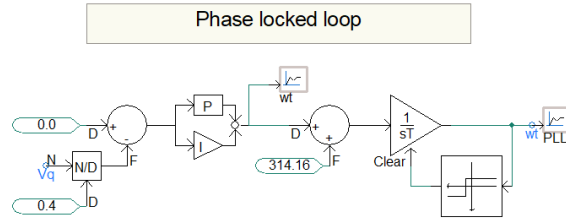


Figure 4.6: SRF-PLL control block implemented for the system

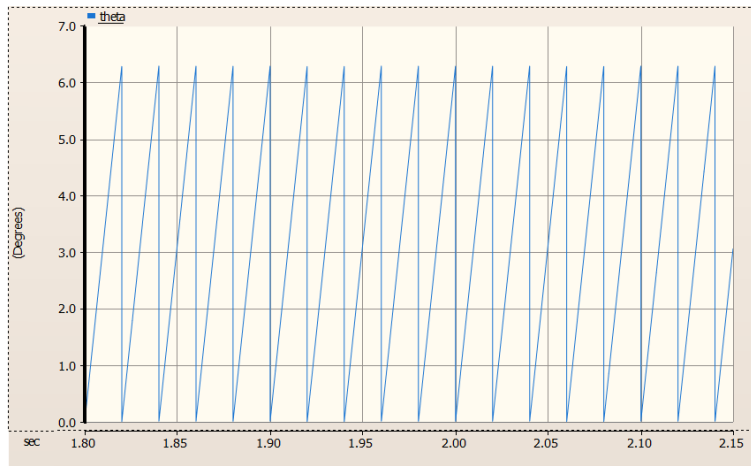


Figure 4.7: Waveform of angle θ for proper synchronization

4.4 Control methods

In this section the four proposed controllers which are based on the theoretical analysis from the previous chapter, will be reviewed. With similar control object and connected to similar half-bridge inverter, the controllers are different from one another in terms of its methodology.

4.4.1 Design of 1st controller

Required input information for the PWM scheme illustrated in Fig.4.8 are the angle θ and the magnitude V_m . Information on angle and magnitude are essential to generate the reference three phase voltages described in equation (4.1). Control of the power flow is embedded in the generation of desired voltages in natural frame. Based on the theory analysis from section 3.7, the active power

can be controlled by regulating the angle, δ , between sending end voltage and the receiving end voltage, shown in Fig3.14. In a similar manner, the reactive power Q is controlled by regulating the magnitude of the dq-component for the sending end voltage and its current.

$$\begin{aligned}
 V_{a.ref} &= V_m \cos\theta \\
 V_{b.ref} &= V_m \cos\left(\theta - \frac{2\pi}{3}\right) \\
 V_{c.ref} &= V_m \cos\left(\theta + \frac{2\pi}{3}\right)
 \end{aligned} \tag{4.1}$$

Fig.4.8 shows the proposed design for the first controller. P and Q control are controlled independently from each other. Active power control is directly controlled through the dc-link voltage control. A detailed block of the dc-link voltage controller is provided in Fig.4.9. The error between dc-link voltage V_{pv} and MPP voltage V_{MPP} is decreased using a compensator block of PI controller ($K_p = 1$ and $K_i = 0.01$). Output angle generated from the PLL control, ωt , is fed as a feedforward term to avoid unwanted start-up transient. Output of the dc-link control is the angle denoted as alpha, which comply with the θ shown in equation (4.1).

The magnitude control block is used to control the reactive power flow. A direct method is applied to control the reactive power. Detail of the controller is given in Fig.4.10. Q can be controlled directly by a compensator block where the measured value of Q is controlled to be equal to desired value Q_{ref} (Fig.4.10a). Fig.4.10b shows another method to control the reactive power flow by controlling the sending end voltage V_{inv} to equal to a desired value of 1. As mentioned in section 3.x, gains for controllers are decided based on trial and error method and are summarized in Table4.3.

1st controller	Proportional	Integral
DC-link control	1	0.01
Direct Q control	0.001	0.025
Direct V_{inv} control	1	0.1

Table 4.3: PI controller gains for 1st controller

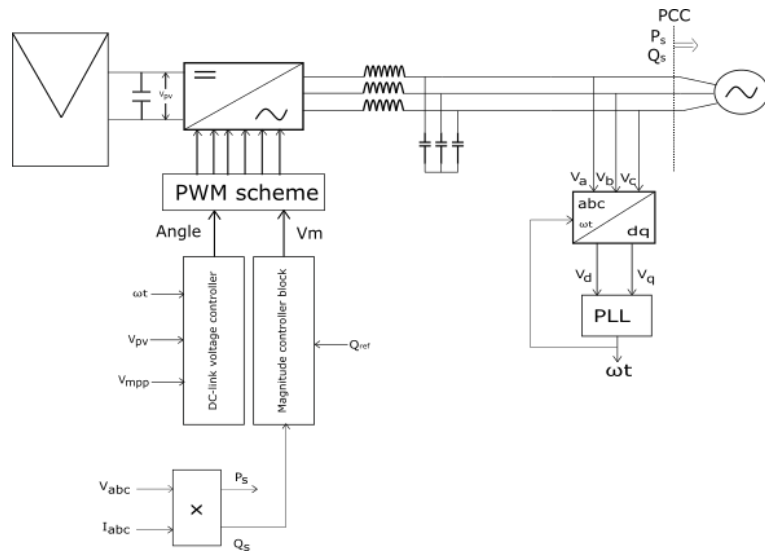


Figure 4.8: Control topology for the first controller

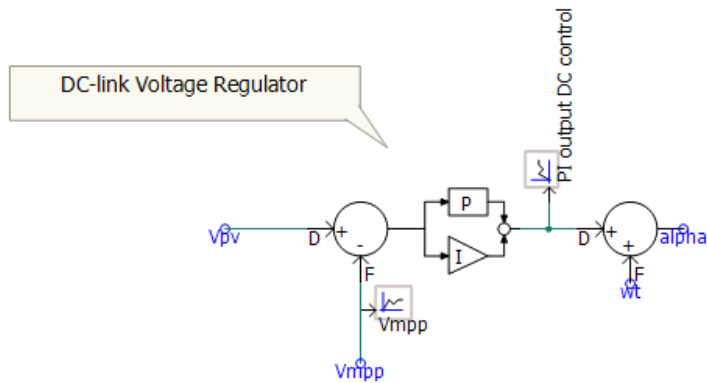


Figure 4.9: DC-link voltage control block for the first controller

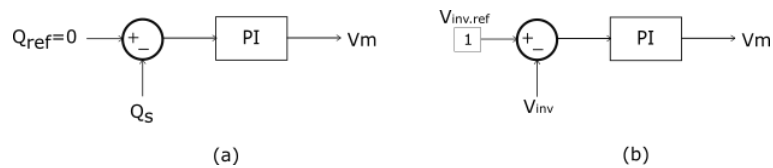


Figure 4.10: Inside the magnitude control block a) Q control and b) V_{inv} control

4.4.2 Design of 2nd controller

Fig. 4.11 shows the control topology for the second controller. In the previous controller, a grid connected control was achieved through control of voltage parameter in natural reference frame. Control of parameters in synchronous frame (d-q) has been applied for the 2nd control. Using Park's transformation, current and voltage parameters are transformed from natural frame to synchronous frame to control the components in dq-frame. Before the voltages are sent to the SPWM scheme, desired current and voltage parameters are transformed back to natural frame using inverse Park's transformation.

DC-link voltage control is a part of the active power control for the system. PI controller is used as a compensator block for the desired voltage generated from MPPT control block and the dc-link voltage V_{pv} .

To achieve unity PF control, the reactive power needs to be equal to zero. In the second controller this is achieved by controlling the q-component of the inverter current shown in fig.3.13. This is shown in Fig. 4.11 where a PI controller is used to reduce the error between measured I_q and the desired $I_{q.ref}$. Output is a current value in d-component $I_{inv.d}$. The desired $V_{d.ref}$ is generated with the addition of 489V.

2nd controller	Proportional	Integral
DC-link control	1	0.1
Q control	1	0.1

Table 4.4: PI controller gains for 2nd controller

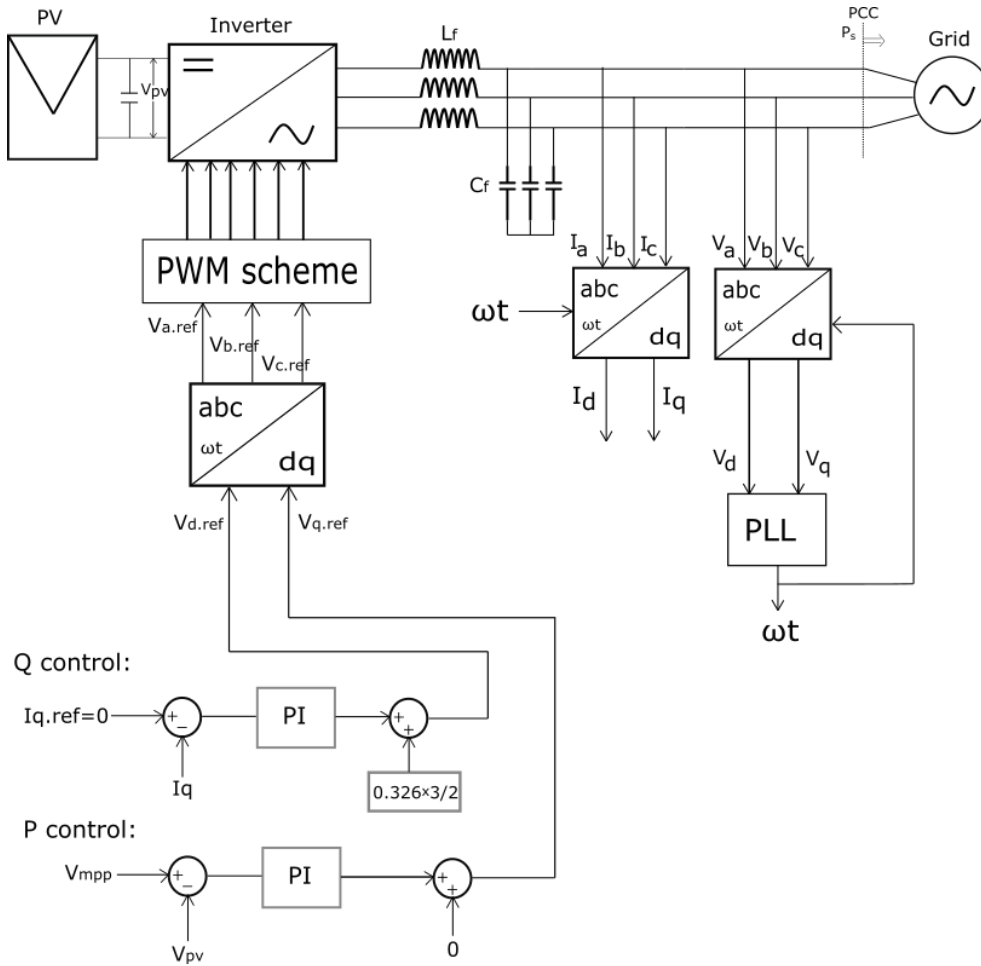


Figure 4.11: 2nd control block

4.4.3 Design of 3rd controller

A cascaded control was implemented for the third controller of the study. According to [14] having controller with inner- and outer loop is most common control seen for the distributed system. As it can be seen in the results part in section 4.5.3, undesired results were attained when two PI controllers were implemented in the system. The general structure of the control block for the third controller is shown in Fig.4.12. Two different methods are applied here for the active power control and the reactive power control block. Differences are in the number of PI controllers applied in the control of active power. In the first method shown in Fig.4.13, the active power flow is controlled by dc-link voltage control. The current output of the dc-link voltage control is used to generate the desired $V_{q.ref}$ using decoupling term and a voltage feedforward term.

Active power in the second method is controlled by one cascaded control loop, where the inner loop is current controlled and the output is a dc-link voltage control. Control block for the second

method is depicted in Fig.4.14. Desired current $I_{d.ref}$ is generated as output from the dc-link voltage control. The current control loop consist of a PI controller to reduce the error between the reference current value and the measured current value of the d-component. Then similar to the first method, controller uses decoupling terms and voltage feedforward to generate the desired $V_{d.ref}$.

For the reactive control for both methods uses a PI controller block to reduce the error between desired current $I_{q.ref}$ and the measured current value I_q . Using a decoupling term and voltage feedforward term similar to the active power control, required voltages are generated as output. Reference value of the voltage in d-component is generated from the first method, while the second method generates the reference voltage value of the q-component.

Inverse park transformation is applied to transform the desired values in synchronous frame to natural frame, $dq \rightarrow abc$. Then the desired voltage values in natural frame $V_{abc.ref}$ with phase grid angle obtained from the PLL control, are injected to the PWM scheme to generate the switching signals for the controllable IGBT switches in the half-bridge inverter. Summary of the PI controller gains chosen for the controller in first and second method are given in Table4.5 and in Table4.6

3rd control: 1st method	P	I
Q control	0.25	0.01
DC-link voltage control	0.1	0.01

Table 4.5: Proportional gain and Integral gain for 1st method controller

3rd control: 2nd method	P	I
Q control	0.25	0.01
DC-link voltage control	0.1	0.01
Inner control	0.1	0.01

Table 4.6: Proportional gain and Integral gain for 2nd method controller

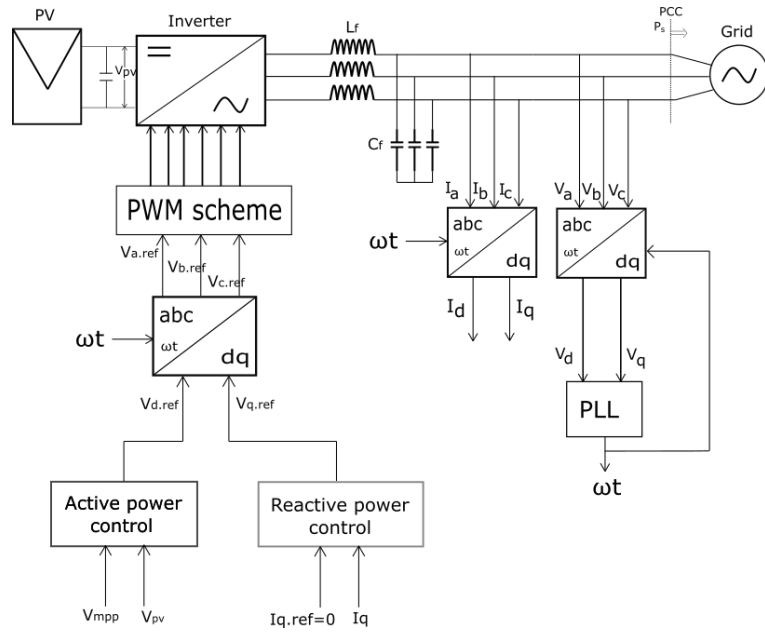


Figure 4.12: 3rd control block

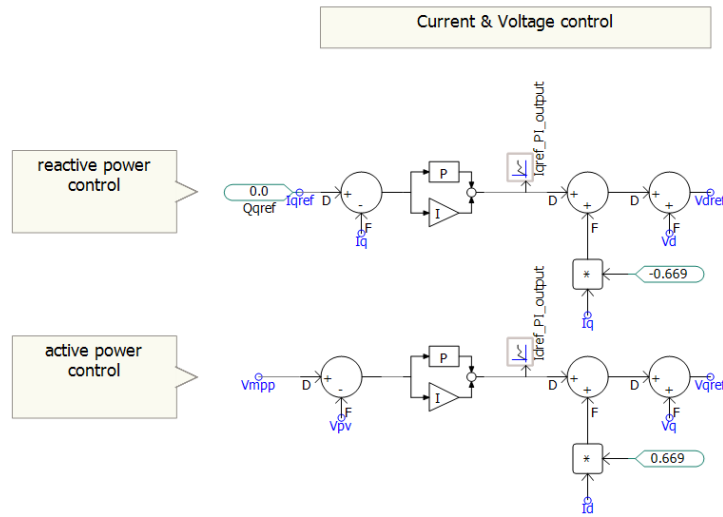


Figure 4.13: First method with one PI-controller

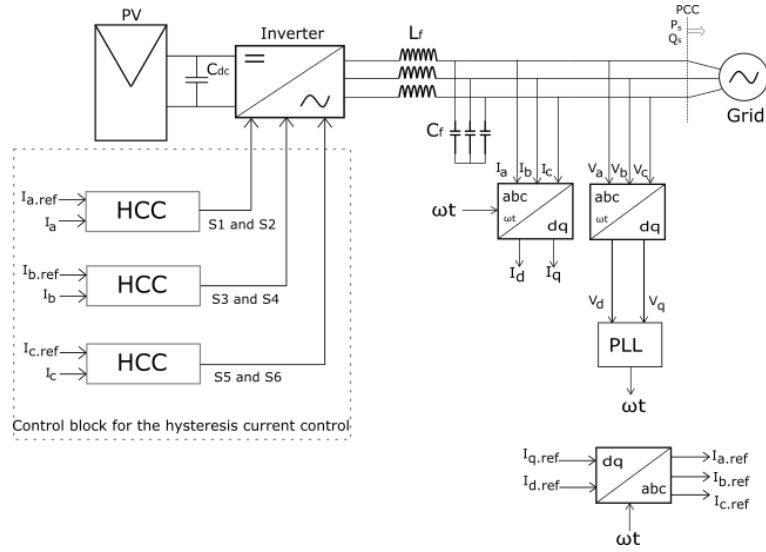


Figure 4.15: Hysteresis control block

Current and voltage values sensed at the PCC are transformed from natural frame to synchronous frame $abc \rightarrow dq$, using Park's transformation. Since it is easier to now implement control in two-phase, reference values can be found. Voltage values V_{dq} are applied to the PLL block to generate grid phase angle. Following equation with reference active and reactive power is used to find the desired current component:

$$\begin{aligned} P_{ref} &= V_{inv.d}I_{d.ref} + V_{inv.q}I_{q.ref} \\ Q_{ref} &= V_{inv.q}I_{d.ref} - V_{inv.d}I_{q.ref} \end{aligned} \quad (4.2)$$

voltage values in equation (4.2) can be considered to equal the grid voltage (326V) when the system is properly synchronized. Which means, from the above equation, control of the power is dependent on the current components. With a proper synchronization with the grid accomplished by PLL control, the q-component is zero since the voltage d-component aligns with the grid voltage vector, equation (4.2) can be rewritten as:

$$\begin{aligned} P_{ref} &= V_{inv.d}I_{d.ref} \\ Q_{ref} &= -V_{inv.d}I_{q.ref} \end{aligned} \quad (4.3)$$

DC-link voltage controller is designed for active power control generating $I_{d.ref}$ as output while the reactive power is directly controlled to be zero. A detailed description of the control is shown in Fig.4.16. Using the inverse Park's transformation, the reference currents in dq-components can be transformed to abc-frame.

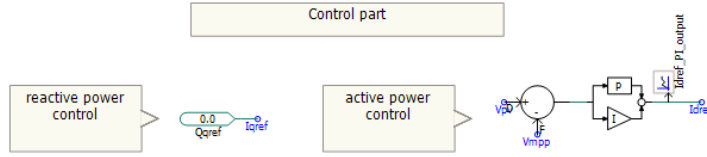


Figure 4.16: HCC: Active and reactive power control

Switching signals to the inverter are controlled using a HCC control block. Each current phases are controlled independently as shown in Fig.4.15. As shown in Fig.4.17, the controller consist of a feedforward term and a feedback technique. Purpose of HCC control is achieved through this block enabling constant switching frequency f_{sw} and a good dynamic response. Control block in Fig.4.17 is for phase a, a similar control is applied for the other two phases that are displaced by 120° .

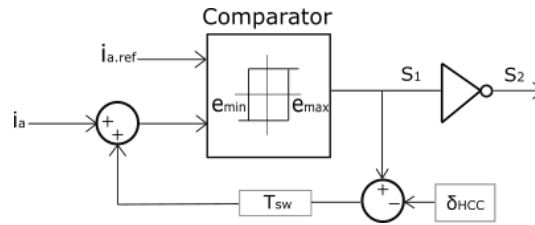


Figure 4.17: HCC control block for phase a

4.5 Simulation Results

Results and discussion for the proposed controllers for grid-connected PV system are provided in this section.

4.5.1 1st Controller

A simple control design has been implemented for the first controller in this study. This benefits in a simple circuitry and design for the system. Fig.4.18 shows the results from PWM generation where the desired generated voltage waveforms $V_{abc.ref}$ are compared with a carrier waveform. With the control, a modulation index equal to 0.96 is achieved which complies with the requirement of $m_a \leq 1$. Generated current and voltage waveform are depicted in same graph in fig.4.19 under STC. Peak value voltages are close to the desired peak value of grid voltage, 325V and the current is measured to 12.6A.

A slight difference can be seen in the measured current under STC and site condition. The voltage injected to the grid is equal to 323V under site condition and the current is measured 10.9A (Fig.4.19b). With increase in irradiance the current value decreases while the voltage increase. The opposite is true when the temperature increases.

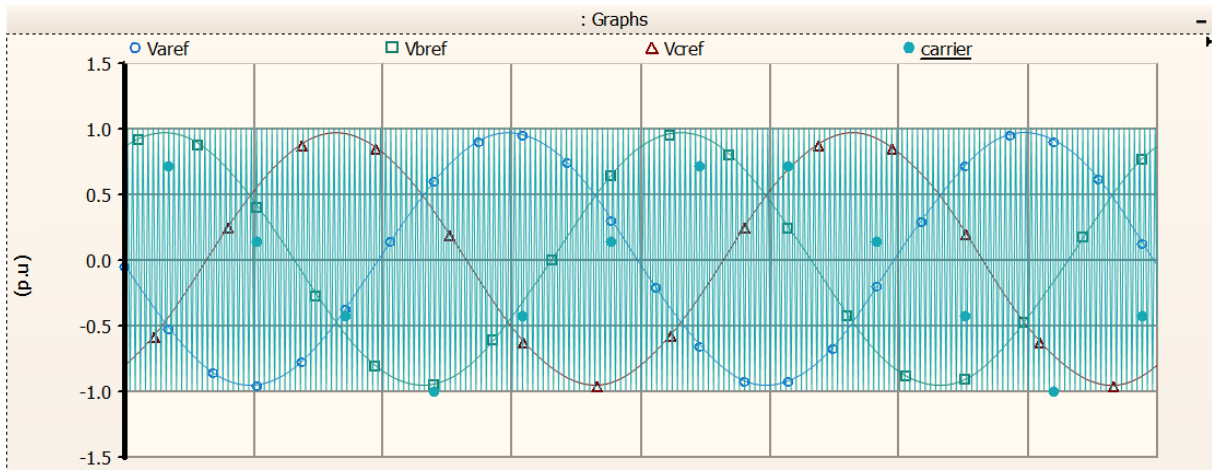
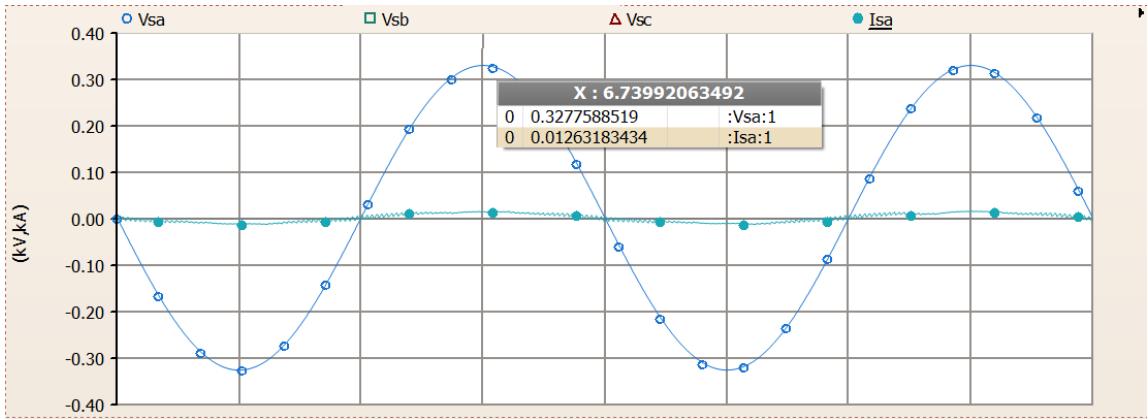
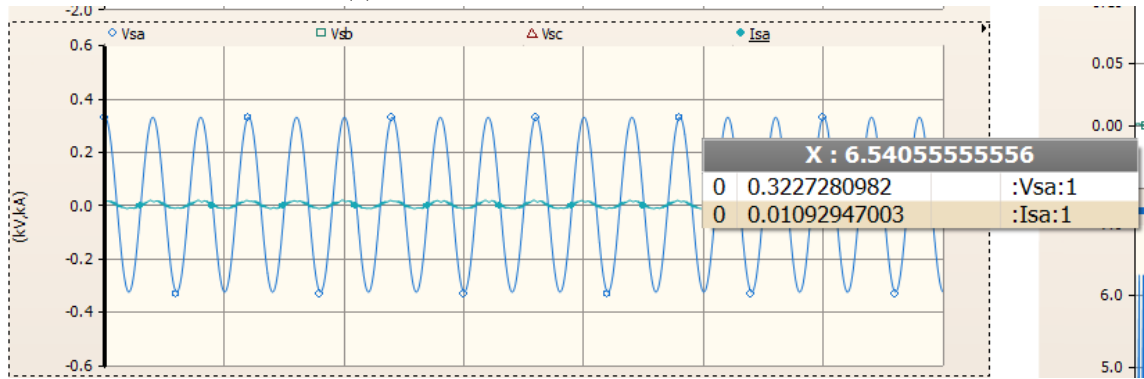


Figure 4.18: 1st controller: Reference voltage waveform vs the carrier waveform

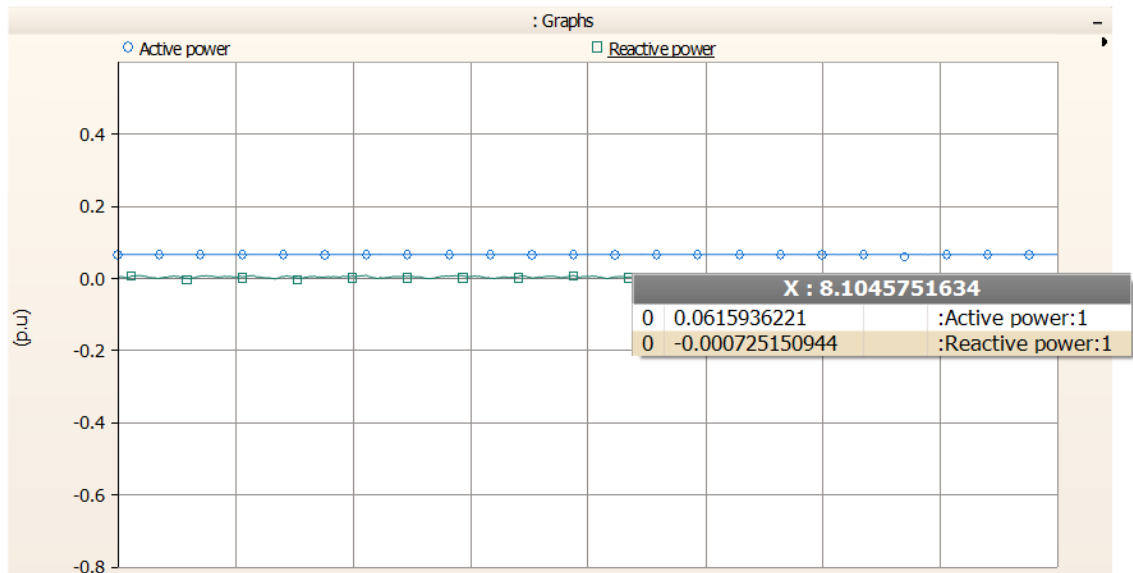


(a) Current and voltage waveform at STC

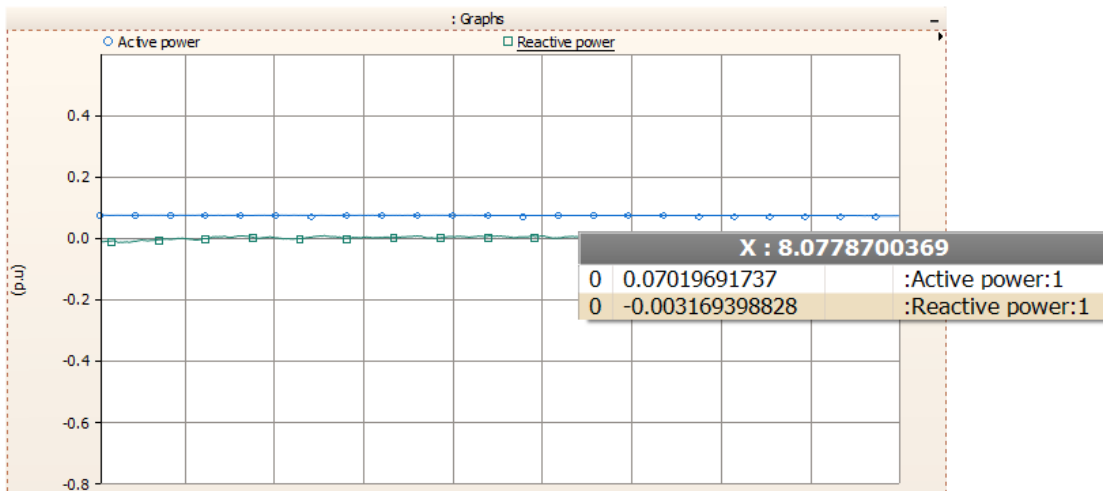


(b) Current and voltage at site condition

Figure 4.19: Voltage current waveforms from 1st control



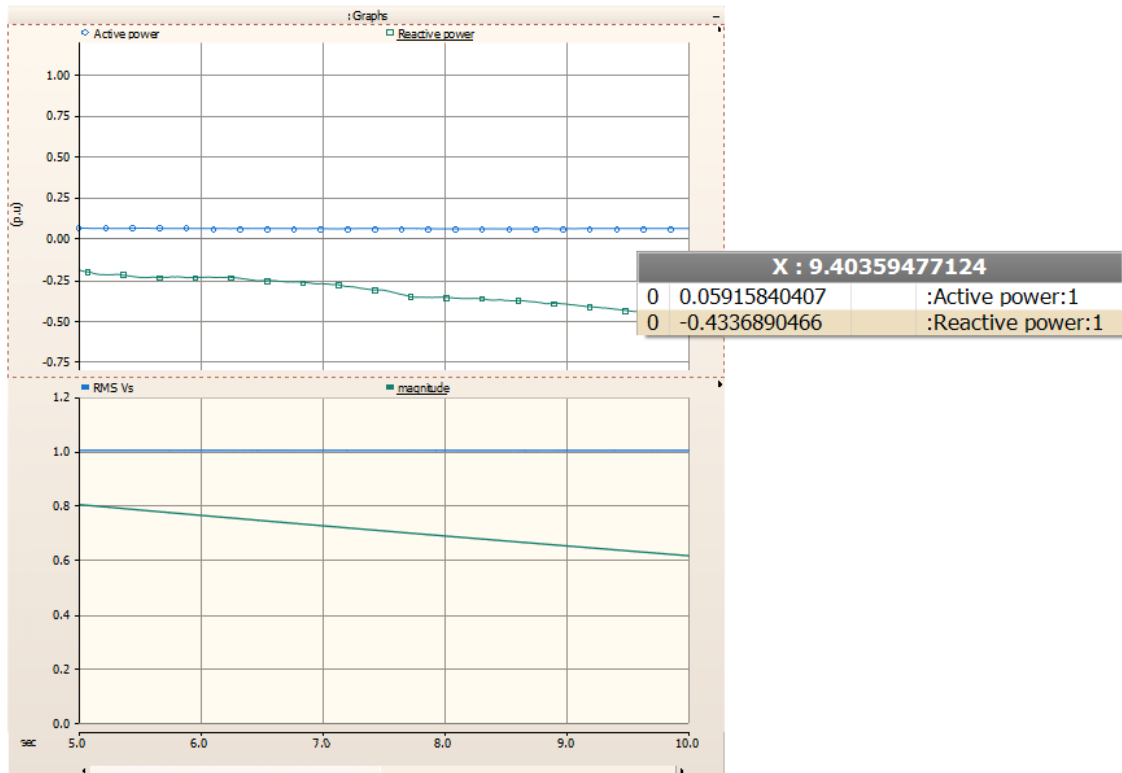
(a) Active and reactive power at STC



(b) Active and reactive power at site condition

Figure 4.20: Active and reactive power from 1st control

Results of the waveforms for the active and reactive power under both STC (fig.4.21a) and under site condition (Fig.4.21b) are given in fig.4.20. With output active power of 7kW under STC and 7.2kw under site condition, the efficiency for the controller under is given to be around 97%.



(a) Active and reactive power for control of V_{inv}



(b) Current and voltage waveform

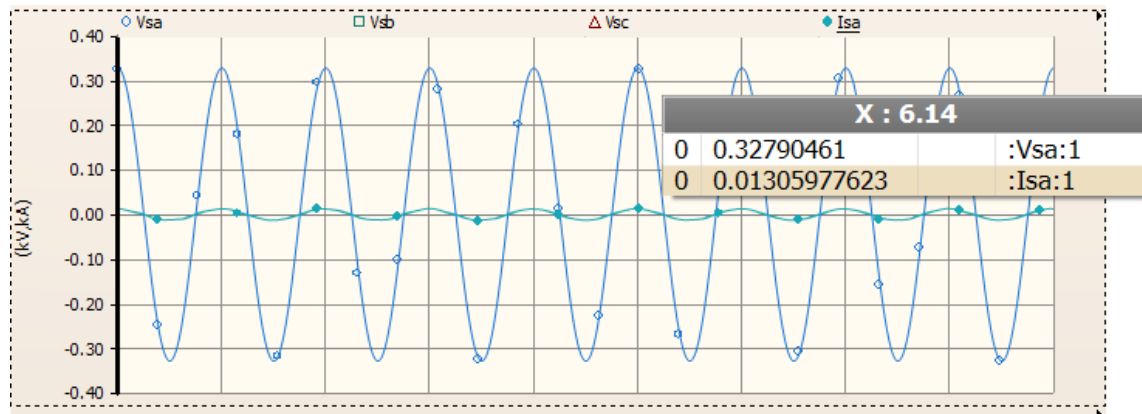
Figure 4.21: Simulation results from direct control of V_{inv}

Fig.4.21 shows the results of the simulation for the first controller when V_{inv} was directly controlled instead of Q . Unsatisfactory results are attained from this type of control. A high value of peak current has been observed in Fig.4.21b, approximately 80A. This is a result of the current

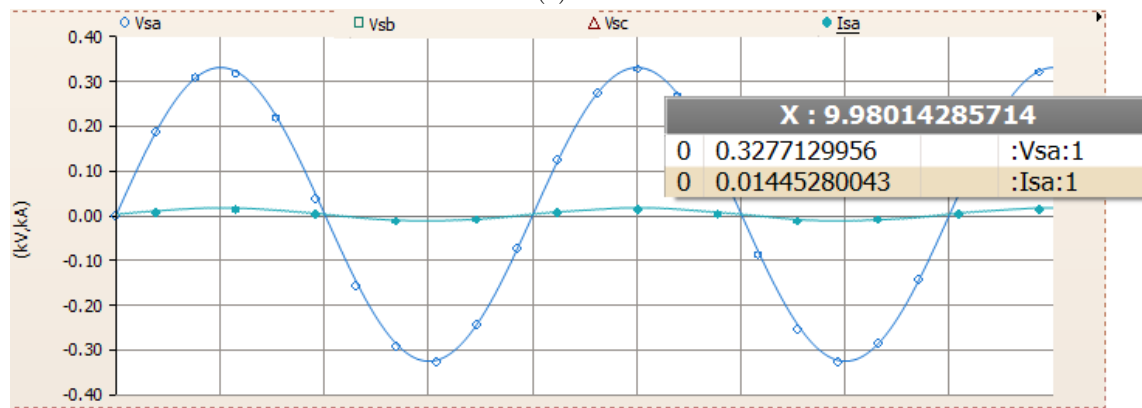
waveform is not in phase with the voltage waveform which produces reactive power. A steadily decrease of the magnitude value without stabilization is seen in Fig.4.21a, this shows that direct control of Q is a better option over the direct control of V_{inv} .

4.5.2 2nd Controller

Results for the controller with current control applied additionally to the voltage is shown in this section. Control of the current is essential to secure and stable operation. In case of faults occurs on the system, the current can be disrupted and uncontrollable which leads to detrimental damages of the system. From the waveforms seen in Fig.4.22, desired results have been realized as the current are in phase with the voltage. This means, unity power factor operation is achieved for the system.

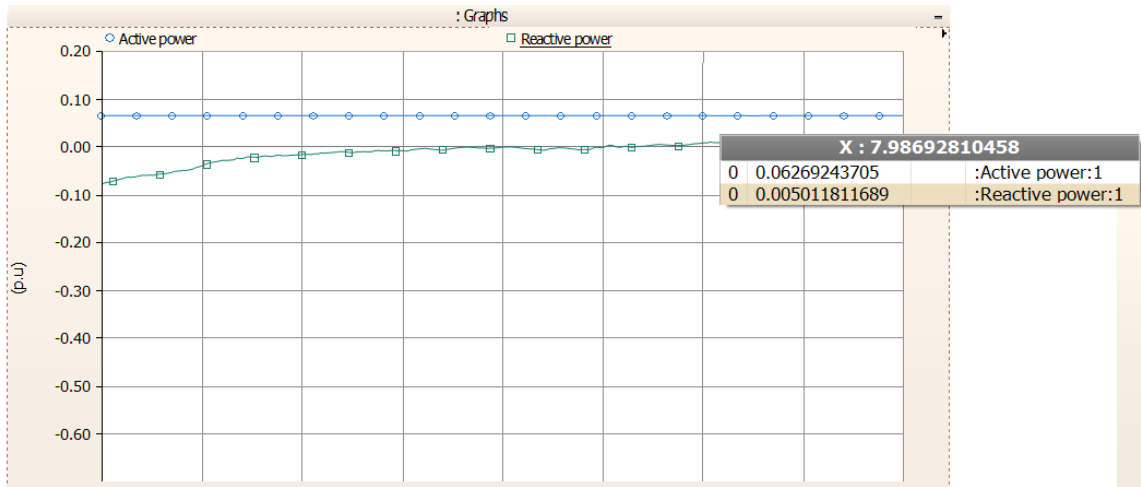


(a) STC

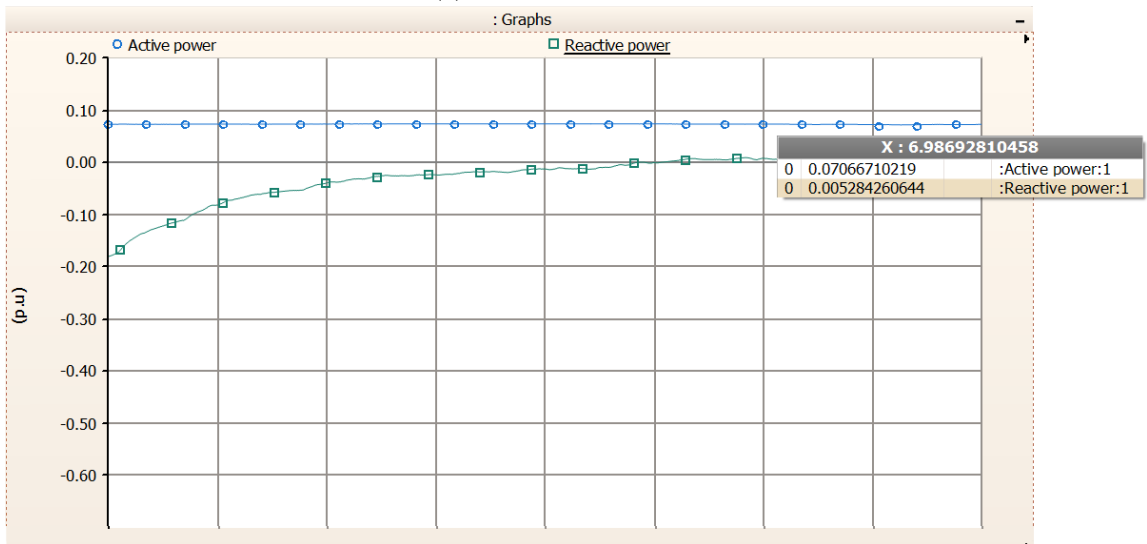


(b) Site condition

Figure 4.22: Current and Voltage waveform for 2nd controller in both STC and site condition



(a) PQ control under STC



(b) PQ control under site condition

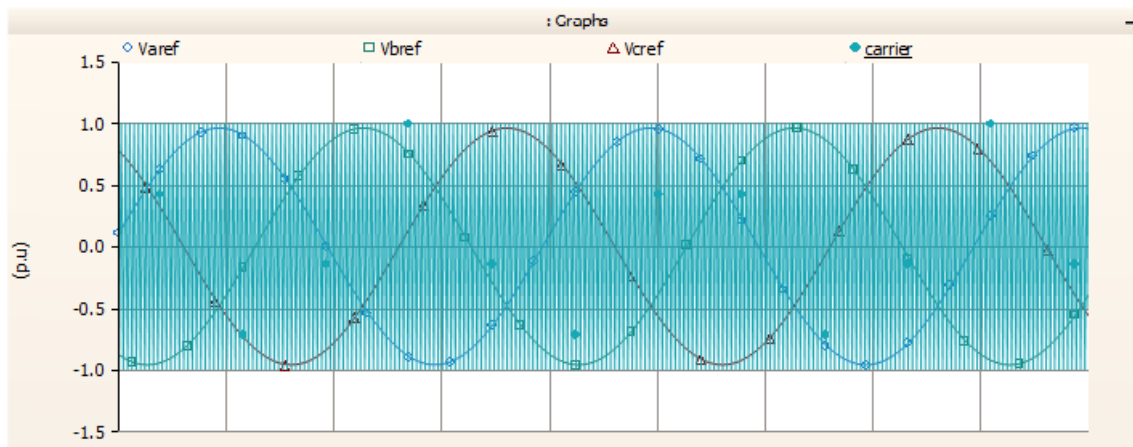
Figure 4.23: Active and reactive power flow control for 2nd controller

4.5.3 3rd controller

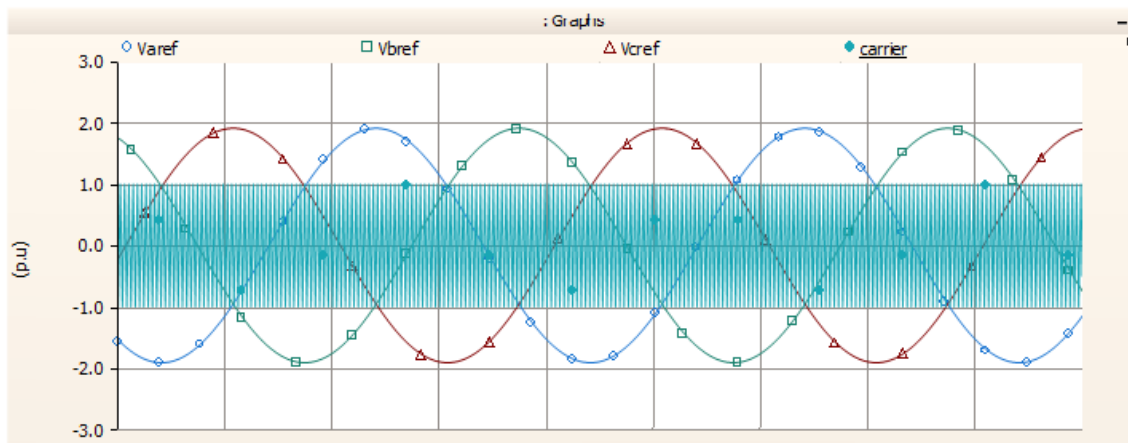
Comparison of the desired voltage waveforms in natural frame with carrier waveform for both methods in 3rd controller is shown in Fig.???. The modulation index for the first method complies with the requirement of $m_a \leq 1$, when one PI controller was applied. While the waveform shown in Fig.4.14, for the cascaded loop in the second method, operation in overmodulation ($m_a > 1$) is achieved. Corresponding results for voltage and current waveform is shown in Fig.4.25, where the current value is high and leads the voltage waveform.

Fig.4.26 shows the simulation for active and reactive power when a cascaded loop was applied for the control of active power, P . Negative value of the power, indicates that the inverter absorbs power instead of supplying to the grid. This is the results of current leading the voltage waveform. Which is why, the second method in 3rd control is not applicable for the control of the grid connected PV system. The reason is the lack of proper modelling of the PI controller gains. Since "trial and error" method is used to chose the proportional and integral gain, increased complexity arises to control oscillation of two PI controllers.

Power flow of the control applied in the first method supplies the grid. Active and reactive control applied in the first method uses only one PI controller each and has desired results compared to cascaded control in this study. In [14] cascaded control are common control. A proper calculation for the gains has been conducted by the author for the system.



(a) Carrier vs three phase voltages in first method



(b) Carrier vs three phase voltages in second method

Figure 4.24: Carrier vs three phase voltages for third controller

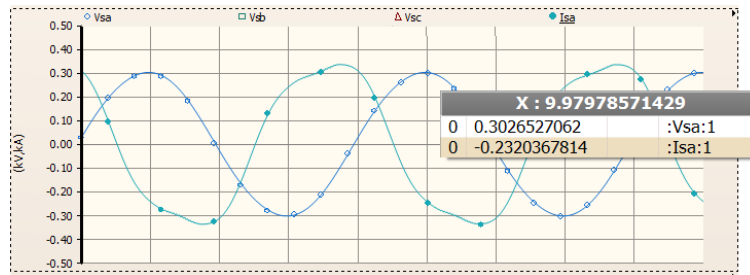


Figure 4.25: Current and voltage waveform of 3rd controller

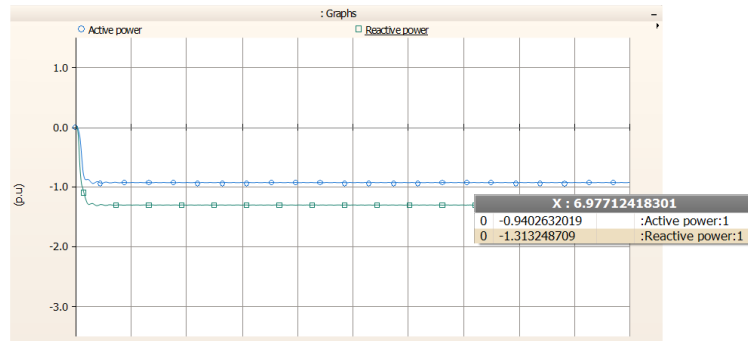


Figure 4.26: Active and reactive power flow for 3rd control

4.5.4 4th controller

A Simulation in both STC and site environmental condition for 4th controller has been provided in this study to analyze how change in temperature and irradiance affects the simulation. Switching frequency and the hysteresis bandwidth where chosen to be 10 kHz and 0.5, designed model block is shown in Fig4.27.

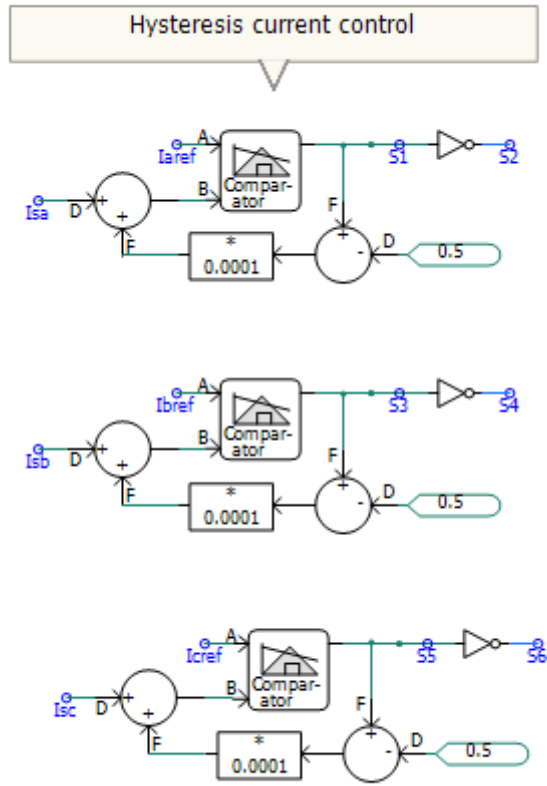


Figure 4.27: HCC control block implemented in PSCAD

Fig.4.28 shows the tracking precision of the HCC block applied for all three current phases. A precise tracking of the reference current with good dynamic response is achieved through HCC. Clearer view of the tracking precision from the applied control is shown in Fig.4.29 where the green waveform is the measured value I_a while the blue curve is reference current $I_{a.ref}$.

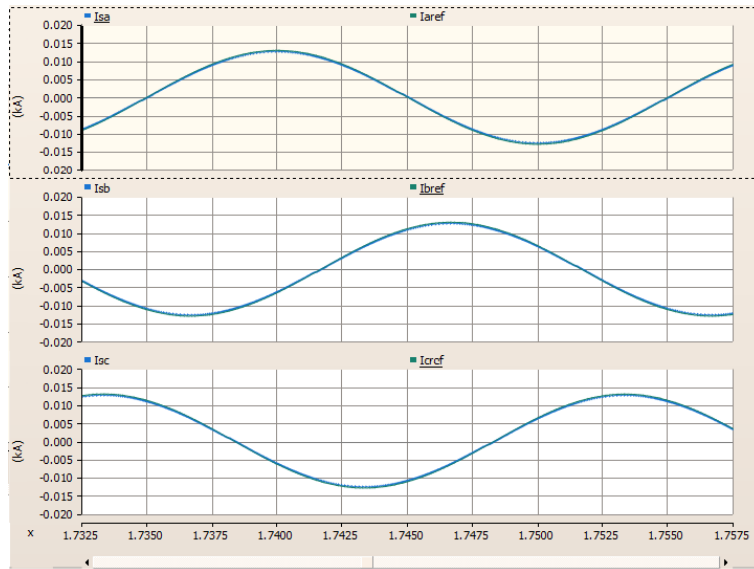


Figure 4.28: HCC tracking precision



Figure 4.29: HCC control tracking precision of phase a current

Simulation results for the active and reactive power at both STC(Fig.4.30) and under site condition (Fig.4.31) is given in the figure below. Results from the HCC control method shows that it is a robust and effective method.

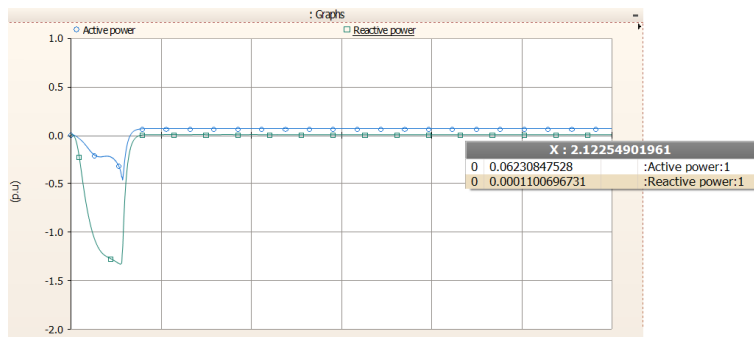


Figure 4.30: Active and reactive power flow with HCC at STC

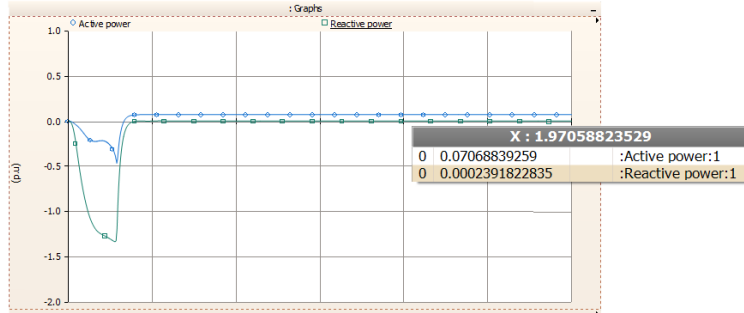


Figure 4.31: Active and reactive power flow with HCC under site condition

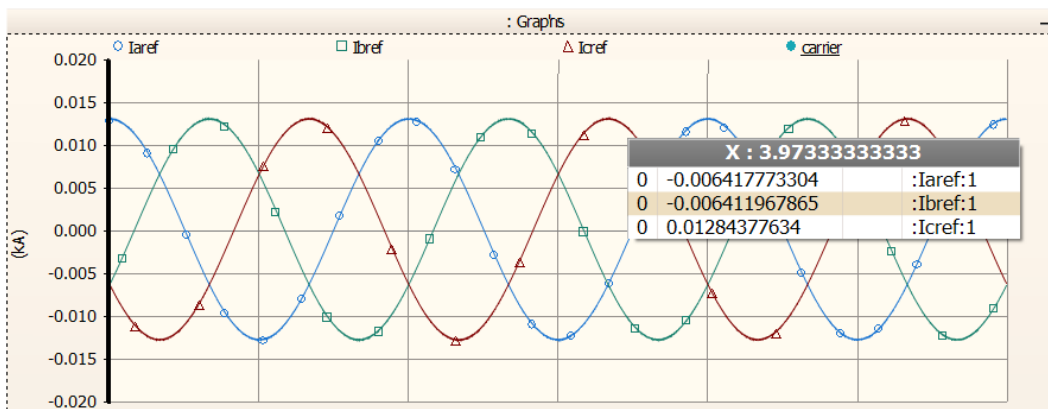


Figure 4.32: HCC: three phase reference currents

Chapter 5

Conclusion & recommendation for future work

5.1 Conclusion and discussion

PV technology has had an exponential growth in the world for past year. With the financial support from the government, Sri Lanka has also had an exponential growth in PV technology and according to [50] it seems to increase. As mentioned in the introduction part, land scarcity will be an issue in the future with increase of conventional PV technology. For this reason, FPV will be viable solution.

For this study, FPV plant in Kilinochchi was considered as a base model. A simulation of a grid connected PV system with a capacity of 6.4 kW has been conducted in this study with focus on the control part. Topology of the system is a single stage, transformerless inverter and the control part consisted of MPPT control, PLL control, dc-link voltage control and power control. Aside from MPPT control and the PLL control, dc-link voltage control and the control of power flow were designed differently for the controllers. A summary of the results from the controllers are provided in Table.5.1. A LC filter was implemented between the inverter and the grid to attenuate the harmonic ripples generated from the inverter. Purpose of the study was accomplished by designing four different control techniques for the grid-connected FPV plant. Effective utilization of the solar resource was achieved, and high quality of power was provided to the grid control techniques that were designed in this study.

	PF	THD%
1st controller	0.97	8.7
2nd controller	0.976	3.12
3rd controller: (2nd method)	—	12.6
4th controller	0.97	0.44

Table 5.1: Control results

MPPT control:

INC method was proposed for the MPPT control to utilize the maximum possible power from the PV array. From the results a precise tracking of the MPP was achieved even during changes in temperature and irradiance. Simulation of the MPPT control started from STC then varied the irradiance from $1000W/m^2$ to $1200W/m^2$ to $800W/m^2$. While the temperature changed from $25^\circ C$ to $30^\circ C$ and $28^\circ C$. Good tracking precision was observed for the first controller. Some ripples were observed when the irradiance was decreased to $800W/m^2$, during this period, the average value of the ripple was tracked. Less ripple was observed when the irradiance increased back to $1000W/m^2$.

A better tracking precision was observed for control 2 and 4. Few ripples were observed under the change of irradiance and temperature. A precise tracking of the V_{MPP} was realized for both controllers tracking the initial value of $V_{MPP} = 677V$. Compared to other controllers, poor tracking was observed for the third controller. This may be because the input voltage to the MPP control block V_{pv} exceeds the defined PV array open circuit voltage of $830V$. A steadily decrease from initial value of the V_{MPP} is observed in the simulation with V_{pv} is constant around $1300V$.

PLL control:

SRF-PLL scheme was applied to extract grid phase angle information for synchronization. From the simulation results of the controllers, it can be observed that synchronization is achieved already achieved from the start, $t=0s$. An instant connection gives good results for the simulation. For the purpose of understanding how a grid-connected system works, simulation of the controllers has been tested under a strong grid condition. To ensure proper PLL control, it must be tested under different grid conditions with harmonics and phase unbalance to see how it reacts under fault conditions.

DC-link voltage control:

DC-link voltage is directly related to the active power production in the system. Constant voltage is realized with the dc-link control, different ways has been implemented to achieve this. According to [24] the control theory is a comparison between the reference voltage at the dc-link with the measured value. Then a PI controller is applied to reduce the fluctuation. For control technique in 1 and 4, the reference value was given as V_{pv} while the measured value was V_{MPP} . This is to regulate the power flow correctly. In control 2 and 3, values were chosen to be opposite of control 1 and 4. This is to ensure the measured voltage at dc link was constant at MPP generated from the MPPT control block. Proposed dc-link voltage controller are proved to be effective based on the simulation.

Proposed Controllers:

Results from the different control techniques applied for the system has been summarized in Table.x showing the power factor of the system (PF) and the harmonic content produced (THD) in the current. Except for the third controller, rest of the control techniques had a system operation close to unity power factor averaging with 0.97. The first control technique which is based on voltage control mode exceeds the THD limit of $< 5\%$ (IEEE 1547).

Among the reviewed techniques, the third controller is least favored for the FPV system. Since an operation of overmodulation is realized when the active power is controlled by using a cascaded loop. P and Q are absorbed by the inverter instead of supplying power to the grid, Fig. 4.25. This also result in high current value which leads the voltage waveform, Fig. 4.26.

The first controller is based on voltage mode, and an effective control is realized where the current generated from the inverter is in phase with grid voltage, Fig.19. Slight deviation from the standard THD limitation, makes this control not applicable for the system. This may be enhanced by implementing an LCL-filter instead of LC-filter for better attenuation of the harmonics. However, having an LCL filter will increase in cost and size of the system.

It can be concluded that either control technique 2 or 4 may be an appropriate control technique that can be applied for the system as the harmonic content for both techniques comply with the limit defined in the standard. Additionally, as the current waveform is phase with the grid voltage, unity power factor is also achieved by the two controllers (Fig. 4.23 and Fig.4.x). The fourth controller which is an HCC is more robust and effective than the conventional method based on reference signal generation [23] with almost no harmonic content.

5.2 Future development for the system

Among the proposed controller, results from the HCC method showed good stability and an effective connection the grid. Simulation conducted in this study was based on steady state condition and to a stiff grid. A Future work needs to consider more realistic circumstances where fault can happen. Islanding detection is a important part of the system that has not been covered in this study. Standards are in place that requires disconnection from the grid in case disturbances or fault.

Inverter in this study was a half-bridge two level inverter, for higher power production multilevel inverter should be considered. The FPV plant in Kilinochchi will look to increase their production, and it would be interesting to investigate further on this for large scale production.

Bibliography

- [1] A.Nicastri and A.Nagliero. *Comparison and evaluation of the PLL techniques for the design of the grid-connected inverter systems*. Tech. rep. 2010 IEEE International Symposium on Industrial Electronics, 2010.
- [2] Adel A.Elbaset and M.S. Hassan. “Introduction and Background of PV systems”. In: *Design and Power quality improvement of Photovoltaic power system*. Springer, pp. 1–17. ISBN: 978-3-319-47463-2.
- [3] Adel A.Elbaset and M.S. Hassan. “Power Quality Improvement of PV System”. In: *Design and Power Quality Improvement of Photovoltaic Power System*, pp. 73–84. ISBN: 978-3-319-47464-9.
- [4] Ajay Kumar, Nitin Gupta and Vikas Gupta. *A Comprehensive Review on Grid-Tied Solar Photovoltaic System*. Tech. rep. India: Malaviya National Institute of Technology Jaipur, Aug. 2017.
- [5] Amirnaser Yazdani and Reza Iravani. “DC/AC Half-Bridge Converter”. In: *Voltage-sourced converters in power systems*. IEEE, Wiley, pp. 23–45. ISBN: 978-0-470-52156-4.
- [6] Amirnaser Yazdani and Reza Iravani. “Grid-imposed frequency VSC system: Control in dq-frame”. In: *Voltage-Sourced Converters in Power systems*. IEEE, Wiley, pp. 204–242. ISBN: 978-0-470-52156-4.
- [7] Andrzej M. Trzynadlowski. “AC to DC Converter”. In: *Introduction to modern power electronics*. Third Edition. John Wiley & Sons, 2016, pp. 115–180. ISBN: 978-1-119-00321-2.
- [8] Anik Goswami, Paromita Sadhu, Utpal Goswami and Pradip Kumar Sadhu. *Floating solar power plant for sustainable development: A techno-economic analysis*. Tech. rep. 2019 American Institute of Chemical Engineers, May 2019.
- [9] B.Hariram and N.S. Marimuthu. *Space vector switching patterns for different applications- a comparative analysis*. Tech. rep. Hong Kong, China: 2005 IEEE International Conference on Industrial Technology, Dec. 2005.
- [10] B.M. Weedy, B.J. Cory, N. Jenkins, J.B. Ekanayake and G. Strbac. “Basic Concepts”. In: *Electric Power Systems*. Fifth Edition. Wiley, pp. 45–78. ISBN: 978-0-470-68268-5.
- [11] Carlos Mateo, Pablo Frias, Rafael Cossent, Paolo Sonvilla and Bianca Barth. *Overcoming the barriers that hamper a large-scale integration of solar photovoltaic power generation in European distribution grids*. Tech. rep. Institute for Research in Technology (IIT), ICAI school of Engineering, June 2017.

- [12] Colm J. O'Rourke, Mohammed M. Qasim, Matthew R. Overlin and James L. Kirtley. *A Geometric Interpretation of Reference Frames and TRansformations: dq0, Clarke and Park*. Tech. rep. IEEE Transactions on Energy Conversion (Volume: 34, Issue: 4, Dec. 2019), Sept. 2019.
- [13] Divya Mittal, Bharat Kumar Saxena and K. V. S. Rao. *Floating solar photovoltaic systems: An overview and their feasibility at Kota in Rajasthan*. Tech. rep. 2017 International Conference on Circuit ,Power and Computing Technologies (ICCPCT), Oct. 2017.
- [14] F.Blaabjerg, R.Teodorescu, M.Liserre and A.V. Timbus. *Overview of control and grid synchronization for distributed power generation systems*. Tech. rep. IEEE Transactions on Industrial Electronics, Oct. 2006.
- [15] F.Blaabjerg, Zhe Chen and S.B. Kjaer. *Power electronics as efficient interface in dispersed power generation systems*. Tech. rep. IEEE Transactions on Power Electronics, Sept. 2004.
- [16] Feng Gao, Ding Li, Poh Chiang Loh, Yi Tang and Peng Wang. *Indirect dc-link voltage control of two-stage single-phase PV inverter*. Tech. rep. 2009 IEEE Energy Conversion Congress and Exposition, 2009.
- [17] Giovanni Lo Calzo, Alessandro Lidozzi, Luca Solero and Fabio Crescimbin. *LC filter design for on-grid and off-grid distributed generating units*. Tech. rep. IEEE Transactions on Industry Applications (Volume: 51, Issue: 2, March-April 2015), Aug. 2014.
- [18] Habbati Bellia, Ramdani Youcef and Moulay Fatima. *A detailed modeling of Photovoltaic module using MATLAB*. Tech. rep. NRIAG Journal of Astronomy and Geophysics, 2014.
- [19] Huafeng Xiao and Shaojun Xie. *Leakage current analytical model and application in single-phase transformerless photovoltaic grid-connected inverter*. Tech. rep. IEEE Transactions on Electromagnetic Compatibility (Volume: 52, Issue: 4, Nov. 2010), Sept. 2010.
- [20] Huzaifa Rauf. *Integrating Floating Solar PV with Hydroelectric Power Plant: Analysis of Ghazi Barotha Reservoir in Pakistan*. Tech. rep. Department of Electrical Engineering, Syed Babar Ali School of Science and Engineering, LUMS, Sector U, DHA, Lahore, Pakistan, Mar. 2019, pp. 816–821. URL: <https://www.sciencedirect.com/science/article/pii/S1876610219302243>.
- [21] Javier Farfan and Christian Breyer. *Combining Floating Solar Photovoltaic Power Plants and Hydropower Reservoirs: A Virtual Battery of Great Global Potential*. Tech. rep. Lappeenranta University of Technology, School of Energy Systems: 12th International Renewable Energy Storage Conference, IRES 2018, Mar. 2018.
- [22] Jiri Lettl, Jan Bauer and Libor Linhart. *Comparison of different filter types for Grid Connected Inverter*. Tech. rep. Department of Electric Drives and Traction, Faculty of Electrical Engineering Czech Technical Universiti in Prague, Mar. 2011.
- [23] Krismadinata, Nasrudin Abd and Jeyraj Selvaraj. *Implementation of hysteresis current control for single-phase grid connected inverter*. Tech. rep. 2007 7th International Conference on Power Electronics and Drive Systems, 2007.
- [24] Marija Vujacic, Manel Hammami, Milan Srdovic and Gabriele Grandi. *Analysis of dc-link voltage switching ripple in three-phase PWM inverters*. Tech. rep. Department of Electrical, Electronic, and Information Engineering, University of Bologna, 40136 Bologna, Italy, 2018.

- [25] Meriem Merai, Mohamed Wissem Naouar, Ilhem Slama-Belkhodja and Eric Monmasson. *An adaptive PI controller design for dc-link voltage control of single-phase grid-connected converters*. Tech. rep. IEEE Transactions on Industrial Electronics, 2018.
- [26] Mohsen Shayestegan. *Overview of grid-connected two-stage transformerless inverter design*. Tech. rep. Journal of Modern Power Systems and Clean Energy (Volume: 6, Issue: 4, July 2018), July 2018.
- [27] Mukund R. Patel. “Photovoltaic Power Systems”. In: *Wind and Solar Power systems*. 2nd edition. Taylor and Francis Group, 2006, pp. 163–181. ISBN: 0-8493-1570-0.
- [28] Munwar Ayaz Memon, Ghullam Mustafa Bhutto and Ehsan Ali Buriro. *Sizing of dc-link capacitor for a grid connected solar photovoltaic inverter*. Tech. rep. Department of Electrical Engineering, Quaid-e-Awam University of Engineering, Science and Technology, 67480, Pakistan, 2020.
- [29] Nasrudin Abd Rahim, Jeyaraj Selvaraj and Krismadinata. *Hysteresis current control and sensorless MPPT for grid-connected Photovoltaic systems*. Tech. rep. 2007 IEEE International Symposium on Industrial Electronics, 2007.
- [30] Ned Mohan, Tore M. Undeland and William P. Robbins. “Switch-mode dc-ac Inverters: dc to sinusoidal ac”. In: *Power Electronics*. Third Edition. John Wiley & Sons, pp. 200–243. ISBN: 978-0-471-22693-2.
- [31] Pouresmaeil, E., Akorede, M.F., Montesinos-Miracle. *Hysteresis current control technique of VSI for compensation of grid-connected unbalanced loads*. Tech. rep. 2012.
- [32] Q. Yao and D.G. Holmes. *A simple, novel method for variable-hysteresis-band current control of a three phase inverter with constant switching frequency*. Tech. rep. Conference Record of the 1993 IEEE Industry Applications Conference Twenty-Eighth IAS Annual Meeting, 1993.
- [33] R.DeBlasio, S.Chalmers and A.J.Anderson. *IEEE Std 929-2000 Recommended Practive for Utility Interface of Photovoltaic (PV) Systems*. Jan. 2000.
- [34] R.DeBlasio, S.Chalmers and Thomas S. Basso. *IEEE application guide for IEEE Std 1547, IEEE standard for interconnecting disrtibuted resources with electric power systems*. 2008.
- [35] Rajimi V. *investigations on Hysteresis-Based Current Control Techniques for Grid Connected Photovoltaic Systems*. Tech. rep. The Journal of Engineering Research, 2014.
- [36] Remus Teodorescu, Marco Liserre and Pedro Rodriguez. “Grid Requirements for PV”. In: *Grid converters for photovoltaic and wind power systems*. IEE, Wiley, 2011, pp. 31–41. ISBN: 978-0-470-05751-3.
- [37] Remus Teodorescu, Marco Liserre and Pedro Rodriguez. “Grid synchronization in single-phase power converters”. In: *Grid converters for Photovoltaic and wind power systems*. IEEE, Wiley, pp. 43–89. ISBN: 978-0-470-05751-3.
- [38] Robert L. Jaffe and Washington Taylor. “The Physics of Energy”. In: Cambridge University Press, Jan. 2018, pp. 465–489. ISBN: 978-1-107-01665-1.
- [39] Rosa A. Mastromauro, Marco Liserre and Antonio DellAquila. *Control Issue in Single-Stage Photovoltaic Systems: MPPT, Current and Voltage Control*. Tech. rep. IEEE Transactions on Industrial Informatics, Feb. 2012.

- [40] S. Narendiran. *Grid tie inverter and MPPT- A review*. Tech. rep. Nagercoil, India: 2013 International Conference on Circuits, Power and Computing Technologies (ICCPCT), June 2013.
- [41] S.B. Kjaer, J.K. Pedersen and F.Blaabjerg. *A review of single-phase grid-connected inverters for photovoltaic modules*. Tech. rep. IEEE Transactions on Industry Applications (Volume: 41, Issue: 5, Sept.-Oct. 2005), Sept. 2005.
- [42] S.B. Kjaer, J.K. Pedersen and F.Blaabjerg. *Power inverter topologies for photovoltaic modules-a review*. Tech. rep. Conference Record of the 2002 IEEE Industry Applications Conference. 37th IAS Annual Meeting (Cat. No.02CH37344), Dec. 2002.
- [43] Saban Ozdemir, Necmi Altin and Ibrahim Sefa. *Single stage three level grid interactive MPPT inverter for PV systems*. Tech. rep. Department of Electrical-Electronics Eng., Faculty of Technology, Gazi University, Ankara, Turkey, 2014, pp. 561–572. URL: <https://www.sciencedirect.com/science/article/pii/S0196890414000934>.
- [44] Sarina Adhikari, Yan Xu, Fangxing Li. *Utility-Side Voltage and PQ control with inverter-based Photovoltaic systems*. Tech. rep. Proceeding of the 18th World Congress The international federation of automatic control, 2011. URL: <https://www.sciencedirect.com/science/article/pii/S1474667016445830>.
- [45] Satyaranjan Jena, B. Chitti Babu, S.R. Samantaray. *Comparative study between adaptive hysteresis and SVPWM current control for grid-connected inverter system*. Tech. rep. Kharagpur, India: IEEE Technology Students’ Symposium, 2011.
- [46] Surajit Chattopadhyay, Madhuchhanda Mitra. “Clark and Park transform”. In: *Electric Power Quality*. Springer, pp. 89–96. ISBN: 978-94-007-0634-7.
- [47] *The thin film flexible floating PV (T3F-PV) array: The concept and development of the prototype*. Tech. rep. URL: <https://www.sciencedirect.com/science/article/pii/S0960148114002584>.
- [48] Tiefu Zhao, Vijay Bhavaraju and Prasanna Nirantare. *Evaluation of commercial scale transformerless solar inverter technology*. Tech. rep. Montreal, Canada: 2015 IEEE Energy Conversion Congress and Exposition (ECCE), Oct. 2015.
- [49] Transmission Divison, Ceylon Electricity Board, Sri Lanka. *LONG TERM GENERATION EXPANSION PLAN 2022-2041*. Tech. rep. Sri Lanka, Oct. 2021, 1–1 to 1–21.
- [50] Transmission Divison, Ceylon Electricity Board, Sri Lanka. *LONG TERM GENERATION EXPANSION PLAN 2022-2041*. Tech. rep., 5–1 to 5–25.
- [51] Trishan ESRAM and Patrick L. Chapman. *Comparison of Photovoltaic Array Maximum Power Point Tracking Techniques*. Tech. rep. IEEE Transactions on Energy Conversion (Volume: 22, Issue: 2, June 2007), May 2007. URL: <https://ieeexplore.ieee.org/abstract/document/4207429>.
- [52] Yaow-Ming Chen; Hsu-Chin Wu; Yung-Chu Chen; Kung-Yen Lee; Shian-Shing Shyu. *The AC line current regulation strategy for grid-connected PV system*. Tech. rep. IEEE Transactions on Power Electronics (Volume: 25, Issue: 1, Jan. 2010), 2009.
- [53] Yazdani, Amirnaser. “Grid-imposed frequency VSC system: control in dq-frame”. In: *Voltage-Sourced converters in Power systems*, pp. 204–245. ISBN: 978-0-470-52156-4.

- [54] Young-Kwan Choi, Nam-Hyung Lee, AN-Kyu Lee and Kern-Joong Kim. *A study on major design elements of tracking-type floating photovoltaic systems*. Tech. rep. Republic of Korea: International Journal of Smart Grid and Clean Energy.
- [55] Yuan-Kang Wu, Jhih-Hao Lin and Huei-Jeng Lin. *Standards and Guidelines for Grid-connected Photovoltaic Generation Systems: A review and comparison*. Tech. rep. IEEE Transaction on Industry Applications, Mar. 2017.
- [56] Yunhui Huang, Xiaoming Yuan, Jiabing Hu and Pian Zhou. *Modeling of VSC connected to weak grid for stability analysis of DC-link voltage control*. Tech. rep. IEEE Journal of Emerging and Selected Topics in power electronics, Apr. 2015.

List of Figures

1.1	Past and the future ORE capacity in Sri Lanka [50]	4
1.2	Impact from VRE sources in different stage [50]	5
2.1	Grid connected, transformer-less PV system	6
2.2	Differences between PV cell, module and array [27]	7
2.3	Equivalent circuit of single-diode solar cell	8
2.4	Caption	8
2.5	Structural topology of PV system a) single-stage inverter and b) two-stage inverter	10
2.6	Centralized inverter topology	12
2.7	String inverter topology	12
2.8	Caption	13
2.9	Caption	13
2.10	Distorted sinusoidal waveform with 3rd, 5th and 7th harmonics	15
2.11	Filter topologies: a) L-filter, b) LC-filter and c) LCL-filter	16
2.12	Structure of floating solar plant	18
2.13	Floating solar plant classification[54]	19
2.14	Fixed-type system[13]	19
2.15	Tracking type[13]	20
2.16	Pontoon based FPV[13]	20
2.17	Flexible type[13]	21
2.18	Submerged Floating PV[13]	21
2.19	Arial view of the pond and the FPV plant	22
2.20	Floating PV plant in Kilinochchi	22
2.21	Overview of the PV module installation	23
2.22	Environmental data of the site from 27th to 28th of May 2020	24
3.1	P-V and I-V curve of for an array	26
3.2	Flowchart for the P&O method	28
3.3	Flowchart for the INC method	29
3.4	DC-link capacitor	30
3.5	Control block for DC-link voltage control	30
3.6	Clark and Park transformation	33
3.7	Pulse width modulation for single phase	35
3.8	PWM for three-phase inverter	35
3.9	Fundamental blocks of PLL	37

3.10	SRF-PLL	37
3.11	Synchronization with SRF-PLL: a) before synchronization and b) synchronized with utility voltage.	38
3.12	Equivalent 1-phase ac circuit	39
3.13	Phasor diagram	39
3.14	Phasor diagram for power flow	40
3.15	Hysteresis current control	42
3.16	Hysteresis current control block	42
4.1	Half-bridge inverter applied for the system with IGBT switches	45
4.2	PV array characterisation under STC	46
4.3	PV array characterisation under site condition	47
4.4	MPPT block: Incremental conductance	48
4.5	Tracking precision from the MPPT control	48
4.6	SRF-PLL control block implemented for the system	49
4.7	Waveform of angle θ for proper synchronization	49
4.8	Control topology for the first controller	51
4.9	DC-link voltage control block for the first controller	51
4.10	Inside the magnitude control block a)Q control and b) V_{inv} control	51
4.11	2nd control block	53
4.12	3rd control block	55
4.13	First method with one PI-controller	55
4.14	Second method with one cascaded loop for the active power control block	56
4.15	Hysteresis control block	57
4.16	HCC: Active and reactive power control	58
4.17	HCC control block for phase a	58
4.18	1st controller: Reference voltage waveform vs the carrier waveform	59
4.19	Voltage current waveforms from 1st control	60
4.20	Active and reactive power from 1st control	61
4.21	Simulation results from direct control of V_{inv}	62
4.22	Current and Voltage waveform for 2nd controller in both STC and site condition	63
4.23	Active and reactive power flow control for 2nd controller	64
4.24	Carrier vs three phase voltages for third controller	65
4.25	Current and voltage waveform of 3rd controller	66
4.26	Active and reactive power flow for 3rd control	66
4.27	HCC control block implemented in PSCAD	67
4.28	HCC tracking precision	68
4.29	HCC control tracking precision of phase a current	68
4.30	Active and reactive power flow with HCC at STC	68
4.31	Active and reactive power flow with HCC under site condition	69
4.32	HCC: three phase reference currents	69
A.1	Solar array designed on PSCAD	1
A.2	Power flow from array to inverter and dc-link capacitor	2
A.3	Clark and Park transformation implemented in PSCAD	4
A.4	Inverse park transformation implemented in PSCAD	5

A.5	Sine PWM applied for the 1st controller	5
A.6	Sine PWM applied for 2nd and 3rd controller	6
A.7	THD% for 1st controller	6
A.8	THD% for 2nd controller	7
A.9	THD% for 3rd controller	7
A.10	THD% for 4th controller	7
B.1	Inverter datasheet	8
B.2	PV module configuration at Kilinochchi	9
B.3	Environmental condition at site	9

List of Tables

- 2.1 SUNNY TRI POWER CORE1 inverter parameters 24

- 4.1 Overview of system parameters for the proposed grid-connected topology 45
- 4.2 PV array parameters 46
- 4.3 PI controller gains for 1st controller 50
- 4.4 PI controller gains for 2nd controller 52
- 4.5 Proportional gain and Integral gain for 1st method controller 54
- 4.6 Proportional gain and Integral gain for 2nd method controller 54

- 5.1 Control results 70

Appendix A

PV topology

A.1 PV array design

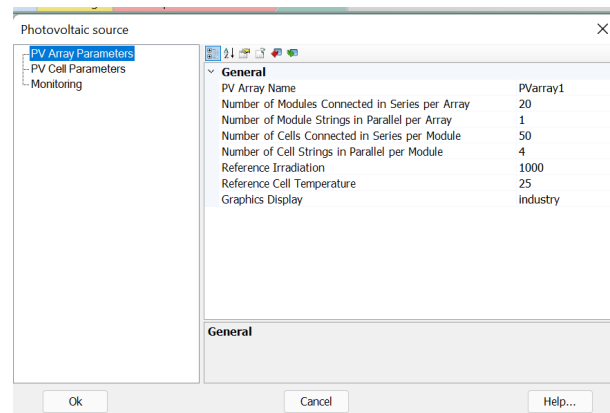
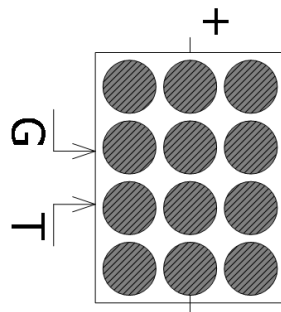


Figure A.1: Solar array designed on PSCAD

A.2 DC-link capacitor calculation

Instantaneous power can be defined as:

$$\begin{aligned}
 P_{out}(t) &= V_g(t)I_g(t) \\
 &= V_{peak}I_{peak}\sin(\omega_g t)\sin(\omega_g t + \phi) \\
 \Rightarrow P_{out}(t) &= V_{peak}I_{peak}\sin^2(\omega_g t) \\
 \Rightarrow P_{out}(t) &= \frac{V_{peak}I_{peak}}{2}(1 - \cos(2\omega_g t)) \\
 P_{out}(t) &= \frac{V_{peak}I_{peak}}{2} - \frac{V_{peak}I_{peak}}{2}\cos(2\omega_g t)
 \end{aligned} \tag{A.1}$$

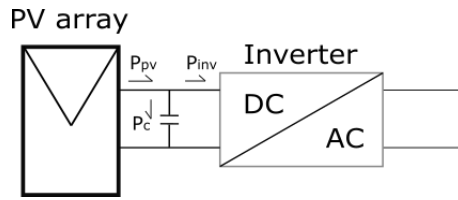


Figure A.2: Power flow from array to inverter and dc-link capacitor

Power flow from Fig.A.2 can be explained as:

$$\begin{aligned}
 P_{pv} &= P_{inv} + P_c \\
 \Rightarrow P_{inv} &= P_{pv} - P_c \\
 P_{inv} &= P_{pv} - i_c V_{dc} \\
 P_{inv} &= P_{pv} - C_{dc} V_{dc} \frac{dV_{dc}}{dt}
 \end{aligned} \tag{A.2}$$

(A.1) can be simplified to be $P_{out}(t) = \frac{V_{peak}I_{peak}}{2}$ as the last term is equal to zero because of the symmetry in three phase. Then, $P_{pv} = P_{inv} = P_{out}$ could be consider if losses are ignored and a constant voltage is maintained at PV terminals.

$$\begin{aligned}
 P_{inv} &= \frac{V_{peak}I_{peak}}{2} - C_{dc}V_{dc} \frac{d\overline{V_{dc}}}{dt} \\
 \Rightarrow C_{dc} &= \frac{S}{2\omega_g V_{dc} \overline{V_{dc}}} \sin(2\omega_g t)
 \end{aligned} \tag{A.3}$$

Voltage defined in (A.3) reaches its maximum at $\omega_g t = \frac{\pi}{4}$ then the equation can be simplified as:

$$C_{dc} = \frac{S}{2\omega_g V_{dc} \overline{V_{dc}}} \tag{A.4}$$

The value of voltage ripple $\overline{V_{dc}}$ is typically chosen to be a value below 8.5%. The DC-link capacitor for the system is kept to 8.5% and the calculation is given as:

$$\begin{aligned}
C_{dc} &= \frac{S}{2\omega_g V_{dc} \bar{V}_{dc}} \\
C_{dc} &= \frac{6.4 \text{ VA}}{2 \cdot 100\pi \cdot 677 \text{ V} \cdot (677 \text{ V} \cdot 8.5\%)} \\
C_{dc} &= 260 \mu\text{F}
\end{aligned} \tag{A.5}$$

A.3 LC-filter calculation

Selecting maximum current ripple to be 10% of the rated current [3]:

$$\begin{aligned}
\Delta i_{Lmax} &= 10\% \cdot i_{rated} \\
&= 10\% \cdot 9.4 \text{ A} \\
&= 0.94 \text{ A}
\end{aligned}$$

Calculation of filter inductor :

$$\begin{aligned}
\Delta i_{Lmax} &= \frac{1}{8} \cdot \frac{V_{dc}}{L_f \cdot f_{sw}} \\
\Rightarrow L_f &= \frac{1}{8} \cdot \frac{V_{dc}}{\Delta i_{Lmax} \cdot f_{sw}} \\
&= \frac{1}{8} \cdot \frac{677 \text{ V}}{0.94 \text{ A} \cdot 10 \text{ kHz}} = 9 \text{ mH}
\end{aligned}$$

Calculation for the filter capacitor [3]:

$$\begin{aligned}
C_f &= 10\% \frac{P_{rated}}{3 \cdot 2\pi f \cdot V_{rated}^2} \\
&= 10\% \frac{6.4 \text{ kW}}{3 \cdot 2\pi 50 \text{ Hz} \cdot 677^2 \text{ V}} \\
&= 1.5 \mu\text{F}
\end{aligned}$$

A.4 Clark and Park transformation on PSCAD

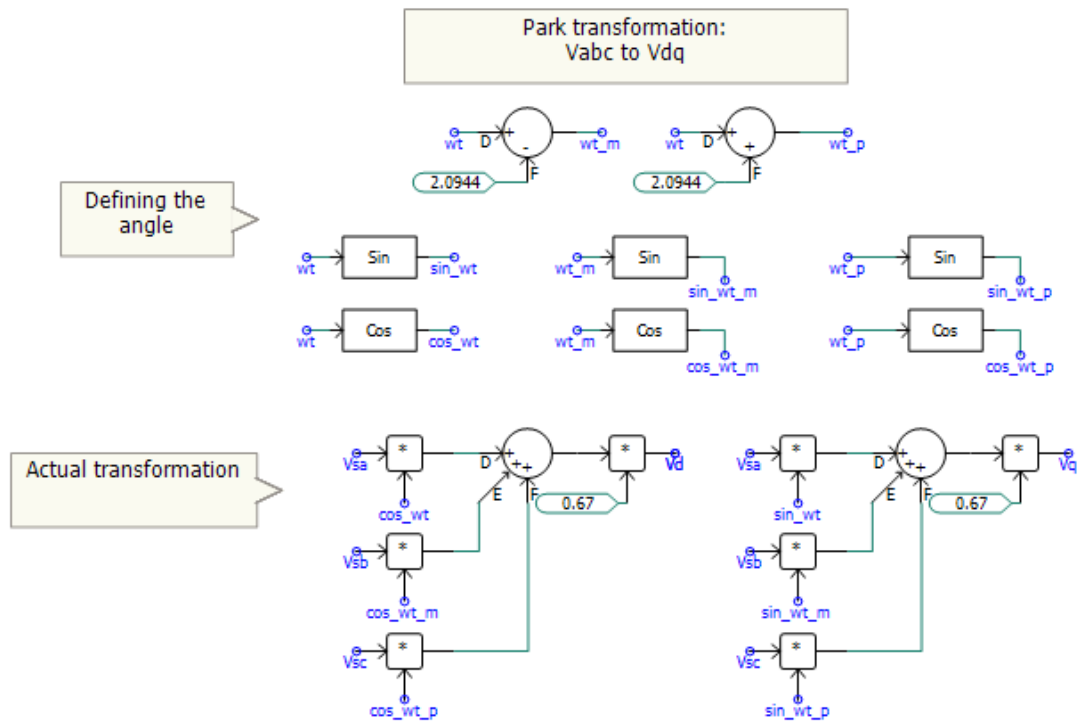


Figure A.3: Clark and Park transformation implemented in PSCAD

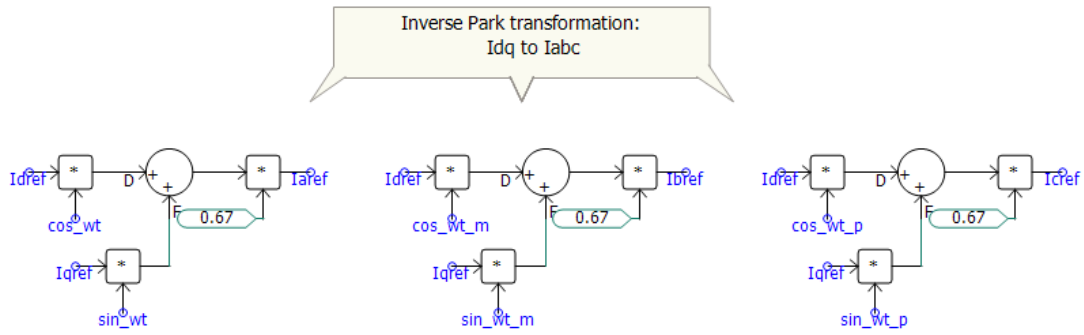


Figure A.4: Inverse park transformation implemented in PSCAD

A.5 Pulse width modulation scheme

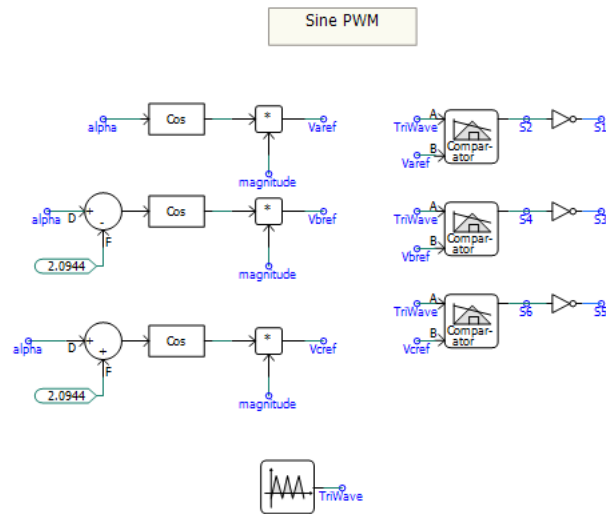


Figure A.5: Sine PWM applied for the 1st controller

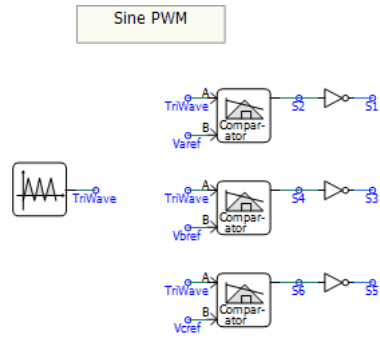


Figure A.6: Sine PWM applied for 2nd and 3rd controller

A.6 THD

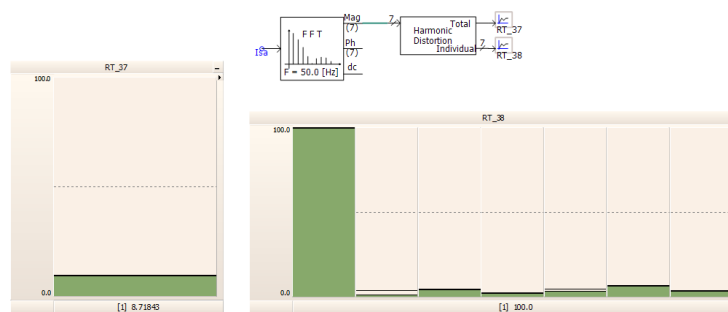


Figure A.7: THD% for 1st controller

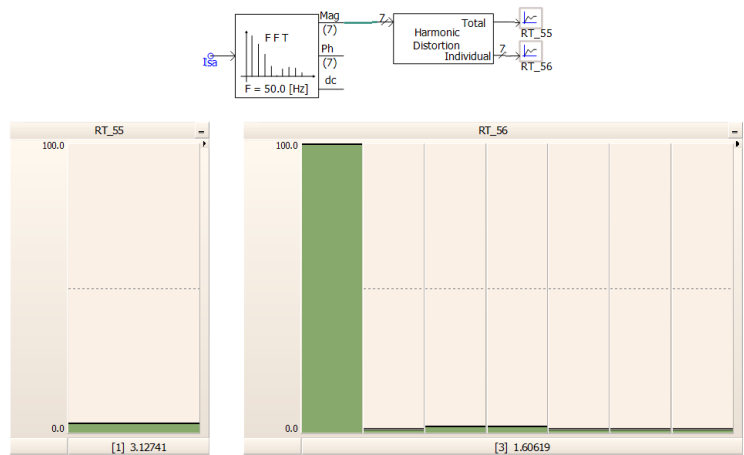


Figure A.8: THD% for 2nd controller

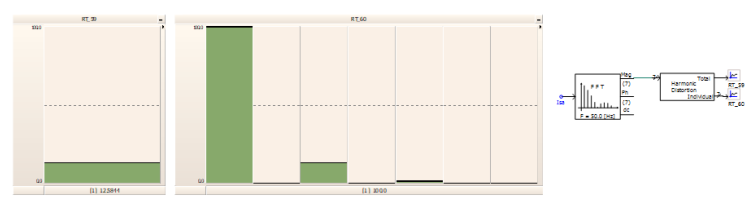


Figure A.9: THD% for 3rd controller

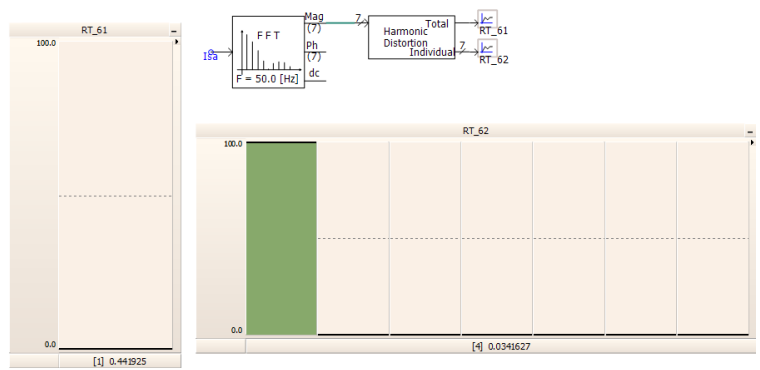


Figure A.10: THD% for 4th controller

Appendix B

Data about the FPV plant in Kilinochchi

B.1 SUNNY TRI POWER CORE1 Datasheet

Technical Data	Sunny Tripower CORE1	Technical Data	Sunny Tripower CORE1
Input (DC)		Efficiency	
Max. generator power	75000 Wp STC	Max. efficiency / European efficiency	98.1% / 97.8%
Max. input voltage	1000 V	General data	
MPP voltage range / rated input voltage	500 V to 800 V / 670 V	Dimensions [W/H/D] without feet or DC load break switch	569 mm / 733 mm / 621 mm [22.4 in / 28.8 in / 24.4 in]
Min. input voltage / start input voltage	150 V / 188 V	Weight	84 kg [185 lb]
Max. operating input current / per MPPT	120 A / 20 A	Operating temperature range	-25°C to +60°C [-13°F to +140°F]
Max. short circuit current per MPPT / per string input	30A / 30A	Noise emission [typical]	< 65 dB(A)
Number of independent MPPT inputs / strings per MPPT input	6 / 2	Self-consumption [at night]	4.8 W
Output (AC)		Topology / Cooling concept	Transformerless / OptiCool
Rated power [at 230 V, 50 Hz]	50000 W	Degree of protection [as per IEC 60529]	IP65
Max. apparent AC power	50000 VA	Climatic category [according to IEC 60721-3-4]	4K4H
AC nominal voltage	220 V / 380 V 230 V / 400 V 240 V / 415 V	Max. permissible value for relative humidity [non-condensing]	100%
AC voltage range	202 V to 305 V	Features / functions / accessories	
AC grid frequency / range	50 Hz / 44 Hz to 55 Hz 60 Hz / 54 Hz to 65 Hz	DC connection / AC connection	SUNCLIX / screw terminal
Rated power frequency / rated grid voltage	50 Hz / 230 V	Mounting feet	●
Max. output current / Rated output current	72.5 A / 72.5 A	LED indicators [status / fault / communication]	●
Output phases / AC connection	3 / 3-[N]PE	LC display	○
Power factor at rated power / Adjustable displacement power factor	1 / 0.0 leading to 0.0 lagging	Interface: Ethernet / WLAN / RS485	● [2 ports] / ● / ○
THD	< 3%	Data interface: SMA Modbus / SunSpec Modbus / Speedwire, Webconnect	● / ● / ●
Protective devices		Multi-Function relay / Expansion Module Slots	● / ● [2 ports]
Input-side disconnection device	●	Shade management SMA ShadeFix / Integrated Plant Control / Q on Demand 24/7	● / ● / ●
Ground fault monitoring / grid monitoring	● / ●	Off-grid capable / SMA Fuel Save Controller compatible	● / ●
DC reverse polarity protection / AC short-circuit current capability / galvanically isolated	● / ● / -	Guarantee: 5/10/15/20 years	● / ○ / ○ / ○
All-pole sensitive residual-current monitoring unit	●	Certificates and permits [more available on request]	ANRE 30, AS 4777, BDEW 2008, C10/11/2012, CE, CB 0-16, CEI 0-21, EN 50438:2013*, G59/3, IEC 60068-2-4, IEC 61727, IEC 62109-1/2, IEC 62116, MEA 2016, NBR 16149, NEN EN 50438, NRS 097-2-1, PEA 2016, PFC, RD 1699/413, RD 661/2007, Res. n° 7/2013, S4777, TCR 04, TR 3-2-2, UL/IEC 15-712-1, VDE 0126-1-1, VDEARN 4105, VWR 2014, PO 12.3, NTC0-NTC5, GC 8 9H, PR20, DEWA
Protection class [according to IEC 62109-1] / overvoltage category [according to IEC 62109-1]	I / AC: III; DC: II	* Does not apply to all national appendices of EN 50438	
AC/DC surge arrester [type 2, type 1/2]	○	● Standard features ○ Optional - Not available	
		Data at nominal conditions - status 02/2020	
		Type designation	STP 50-40

Figure B.1: Inverter datasheet

B.2 PV module topology

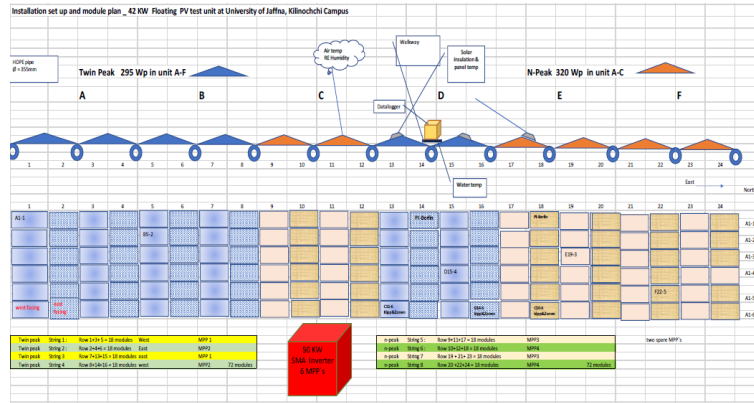


Figure B.2: PV module configuration at Kilinochchi

B.3 Environmental condition

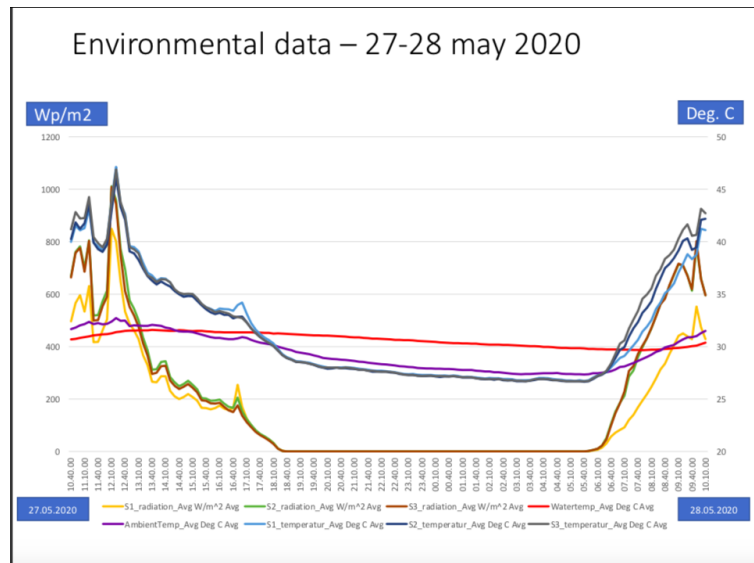


Figure B.3: Environmental condition at site